

# Colloidal quantum dots for bioscience applications

David Cunnah

UMI Number: U518441

All rights reserved

INFORMATION TO ALL USERS

The quality of this reproduction is dependent upon the quality of the copy submitted.

In the unlikely event that the author did not send a complete manuscript and there are missing pages, these will be noted. Also, if material had to be removed, a note will indicate the deletion.



UMI U518441

Published by ProQuest LLC 2013. Copyright in the Dissertation held by the Author.  
Microform Edition © ProQuest LLC.

All rights reserved. This work is protected against  
unauthorized copying under Title 17, United States Code.



ProQuest LLC  
789 East Eisenhower Parkway  
P.O. Box 1346  
Ann Arbor, MI 48106-1346

## ***Acknowledgements***

My thanks go out to my supervisors, Peter Blood and Huw Summers, who oversaw my work throughout the last few years. Without your patience and experience I would not have been able to begin, let alone finish, this work.

I must offer equal thanks to my fiancée Anna, who has been a rock to me at every turn of these last four years and was always willing to lend a listening ear when the struggles of completing a PhD were beginning to overwhelm me. I promised you I would get this finished before marrying you, and will fulfil my promise with a few days to spare!

To all of the people with whom I shared office and lab space, as well as lunches and drinks, I am indebted to you for making the day to day work a far more enjoyable experience. The many pubs and cafes which furnished us with said food and drink, I salute you!

I give a special mention for my soon to be best man David Porter, whose daily lunch trips were an invaluable opportunity to vent the frustrations of PhD life. Your ability to complete your PhD in 3 years also gave me the shove in the right direction I had needed in order to get on with the work needed to complete my own.

I could go on but I will also give my thanks to the others who attended and organised the Cardiff Redhawks ice hockey training and the Monday football sessions with me. They were always a great way of turning my attention away from my work, although I suspect that I spent a good few tired mornings being less productive because of them.

I also offer my thanks to EPSRC for their financial support during my time producing this thesis.

## **Abstract**

In this thesis I have produced results to characterise the effect of environmental factors on colloidal quantum dots, with a specific view to describing behaviour observed in biomedical imaging applications. I have used photoluminescence and absorption measurements to characterise the physical and electronic state of the dots, while developing an analytic technique to characterise their behaviour.

Initially 610nm cadmium selenide/ zinc sulphide colloidal quantum dots in a PMMA matrix showed photo-sensitive emission dynamics which were described using a two state model for the population. We show that competing processes act to increase and decrease the population's radiative efficiency. We attribute these processes to photo-driven passivation of non-radiative surface states and photo-driven oxidation of the dot surface respectively.

Results from photo-activation and absorption studies are used, in conjunction with manufacturer data, to demonstrate calculation of the concentration of a dot ensemble using absorption and extinction co-efficient data. Combining this data with photo-activation rates it was possible to calculate the probability of photo-activating a colloidal quantum dot upon absorption of a photon.

Finally 655nm quantum dots were functionalised in pH buffers in order to simulate a cellular environment. By observing the environmentally sensitive behaviour of the dots under various conditions we were able to propose a physical mechanism for the observed behaviour and point to implications for the use of dots in biomedical imaging and treatment.

## Table of Contents

<b>1. Introduction .....</b>	<b>4</b>
1.1 Aims and Motivation.....	4
1.2 Methodology.....	5
1.3 Thesis Structure .....	5
1.4 References .....	6
<b>2. Background .....</b>	<b>8</b>
2.1 An Overview of Quantum Dots.....	8
2.2 Semiconductors and their Behaviour.....	9
2.3 Optical and Electrical Properties of Nanocrystals.....	14
2.4 Quantum Dot Fabrication .....	24
2.5 Quantum Dot Applications.....	26
2.6 Conclusions .....	34
2.7 References .....	34
<b>3. Development of Experimental Techniques.....</b>	<b>40</b>
3.1 Introduction .....	40
3.2 Sample Preparation and Characterisation.....	42
3.3 Photoluminescence Measurements.....	45
3.4 Absorption Measurements.....	55
3.5 Summary.....	65
3.6 References .....	65
<b>4. Characterisation of Photo-Dynamics of 610nm CdSe/ZnS core-shell hydrophobic colloidal quantum dots in PMMA .....</b>	<b>66</b>
4.1 Introduction .....	66
4.2 Effect of Functionalisation in PMMA.....	66

4.3 Photo-Dynamic Behaviour .....	68
4.4 Measurements .....	74
4.5 Discussion.....	77
4.4 Conclusions .....	81
4.6 References .....	82
<b>5. Calculation of Optical Cross Section and Photo-Activation Probability in 610nm CdSe/ZnS Colloidal Quantum Dots in PMMA .....</b>	<b>83</b>
5.1 Introduction .....	83
5.2 Calculation of the Optical Cross Section.....	83
5.3 Results .....	91
5.4 Analysis and Proposed Physical Model.....	94
5.5 Conclusions .....	98
5.6 References .....	99
<b>6. Optical Study of 655nm Untargeted CdSe/ZnS Colloidal Quantum Dots in pH Buffer Solutions .....</b>	<b>100</b>
6.1 Introduction .....	100
6.2 Effect of Functionalisation into pH Buffers (Stage I) .....	101
6.3 Transient Absorption Measurements.....	102
6.4 Analysis of Results .....	109
6.5 Discussion.....	119
6.6 TEM and EDX measurements.....	122
6.7 Conclusions and Application.....	127
<b>7. Conclusions and Further Work.....</b>	<b>130</b>
7.1 Conclusions .....	130
7.2 Further Work .....	132

## **1. Introduction**

The focus of this thesis is to gain a greater understanding of the optical behaviour of colloidal quantum dots, especially in cellular environments, by observing optical behaviour in pH buffers. In this section I will explain the motivation behind the work which I have undertaken, and explain how this work provides original results which increase the understanding of the processes which drive colloidal quantum dot behaviour.

### **1.1 Aims and Motivation**

Colloidal quantum dots possess a number of characteristics, such as size-selective emission wavelength, broad absorption spectra and relatively high photostability, which make them more desirable for imaging in biological systems than traditional dyes, as well as possessing potential in medical diagnostics and treatment [1,2,3] due to the possibility of attaching targeting molecules to the dot surface.

In order for these advantages to be fully harnessed a better understanding of the effect of environmental conditions [4,5] on the dot behaviour is required. In the field of cellular imaging the process by which dots are ingested by cells is endocytosis. The pathway taken by the dot after uptake into the cell involves increasingly acidic environments, and it is the effect of these environments upon the dot which we primarily aim to gain a greater understanding of, as environmentally and optically induced changes in the dot emission intensity and wavelength can lead to erroneous observations in studies where they are utilised as markers.

In order to attain the above objective we begin by seeking to gain a picture of the processes driving dot behaviour in a more controlled environment, specifically in PMMA in the first case. We subsequently incorporate dots into a ‘simulated cell’

whereby acidic environments which mimic those found in cells are used to gain a specific understanding of expected behaviour in these conditions and the results compared to the work in PMMA in order to create a more complete picture of the processes involved.

This work is of significant value to the fields of *in vivo* and *in vitro* studies, as we shall investigate not only the changes that one should expect in the dot's optical behaviour, but also how the resulting by-products may effect tandem measurements, the cell itself and possible implications of dot toxicity.

## **1.2 Methodology**

In order to achieve the objectives of this work I measure photoluminescence and absorption spectra in order to characterise the colloidal quantum dots in pH buffers which are used to simulate cellular environments. I have developed a system whereby photoluminescence and absorption can be measured simultaneously and, by containing the dots within a capillary, study the same population of dots consistently over long timescales.

## **1.3 Thesis Structure**

In Chapter two I introduce colloidal quantum dots, beginning with a brief history of their emergence. I then summarise the key elements of semiconductor technology surrounding colloidal dots and go onto discuss elements of their specific optical behaviour. I introduce some of the main methods used for colloidal quantum dot fabrication and conclude by discussing the areas in which they are commonly applied.

In Chapter three I introduce the measurement techniques used to observe the dots, as well as the methods used to functionalise the dots for study. I also compare

some methods used to study dots in other work and justify our choice of method. In this chapter I also explain some of the theory behind the methods used and present typical results.

In Chapter four I show studies of photo-dynamic behaviour in colloidal quantum dots in a PMMA matrix over several hours. A model of a two state system is used to describe the behaviour and compared to results.

In Chapter five I use optical absorption measurements on dots in PMMA to obtain values of concentration and using the optical cross section I calculate the probability of photo-activating a dot upon absorption of an incident photon. Combining this with results from Chapter four allows development of a physical picture of the processes involved.

In Chapter six dots are prepared in two different pH buffers and their optical properties are studied in a variety of optical conditions; under no illumination, under low intensity white light illumination and under high intensity excitation. I analyse these results and develop a hypothesis for the observed mechanisms, which is tested by data supplied from Leeds University in order to develop a more specific picture than that in Chapter five and then draw conclusions which apply to the use of colloidal quantum dots in the biosciences.

## **1.4 References**

- [1] X. Michalet, F. F. Pinaud, L. A. Bentolila, J. M. Tsay, S. Doose, J. J. Li, G. Sundaresan, A. M. Wu, S. S. Gambhir, S. Weiss *Science*, 307, 5709 (2005)
- [2] X. Gao, Y. Cui, R.M. Levenson, L. W. K. Chung, S. Nie, *Nature Biotechnology*, 22, 8 (2004)
- [3] D. R. Larson, W. R. Zipfel, R. M. Williams, S. W. Clark, M. P. Bruches, F. M. Wise, M. W. Webb, *Science*, 300, 5624 (2003)

[4] S. R. Cordero, P. J. Carson, R. A. Estabrook, G. F. Strouse, S. K. Buratto, *J. Phys. Chem. B*, 104, 12137, (2000)

[5] J. Muller, J. M. Lupton, A. L. Rogache, J. Feldmann, D. V. Talapin, H. Weller, *App. Phys. Lett.*, 85, 381, (2004)

## **2. Background**

This section serves as an introduction to core concepts which influence colloidal quantum dot behaviour, as well as an introduction to the fields of work into which ours is relevant, specifically optoelectronics and biological imaging.

### **2.1 An Overview of Quantum Dots**

Colloidal Quantum Dots (CQDs) or Nanocrystals, as they have become known, present a unique opportunity to study the behaviour of material evolution between molecular and bulk states. QDs possess several fascinating properties which arise due to the confinement of the electron and hole to a region which is smaller than the Bohr radius. QDs differ in size from a few nanometres up to tens of nanometres, and it is the possibility to strongly influence the optical and electrical properties of devices fabricated from a single material by simply varying their size which has generated so much interest in QDs over the past two decades. A number of review articles exist which summarise some of the work which has been undertaken on such systems [1,2,3,4].

The properties of quantum dots have led to a great deal of interest in their incorporation into a number of fields including optoelectronics [5,6,7] and medical imaging, diagnosis and treatment[8,9,10]. The appeal of quantum dots in these areas arises due their size tunable properties and high potential quantum yields compared to traditional material systems and their ease of bio-conjugation due to a chemically customisable surface.

A number of studies have been performed on the evolution of the dot properties, specifically emission and absorption, from the bulk state down to the so called strong confinement regime [11,12,13,14,15]. These studies allow observation of the development of the energy level structure.

Historically it was during the late 70s that studies began on the size-dependent properties of quasi 2-D structures, so-called quantum wells, in which the size of the confining well was smaller than the Bohr radius in one dimension, resulting in two degrees of electronic freedom (hence two dimensional)[16,17]. Later came the realisation of 1-D structures, so called quantum wires, which could be grown by epitaxial methods such as molecular beam epitaxy (MBE) [18,19] and more recently by wet synthesis methods[20]. Quantum dots represent the final incarnation of the concept; structures in which there exist zero degrees of electrical freedom, hence zero dimensional structures.

## **2.2 Semiconductors and their Behaviour**

A semiconductor is a material whose conductivity increases with increasing temperature from a point where it is an insulator at 0K due to full occupation of the lower energy band. This occurs due to thermal effects allowing the electron to cross the bandgap into the conduction band. A bandgap of 4eV is usually arbitrarily used as the dividing line between semiconductor and insulating materials at room temperature. Semiconductor properties are dictated by their crystal structure. Solving Schrödinger's equation for a periodic potential describing the regular arrangement of atoms in a crystal yields a forbidden energy range in which the electron may not exist.

### 2.2.1 Direct and Indirect Band Gap Semiconductors

Semiconductors are commonly separated into two groups, direct gap and indirect gap materials. Silicon is an example of an indirect gap material while Cadmium Selenide is an example of a direct gap semiconductor. The primary difference lies in the nature of the conduction band to valence band transition in each material. The E-k curve is commonly used to describe the relationship between the wavevector associated with an electron and the energy state of said electron. In Direct band gap materials the conduction (valence) band E-k curves have a minimum (maximum) at  $k=0$ . This means direct transitions produce a photon since the k-vector of the electron hole pair is effectively zero, allowing conservation of momentum during the recombination event without production of a phonon. In indirect gap materials the conduction band has a non  $k=0$  minimum (the maximum of the valence band is necessarily at  $k=0$  by definition) which results in the production of a phonon in order to satisfy conservation of momentum in the process.

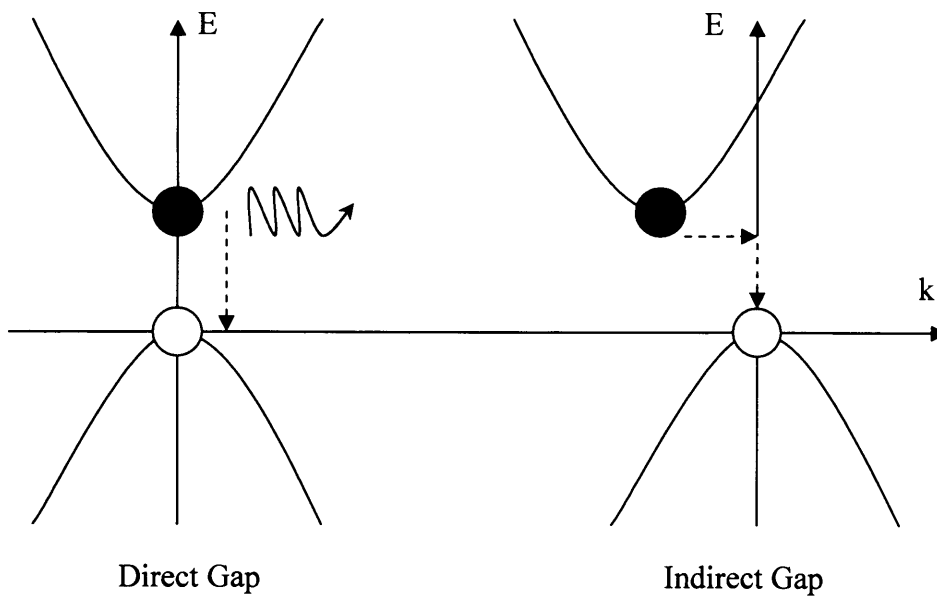


Figure 1 Diagram illustrating production of a photon via recombination in a direct band gap material, and a phonon due to recombination in an indirect semiconductor material.

The bands in semiconductors are approximated as parabolic near the band edge as a function of  $k$ , and below we assume the maximum of the valence band defines  $E=0$ . For the conduction band and valence band respectively this is expressed as:

$$E = E_g + \frac{\hbar^2 k^2}{2m_e} \quad \text{and} \quad E = -\frac{\hbar^2 k^2}{2m_h}$$

**Equation 1**

### 2.2.2 Effective Mass

The concept of effective electron and hole mass in semiconductors arises due to the wave-packet dynamics which represent a localised particle. Equation 2 is the result of applying Newton's law to a particle of mass  $m_e$  (i.e. an electron) in a parabolic energy band, under the influence of some electric field. It describes the mass that the particle appears to carry in a semi-classical model.

$$m_e = \frac{\hbar^2}{\left(\frac{d^2 \epsilon}{dk^2}\right)}$$

**Equation 2**

As is evident in Equation 2, the shape of the E-k curve determines the effective mass, with a sharper parabola yielding a lower effective mass and vice versa.

### 2.2.3 The Exciton

In semiconductor physics, and especially in confined systems, it is often appropriate to describe the behaviour of the exciton, an electron and its corresponding hole which are bound to each other via the Coulomb force. Within a crystal lattice they allow the description of energy transport without the transport of charge. Fox [21] describes excitons as “electron-hole pairs bound together in stable orbits by the mutual Coulomb attraction between them”.

Excitons are usually described as Wannier-Mott excitons, or Frenkel excitons. While a Wannier-Mott exciton is free to move in the crystal lattice while the Frenkel exciton is localised on an atomic site. Figure 2 illustrates the difference between the two concepts, and also a point which shall become important in later discussions, specifically the situation where the exciton occupies a crystal which is smaller than its natural separation (the Bohr radius, described further in 2.3.1) of the electron hole pair. When this is the case the term ‘strong confinement’ is used to describe the effect on the system’s electronic states, and is discussed further in 2.3.1.

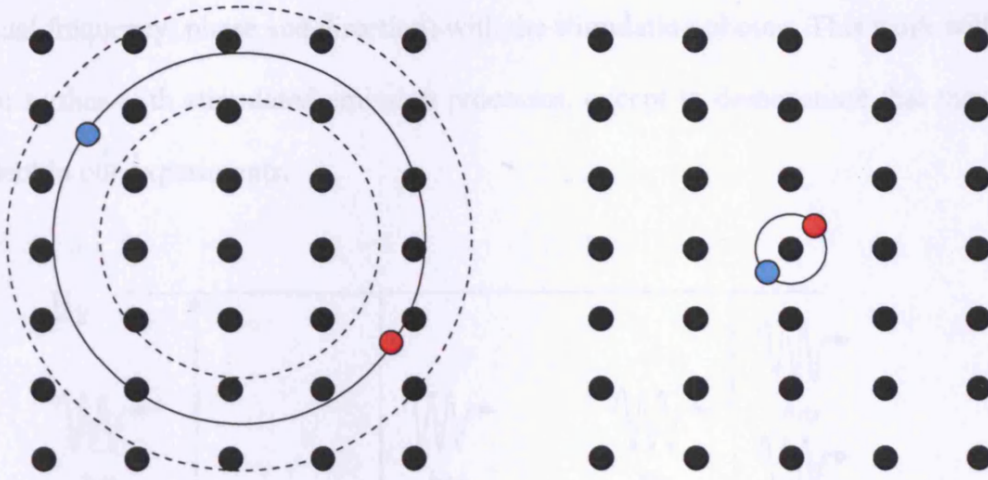


Figure 2 Illustration of a free exciton and a tightly bound exciton. In the image of the free electron the dotted lines indicate a cross section through a cluster which would be considered to be within and without the strong confinement regime, with the larger circle indicating the cluster which is outside of the strong confinement regime. Adapted from [70].

### 2.2.4 The Einstein Picture of Absorption and Emission

Here I briefly outline an approach to describing the optical transitions in a material which was developed by Einstein [22].

We begin by considering that an electron occupying some energy state  $E_1$  may undergo a transition to a higher energy state  $E_2$  via absorption of a photon of energy  $\hbar\omega$  given that the condition outlined in Equation 3 is satisfied.

$$E_2 - E_1 = \hbar\omega$$

Equation 3

Conversely an electron in  $E_2$  can relax back to  $E_1$ , emitting a photon of energy  $\hbar\omega$ . This process will occur after some time in a spontaneous manner, but may

be stimulated by an incoming photon. The resulting emitted photon will be coherent (equal frequency, phase and direction) with the stimulating photon. This work will not deal further with stimulated emission processes, except to demonstrate that they are absent in our experiments.

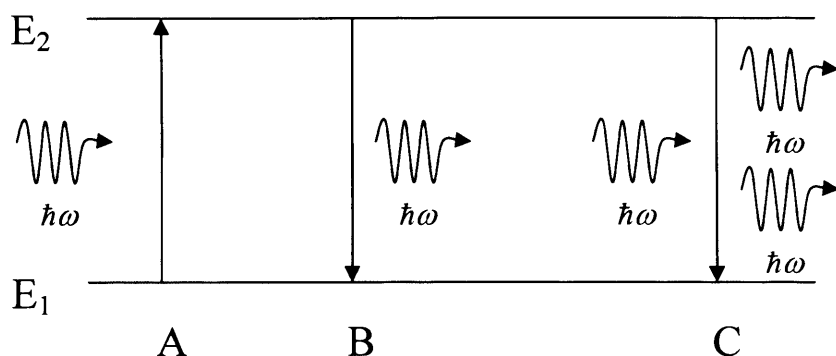


**Figure 3** Depiction of absorption and emission processes in a two level system. In A a photon whose energy satisfies Equation 3 is absorbed and the absorbing electron is excited to state  $E_2$ . In B the electron relaxes back to  $E_1$  emitting a photon of energy  $\hbar\omega$ , and in C a photon stimulates the relaxation of the electron, resulting in emission of a photon coherent with the stimulating photon.

## 2.3 Optical and Electrical Properties of Nanocrystals

As outlined above, one of the most fascinating properties of nanocrystals is their unique behaviour due to the confinement of the electron hole pair in all three dimensions. Here we outline some of the key features of nanocrystals and compare these to those of bulk and molecular systems.

### 2.3.1 Quantum Confinement

The effect of exciton confinement in three dimensions leads to the novel size dependent emission wavelength of colloidal quantum dots. Confinement arises due to the relatively narrow bandgap of the dot material compared to its surrounding matrix,

resulting in a three dimensional well in which the carrier is confined. In practice dots are usually coated with a wider bandgap shell in order to reduce surface defect recombination. Figure 4 depicts the physical and electronic structure of the dot and its band gap. The effective confinement of the dot is influenced by the matrix into which it is placed, however for most systems the bandgap of the matrix will be much larger than that of the dot or its shell.

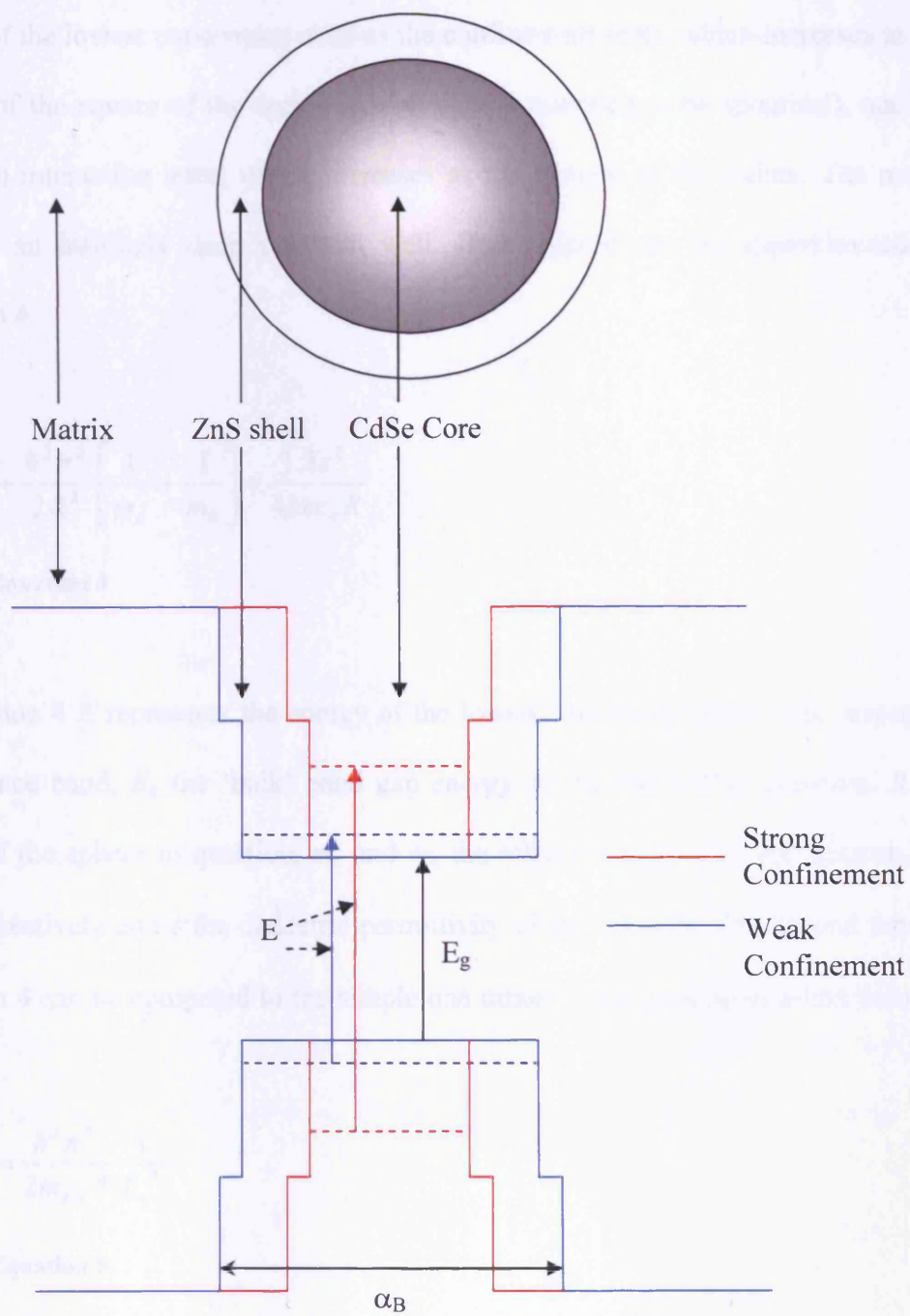


**Figure 4** Diagram depicting energy gap in a CdSe/ZnS core shell quantum dot. The core has a relatively narrow bandgap while the shell and matrix have increasingly larger bandgaps which leads to confinement of carriers within the core, entering the strong confinement regime when the well width is below the Bohr radius.

The effect of quantum confinement on the band gap of the material system was characterised by Brus in 1983 [1]. Brus identified the main influences on the energy of the lowest unoccupied state as the confinement term, which increases as the inverse of the square of the radius (the particle is assumed to be spherical), and the Coulomb interaction term, which increases as the inverse of the radius. The model assumes an infinitely deep potential well. Brus' model can be approximated by Equation 4

$$E = E_g + \frac{\hbar^2 \pi^2}{2R^2} \left[ \frac{1}{m_e} + \frac{1}{m_h} \right] - \frac{1.8e^2}{4\pi\epsilon\epsilon_0 R}$$

**Equation 4**

In Equation 4  $E$  represents the energy of the lowest unoccupied state with respect to the valence band,  $E_g$  the 'bulk' band gap energy of the material in question,  $R$  the radius of the sphere in question,  $m_e$  and  $m_h$  the effective masses of the electron and hole respectively and  $\epsilon$  the dielectric permittivity of the material. The second term in Equation 4 can be compared to the simple one dimensional particle-in-a-box solution of

$$E_{e,h}(z) = \frac{\hbar^2 \pi^2}{2m_{e,h}} \frac{1}{L_z^2}$$

**Equation 5**

by realising that the contribution to the total bandgap shift will be the sum of the electron (CB) and hole (VB) contributions. The third term in Equation 4 is simply the Coulomb interaction between an electron and a hole at a distance  $R$ . This formula

breaks down for large R (specifically  $R > \alpha_B$ , the Bohr Radius-see below), since the separation of the charges will no longer be equal to R.

Using standard data for CdSe [23, 24], the predicted change in the energy of the first state due to confinement and the Coulomb interaction are illustrated in Figure 5.

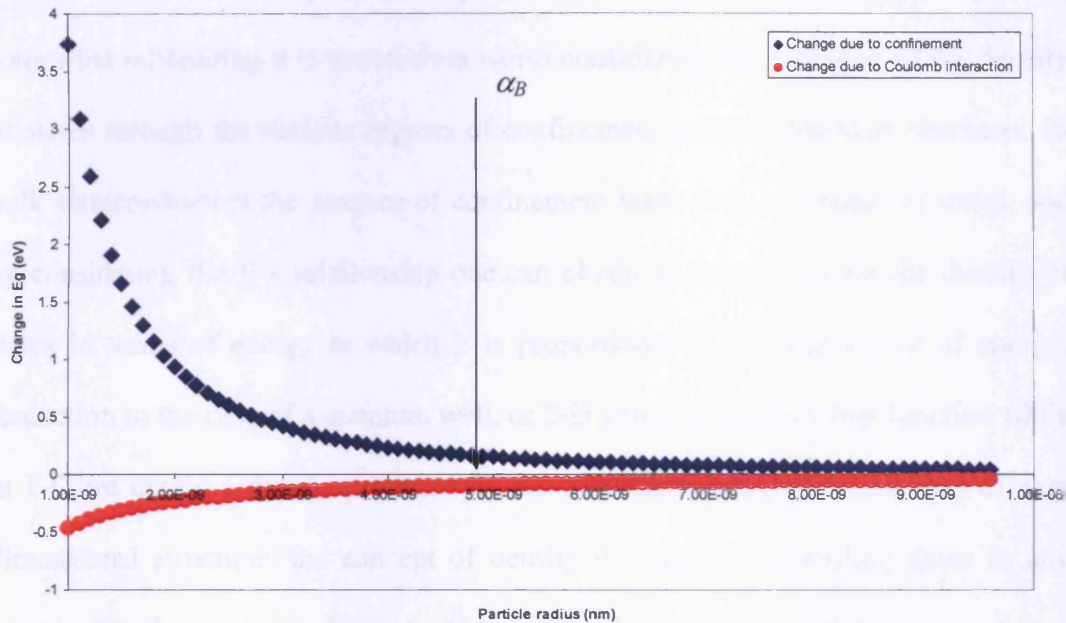


**Figure 5** Expected change in the effective band gap of CdSe due to confinement effects and Coulomb interaction.

A system is commonly thought to be in the ‘strong confinement’ regime when the physical size of the system is comparable to or smaller than the Bohr radius of the exciton, defined as;

$$\alpha_B = \epsilon_0 \epsilon h^2 / \pi \mu e^2$$

**Equation 6**

where  $\alpha_B$  is the Bohr radius,  $\epsilon_0$  the permittivity of free space,  $\epsilon$  the dielectric constant of the material and  $\mu$  the reduced effective mass of the electron hole pair. As shown in Figure 5, the Bohr radius of CdSe is around 4.9nm.

### 2.3.2 Density of States

While the concept of density of states in a zero dimensional structure is somewhat misleading it is nonetheless worth considering the evolution of the density of states through the various degrees of confinement in semiconductor structures. In bulk semiconductors the absence of confinement leads to a continuum of states, and by considering the E-k relationship one can obtain an expression for the density of states in terms of energy in which it is proportional to the square root of energy. Reduction to the case of a quantum well, or 2-D structure yields a step function while in 1-D we obtain a function dictated by the Heaviside function. In the case of zero dimensional structures the concept of density of states is misleading since in any given entity the states are discrete and hence the density of states function appears as a delta function. A more useful application of the concept arises when considering the broadening of the delta function due to inhomogeneous and homogeneous distributions of size in ensembles of zero dimensional structures.

### 2.3.3 The Role of Surface States

As crystalline structures approach smaller sizes the effect of surface states begins to become a significant factor in their behaviour. This occurs due to the rapid increase in the fraction of atoms existing at the material interface to the number of atoms in the crystallite. Atoms at the surface have unpassivated, so-called 'dangling' bonds, whose interaction influences the electronic structure of the system. The effect of these dangling bonds is illustrated in Figure 6. The surface states form a number of

energy states within the band gap of the dot. The vast majority of recombination via these states is non-radiative and if the surface states are not well passivated will severely diminish the radiative efficiency of the dot.

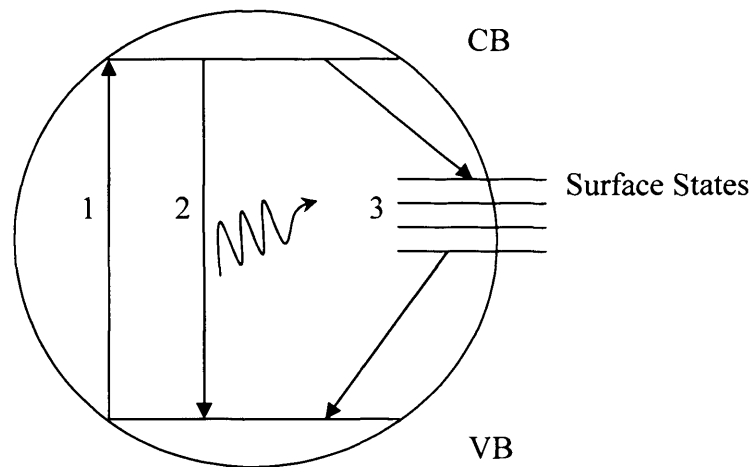


**Figure 6 Diagram depicting recombination routes in a colloidal quantum dot. 1) A photon is absorbed, exciting an electron into the conduction band and leaving a hole in the valence band. 2) The electron either recombines radiatively, producing a photon or 3) recombines non-radiatively via surface states.**

In practise the shell layer of wider bandgap material goes some way to passivating the surface of dots which possess this structure. In order to further stabilise the dot surface it is common practise to coat the dot surface with a polymeric material in order to further passivate any dangling surface bonds.

### **2.3.4 Single Dot Blinking**

Nirmal et al. reported colloidal quantum dot blinking in 1996 [25], having observed discrete on and off states in the fluorescence of single quantum dots. Despite extensive studies in subsequent years the precise nature of the process is still not well understood, although it is widely accepted that surface charging plays a part in the

behaviour. Although not the focus of this document the reader should be aware of the potential applications of such a process if it can be controlled, including data storage for quantum computation. Ultimately it is the adjustment of ‘on’ and ‘off’ states in ensembles which leads to the photodynamic behaviour discussed in detail below.

### **2.3.5 Reversible and Irreversible Photo-Dynamic Behaviour**

In colloidal quantum dot ensembles the photoluminescence efficiency can be dramatically altered by application of optical [26] excitation. Despite a wealth of work on the area there remains ambiguity as to the precise source of this behaviour.

Photo dynamic behaviour has been shown to be very sensitive to environmental factors, such as presence of water molecules [26] and oxygen [27]. This has led to a consensus that, as with blinking, the driving force behind the process is linked to the charging of the dot surface and that the neutralisation of surface charge is due to environmental ions.

Typically photo-dynamic behaviour is described as reversible or irreversible. Reversible behaviour is usually attributed to charging processes at the dot surface whereas irreversible changes are supposed to be driven by permanent physical changes in the dot structure such as photo-oxidation.

### **2.3.7 Optical Absorption and Absorbance**

Fundamentally the absorption of a material is determined by the interaction of light and matter. In semiconductor physics as well as other areas it is convenient to define the absorption of a material by the absorption co-efficient, usually expressed as  $\alpha(h\nu)$ , which is defined as the relative rate of the decrease of light intensity,  $I(h\nu)$ , along its propagation length  $x$  [28]. Equation 7 is true for  $dx \gg \lambda$ .

$$\alpha(h\nu) = \frac{1}{I(h\nu)} \frac{dI(h\nu)}{dx}$$

**Equation 7**

In many studies it is convenient to define the absorbance of a material,  $A$ , which is expressed as [29];

$$A = -\log_{10} T$$

**Equation 8**

where  $T$  is the fractional transmittance of the material ( $I(x)/I(0)$ ). The above is often called Beers Law, after the author of the paper in reference 29. Beer also demonstrated that;

$$A = \varepsilon CL$$

**Equation 9**

where  $\varepsilon$  is the extinction co-efficient of the material,  $C$  is the concentration of absorbing material within some transparent dilution and  $L$  is the path length. When using this expression one must be careful with definition of  $\varepsilon$ , especially in the field of colloidal quantum dots, since the constant may be defined as the extinction per unit length per mole of material in synthesis (i.e. molar concentration of synthesis solution) or it may be the extinction per unit length per mole of quantum dots (i.e. Avogadro's Number of quantum dots). One must also carefully consider the wavelength at which any measurements are made. Many studies of colloidal dots assume  $\varepsilon$  to be measured at the band-edge, and the expected behaviour as the dot size

changes is necessarily different both at different wavelengths and for different definitions of  $\varepsilon$ .

When considering the oscillator strength (the ratio of the optical cross section to that expected from a classical oscillator, which is closely related to the extinction co-efficient), we begin by considering that at high energies the absorption spectra of colloidal quantum dots become featureless and equivalent to the bulk material system. As such the extinction co-efficient of an ensemble should be identical to that of a film of bulk material, having the same amount of material, along the same path. This is not the case, however, at lower energies where the evolution of discrete states leads to more complex behaviour of the oscillator strength.

Because colloidal dots are usually studied in some co-ordinating solvent it is necessary to consider the local field correction factor,  $|f(\omega)|^2$  based on the Bruggeman effective media theory [30,31]. The optical cross section,  $\sigma_a(\omega)$  per dot in the high energy regime can be shown to be [32];

$$\sigma_a(\omega) = \frac{4}{3} \pi R^3 \frac{n_1}{n_2} |f(\omega)|^2 \alpha_b(\omega)$$

**Equation 10**

where  $n_{1,2}$  are the real parts of the refractive indices of the semiconductor and solvent respectively,  $\alpha_b(\omega)$  is the bulk absorption co-efficient at a frequency  $\omega$  and  $|f(\omega)|^2$  is given by;

$$f(\omega) = \frac{3m_2^2}{m_1^2 + 2m_2^2}$$

**Equation 11**

where  $m_{1,2}$  are the complex indices of refraction.

It is worth noting at this point that Leatherdale [32] observed that the effect of the local field correction factor,  $f(\omega)$ , was much lower in practise than in theory. This was attributed to the low refractive index ligand shell acting as a screen for the effect.

As Equation 10 shows, we expect a cubic relationship between the cross section per dot and the radius in the high energy regime. Conversely, many experimental [33] and theoretical [2,34] works have demonstrated that the cross section per dot is independent of dot size at the band gap.

## **2.4 Quantum Dot Fabrication**

Wet chemical synthesis is the most common method for the fabrication of nanocrystals. For clarity, it should be made clear here that we shall be discussing structures in which there exists a strong confinement of the exciton, called nanocrystals henceforth, as opposed to self assembled quantum dots produced by the so called Stranski-Krastanow (SK) method, in which the presence of a wetting layer as well as the formation of ternary dots inhibits the effective 3-D confinement of the dots [35,36,37,38].

It has recently been shown that epitaxial growth of nanocrystals can be achieved [39], however, since this work will focus exclusively on nanocrystals fabricated in solution this chapter will focus on this method.

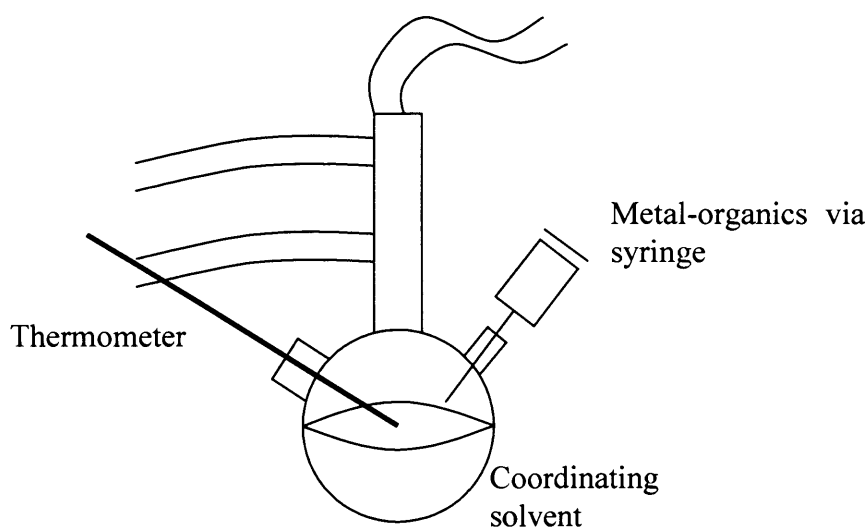


**Figure 7 Diagram depicting setup for wet synthesis of colloidal quantum dots. The precursor metals are injected via the syringe while the temperature is adjusted and monitored in order to control nucleation and growth. Adapted from Ref. 41**

The two critical steps in the production of nanocrystals in solution involve initial nucleation and subsequent growth [40], while improvement of the monodispersity of the solution can be achieved via so-called focusing of the size distribution and Ostwald ripening. Each of the steps is outlined below:

- Nucleation involves rapid addition of reagents to the reactor chamber containing a co-ordinating solvent (where appropriate this solvent will contain passivating ligands) until their concentration exceeds the nucleation threshold. Nucleation begins and relieves the supersaturation.
- Growth is achieved by controlling the rate at which additional material is added to the solution, such that it does not exceed the rate at which material is added to the growing clusters. The size of the nanocrystals is largely determined by the time over which this process is performed [41].

- If growth during nucleation is small compared to the subsequent growth then the particles become increasingly uniform over time, a process referred to as focusing of the size distribution.
- Ostwald ripening [42,43] involves dissolving smaller nanoparticles, and the growth of larger clusters as they absorb the dissociated material from the smaller particles. This results in a smaller number of nanoparticles with a larger average size.

In reality the product of such synthesis depends strongly on a number of factors such as concentration, temperature, mixing rate and pH of the solution.

Most QD production now occurs in organic solvents, which produces hydrophobic dots which are unsuitable for applications such as biotechnology in which functionalisation into an aqueous environment is necessary. As a result a process known as ligand exchange is often performed, details of which can be found in many relevant works [44,45], where the coating obtained during fabrication is removed and replaced with molecules containing two reactive groups, one of which binds to the dot surface e.g. -SH, and the other hydrophilic to ensure solubility in aqueous environments e.g. -COOH .

## **2.5 Quantum Dot Applications**

This section serves as a review of applications of quantum dots in some key areas, focusing primarily on Opto-Electronic and BioScience applications.

### **2.5.1 Colloidal Quantum Dots in the Bio-Physical Sciences**

CQDs have been exceptionally successful in bioscience applications due to the possibility of functionalising the dot surface for targeted adsorption and immunospecific responses in a wide spectrum of biological systems, from imaging

tumours in mice to tracking the digestive and immune process in singular cells. The sensitivity of colloidal quantum dots to their environment makes them ideal candidates for sensing applications, where environmentally driven changes can be detected in order to better understand the mechanics of biological systems. For the interested reader a number of excellent review papers exist [46-55]. I will here summarise the most important and relevant developments in the field.

The appeal of colloidal quantum dots in biological labelling lies in a number of their properties;

- The size tunability of the dots allows labelling of one entity (such as cell or organ) with multiple dot sizes, providing images resolvable in the wavelength regime. Figure 8 demonstrates dual labelling of a mouse fibroblast cell.
- Dot absorption is broad, while most classical organic dyes demonstrate a narrow absorption spectrum which often overlaps emission, meaning there is necessarily overlap between excitation and photoluminescence. The broad dot absorption allows excitation of multiple dot sources well away from the emitting wavelength. Figure 9 demonstrates typical absorption and emission spectra from an organic dye and a colloidal quantum dot system.
- Dots exhibit relatively high photo-stability in comparison to organic dyes, especially when bio-conjugated. Figure 10 demonstrates the resistance of inorganic quantum dots to photo-bleaching, in comparison to a common organic dye.



Figure 8 Dual labelling of mouse fibroblast cells. Adapted from ref. 53

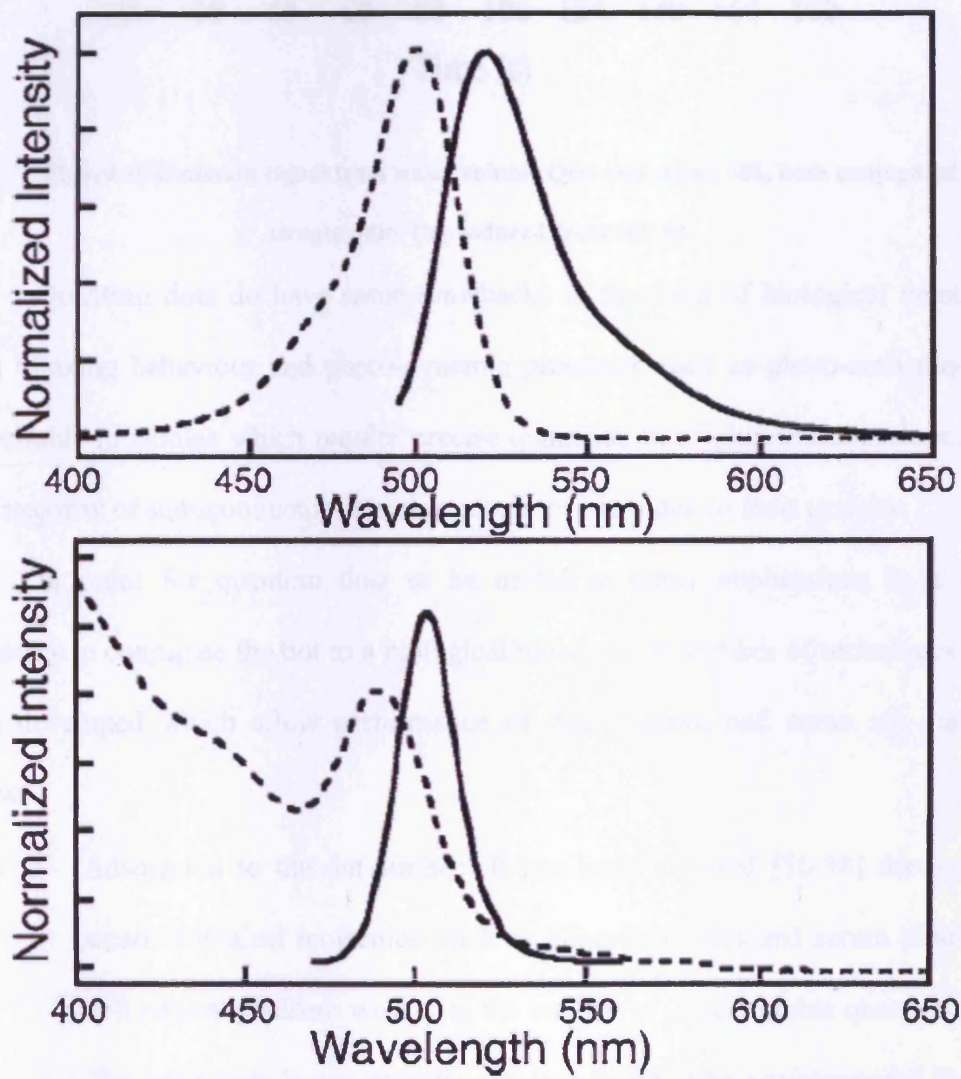


Figure 9 Absorption (dotted) and emission (solid) spectra of fluorescein (top) and water soluble QDs (bottom). Reproduced from ref. 53.

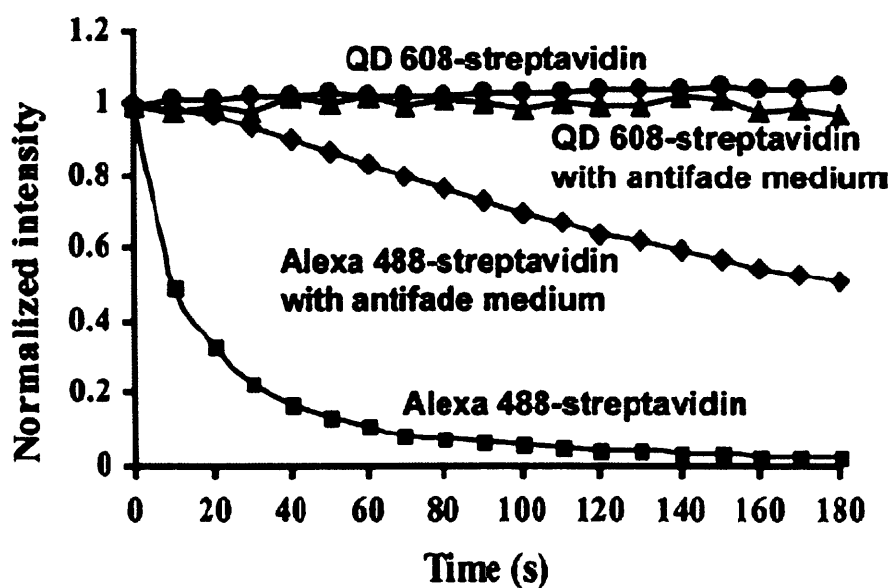


Figure 10 Emission signal from water soluble QDs and Alexa 488, both conjugated with streptavidin. Reproduced from ref. 54.

Quantum dots do have some drawbacks in the field of biological detection. Both blinking behaviour and photo-dynamic processes such as photo-activation are undesirable in studies which require precise quantisation of photoluminescence. The vast majority of semiconductor dots also pose a problem due to their toxicity.

In order for quantum dots to be useful in many applications it is often necessary to conjugate the dot to a biological molecule. A number of techniques have been developed which allow performance of this process, and some are outlined below:

- Adsorption to the dot surface: It has been reported [56-58] that certain small biological molecules, such as oligonucleotides and serum albumins, will naturally adsorb weakly to the surface of water soluble quantum dots. The adsorption is non-specific and is influenced by environmental factors such as temperature and pH.

- **Electrostatic interaction:** The formation of quantum dot bio-molecule conjugates via electrostatic interaction has been reported [59,60] where a protein was attached to a positively charged intermediate which in turn bound to the negatively charged quantum dot surface. The resulting dots demonstrated excellent quantum yield and photo stability.
- **Mercapto exchange:** Various groups have successfully achieved mercapto exchange [61-63] of bio molecules on the surface of quantum dots. Unfortunately the reliance on thiol bonding to the dot surface results in a weak interaction which can cause dots to precipitate from solutions.
- **Cross-Linking:** More stable linkage can be achieved using cross-linking molecules [53, 64-68]. In order for this process to be feasible it is necessary that certain molecular groups exist on the dot surface, and as such it is not possible in all circumstances.

One feature of quantum dots which was developed as a result of necessity is their ability to bind specifically to a location (i.e. a specific cellular environment). Early work on quantum dots used as biological markers showed non-specific binding [67], whereas more recently a better understanding of the surface chemistry of the dots has led to more successful application of specific dot binding to target sites [68].

### **2.5.2 Endocytosis**

The implications of the studies undertaken here are greatest for those using colloidal quantum dots as cellular markers where dots are absorbed into the cell by endocytosis. As such we present here a brief summary of the process and an explanation of the relevance of this work to the field. Much of the work here can be seen in more detail in [69] for the interested reader.

Principally endocytosis involves the uptake and management of extracellular material within a biological cell. Figure 11 demonstrates the important elements of the process; a particle approaches the cellular membrane, which deforms around said particle until it is completely surrounded by the cell. The cell then takes the particle to a series of endosomes where it is processed. The later endosomes have a typical pH of 5.5. Eventually the particle will be placed in a lysosome which has a more acidic pH of around 4.8.

In this document we investigate the effect of the local pH on dot structures in order to better understand the stability and toxicity of the dots when used for imaging techniques which utilise endocytosis for the functionalisation of dots into cellular systems.

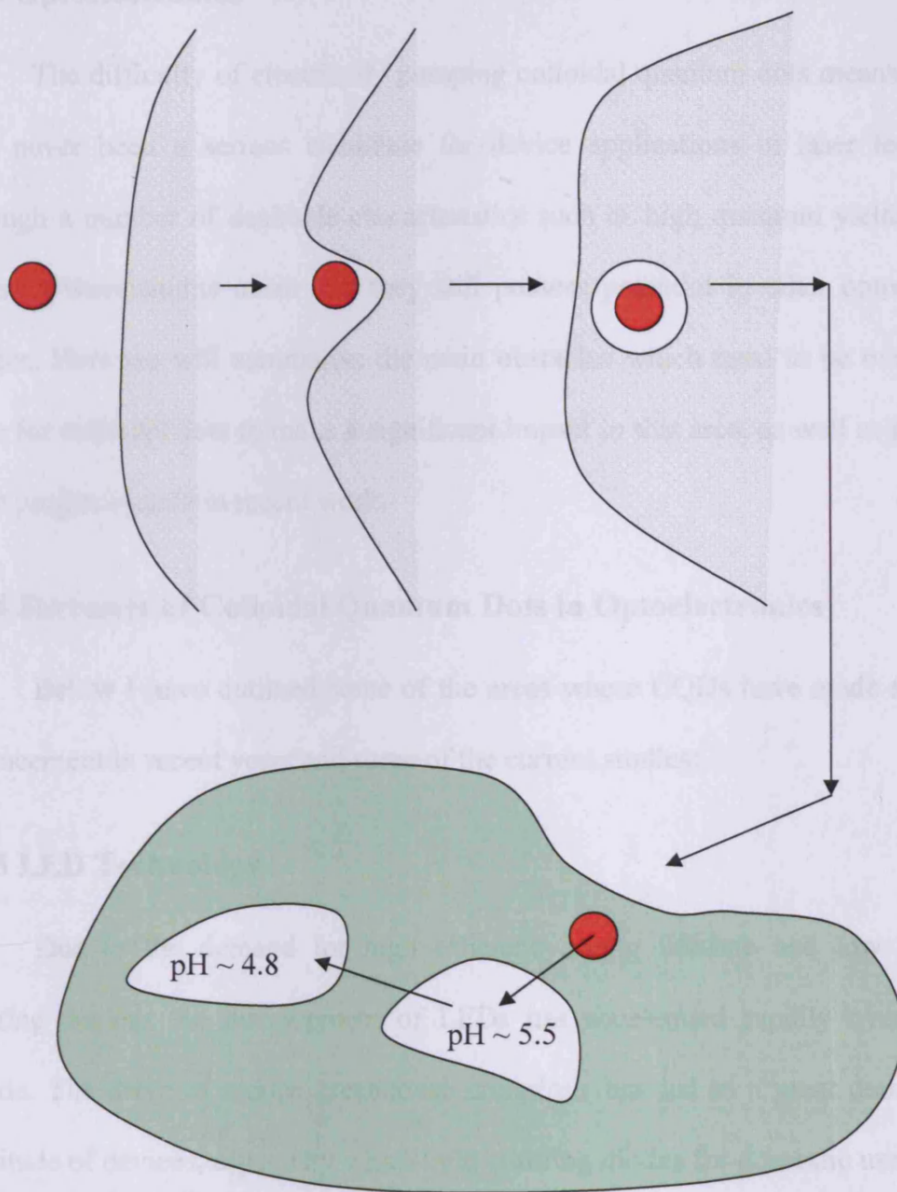


**Figure 11** Highly simplified illustration of the endocytosis process. A dot approaches the cell membrane which deforms around the dot, eventually encapsulating it within the cell. Once inside the absorbed material is taken through a series of endosomes, the so called endocytic pathway. The endosomes have a typical pH of around 5.5. Eventually the dot reaches a lysosome which has more acidic pH of typically 4.8.

### **2.5.3 Optoelectronics**

The difficulty of electrically pumping colloidal quantum dots means that they have never been a serious candidate for device applications in laser technology, although a number of desirable characteristics such as high quantum yields, tunable emission wavelengths mean that they still possess potential in other optoelectronic devices. Here we will summarise the main obstacles which need to be overcome in order for colloidal dots to make a significant impact in this area, as well as presenting some progress made in recent work.

### **2.5.4 Successes of Colloidal Quantum Dots in Optoelectronics**

Below I have outlined some of the areas where CQDs have made significant advancement in recent years and some of the current studies:

### **2.5.5 LED Technology**

Due to the demand for high efficiency, long lifetime and low cost light emitting devices the development of LEDs has accelerated rapidly over the past decade. The drive to reduce greenhouse emissions has led to a great demand for a multitude of devices, especially white-light emitting diodes for domestic use. The size tunability of CQD emission, as well as the possibility of mixing dots of various sizes, make them ideal candidates for such applications and have led to innovation in their functionalisation for such systems.

Using semi-conducting polymers and organic-inorganic hybrid devices LED devices have been demonstrated [70, 71]. Ultimately the real promise of colloidal dots in such systems lies in the ease with which many sizes of colloidal dots may be combined to produce a white light emitting device, while providing excellent efficiency due to their high expected quantum yield.

In order for this field to advance a number of questions must be addressed, specifically:

- The effect of the quantum dot environment on its behaviour in order that selection of organic material, polymers, or any other candidate for the dot matrix can be chosen systematically for best performance
- The long term behaviour of the dots in order that the potential lifetime of any such device in a commercial environment can be established, and ways to improve it can be developed.

## 2.6 Conclusions

In this document we shall attempt to deal with the problem of characterising colloidal quantum dot ensemble behaviour under illumination in order to better understand the mechanics of photo-dynamic behaviour. We use a statistical treatment of photo-activation behaviour as well as absorption behaviour to derive a method which allows calculation of an approximate photo-activation probability per dot upon absorption of a photon.

Furthermore we attempt to simulate cellular environments using pH buffers in order to gain insight into colloidal quantum dot stability and toxicity in such an environment as well as investigate the feasibility of expanding the role of colloidal quantum dots in the detection of environmental pH in cellular imaging.

## 2.7 References

- [1] L. E. Brus, J.Chem Phys, 80, 4403 (1984)
- [2] L. E Brus, Appl Phys A, 53, 456 (1991)
- [3] A. P. Alivisatos, Science, 16, 933 (1996)

- [4] A. P. Alivisatos, *J. Phys Chem*, 100, 13226 (1996)
- [5] V. L. Colvin, M. C. Schlamp and A. P Alivisatos, *Nature*, 370, 354 (1994)
- [6] B.O. Dabbousi, M. G. Bawendi, O. Onitsuka and M. F. Rubner, *Appl Phys Lett*, 66, 1316 (1995)
- [7] J. D. Berger, S. Hallstein, O. Lyngnes, W. W. Ruhle, G. Khitrova, H. M . Gibbs *Phys Rev B*, 55, 4910 (1997)
- [8] X. Michalet, F. F. Pinaud, L. A. Bentolila, J. M. Tsay, S. Doose, J. J. Li, G. Sundaresan, A. M. Wu, S. S. Gambhir, S. Weiss *Science*, 307, 5709 (2005)
- [9] X. Gao, Y. Cui, R.M. Levenson, L. W. K. Chung, S. Nie, *Nature Biotechnology*, 22, 8 (2004)
- [10] D. R. Larson, W. R. Zipfel, R. M. Williams, S. W. Clark, M. P. Bruches, F. M. Wise, M. W. Webb, *Science*, 300, 5624 (2003)
- [11] W. Hoheisel, V. L. Colvin, C. S. Johnson, A. P. Alivisatos, *J. Chem. Phys*, 101, 8455 (1994)
- [12] D. J. Norris, A. Sacra, C. B. Murray, M. G. Bawendi, *Phys. Rev. Lett*, 72, 2612 (1994)
- [13] M. Nirmal, C. B. Murray, M.G. Bawendi, *Phys. Rev. B*, 50, 2293 (1994)
- [14] A. Sacra, D. J. Norris, C. B. Murray, M.G. Bawendi, *J. Chem. Phys*, 103, 5236 (1995)
- [15] A.I. Ekimov, F. Hache, M.C. Schanne-Klein, D. Richard, C. Flytzanis, I. A. Kurdryavtsens, T. V. Yazeva, A. V. Rodina, A. L. Efros, *J. Opt. Soc. Am. B*, 10, 100 (1993)
- [16] R. Dingle, *Advances in Solid State Physics* 21 P.W. (1975)
- [17] A. Harstein, A. B. Fowler, *Proceedings of the Thirteenth International Conference on the Physics of Semiconductors*, 741 (1976)

- [18] J. Tersoff, R. M. Tromp, *Phys. Rev. Lett.*, 70, 2782 (1993)
- [19] S. Tsukamoto, Y. Nagamune, M. Nishioka, Y. Arakawa, *Appl. Phys. Lett.*, 62, 49 (1993)
- [20] K. K. Caswell, C.M Bender, C. J. Murphy, *NanoLetters*, 5, 3, (2003)
- [21] M. Fox, *Optical Properties of Solids*, Oxford University Press, (2001)
- [22] A. Einstein, *Physikalische Zeitschrift*, 18, 121 (1917). Translated in: Haar DT, “The Old Quantum Theory”, Pergamon Press, (1967)
- [23] J. Taylor, C. Ztiratos, M. A. Dubson, *Modern Physics for Scientists and Engineers*, Saunders College Publishing, (1993)
- [24] S. M. Sze, *Physics of Semiconductor Devices*, 2<sup>nd</sup> edition, Wiley Interscience Publishing, (1981)
- [25] M. Nirmal, B. O. Dabbousi, M. G. Bawendi, J. J. Macklin, J. K. Trautman, T. D. Harris, L. E. Brus, *Nature*, 383, 802, (1996)
- [26] S. R. Cordero, P. J. Carson, R. A. Estabrook, G. F. Strouse, S. K. Buratto, *J. Phys. Chem. B*, 104, 12137, (2000)
- [27] J. Muller, J. M. Lupton, A. L. Rogache, J. Feldmann, D. V. Talapin, H. Weller, *App. Phys. Lett.*, 85, 381, (2004)
- [28] “Optical Properties and Spectroscopy of Nanomaterials”, J. Z. Zhang, World Scientific (2009)
- [29] A. Beer, *Annal. Phys. Chem.*, 86, 78 (1852)
- [30] D. Bruggeman, *Ann. Physik*, 24,636, (1935)
- [31] B. E. Launder, *Appl. Phys*, 23, 779, (1952)
- [32] C.A. Leatherdale, W. K. Woo, F. V. Mikulec, M. G. Bawendi, *J. Phys. Chem. B*, 106, 7619, (2002)

- [33] P. Yu, M. C. Beard, R. J. Ellingson, S. Ferrere, C. Curtis, J. Drexler, F. Luiszer, A. J. Nozik, *J. Phys. Chem. B*, 109, 7084, (2005)
- [34] E. Hanamura, *Phys. Rev. B*, 37, 1273, (1988)
- [35] J. Strangl, V. Holy, G. Bauer, R. Murray, *Rev. Mod. Phys.*, 76, 725 (2001)
- [36] T. Walther, A. G. Cullis, D. J. Norris, M. Hopkinson, *Phys Rev Lett*, 86, 2381 (2001)
- [37] A. Rosenauer, D. Gerthsen, D. Van Dyck, M. Arzberger, G. Bohm, G. Abstreiter, *Phys Rev B*, 64, 245334 (2001)
- [38] X. Z. Liao, J. Zou, D. J. H. Cockayne, J. Wan, Z. M. Jiang, G. Jin, K. L. Wang, *Phys. Rev. B*, 65, 153306 (2002)
- [39] W. Heiss, E. Kaufmann, M. Boberl, T. Schwarzl, G. Springholz, G. Hesser, F. Schaffler, K. Koike, H. Harada, M. Yano, R. Leitsmann, L. E. Ramos, F. Beckstedt, *Physica E*, 35, 241 (2006)
- [40] C. B. Murray, C. R. Kagan, M. G. Bawendi, *Ann. Rev. Mater. Sci.*, 30, 545 (2000)
- [41] H. Reiss, *J. Chem. Phys.* 19, 482 (1951)
- [42] Y. De Smet, L. Deriemaeker, R. Finsy, *Langmuir*, 13, 6884 (1997)
- [43] E. T. Gratz, *Scripta Materialia*, 37, 9 (1997)
- [44] C. A. J. Lin, J. K. Li, R. A. Sperling, L. Manna, W. J. Parak, W. H. Chang, *Ann. Rev. Nano Research*, 467 (2007)
- [45] J. Aldana, Y. A. Wang, X. J. Peng, *J. Am. Chem. Soc.*, 123, 8844 (2001)
- [46] A. P. Alivisatos, *Nat. Biotechnol.*, 22, 47, (2004)
- [47] W. J. Parak, D. Gerion, T. Pellegrino, D. Zanchet, C. M. Micheel, *Nanotech*, 14, R15, (2003)
- [48] X. Gao, S. Nie, *Trends Biotechnol.*, 21, 371, (2003)

- [49] X. Michalet, F. Pinaud, D. Lacoste, M. Dahan, M. P. Bruchez, *Single Mol.*, 2, 261, (2001)
- [50] A. J. Suterland, *Curr. Opin. Solid State Mater. Sci.*, 6, 365, (2002)
- [51] W. C. W. Chan, D. Maxwell, X. Gao, R. Bailey, M. Han, S. Nie, *Curr. Opin. Biotechnol.*, 13, 40, (2002)
- [52] A. Watson, X. Wu, M. Bruchez, *Biotechniques*, 34, 296, (2003)
- [53] M. Bruchez, M. Moronne, P. Gin, S. Weiss, A. P. Alivisatos, *Science*, 281, 2016, (1998)
- [54] X. Wu, H. Liu, K. Haley, J. Treadway, *Nat. Biotechnol.*, 21, 41, (2003)
- [55] A. P. Alivisatos, W. W. Gu, C. A. Larabell, *Annu. Rev. Biomed. Eng.*, 7, 55, (2005)
- [56] J. R. Lakowic, I. Gryczynski, Z. Gryczynski, K. Nowaczyk, C. J. Murphy, *Anal. Biochem*, 280, 128, (2000)
- [57] R. Mahtab, H. Harden, C. J. Murphy, *J. Am. Chem. Soc.*, 122, 14, (2000)
- [58] K. Hanaki, A. Momo, T. Oku, A. Komoto, S. Maenosono, *Biochem. Biophys. Res. Commun.*, 302, 496, (2003)
- [59] H. Mattousi, J. M. Mauro, E. R. Goldman, G. P. Anderson, V. C. Sundar, F. V. Mikulec, M.G. Bawendi, *J. Am. Chem. Soc.*, 122, 12142, (2000)
- [60] H. Mattousi, J. M. Mauro, E. R. Goldman, T. M. Green, V. C. Anderson et. al, *Phys. Status Solidi B-Basic Res.*, 224, 227, (2001)
- [61] G. P. Mitchell, C. A. Mirkin, R. L. Letsinger, *J. Am. Chem. Soc.*, 121, 8122, (1999)
- [62] D. M. Willard, L. L. Carillo, J. Jung, A. Van Orden, *Nano-Lett.*, 1, 469, (2001)
- [63] C. Y. Zhang, H. Ma, S. Nie, Y. Ding, L. Jin, *Analyst*, 125, 1029, (2000)

- [64] W. C. Chan, D. J. Maxwell, X. Gao, R. E. Bailey, M. Han, S. Nie, *Curr. Opin. Biotechnol.*, 13, 40, (2002)
- [65] W. C. Chan, S. Nie, *Science*, 281, 2016, (1998)
- [66] D. Gerion, F. Pinaud, S. Williams, W. Parak, D. Zanchet, S. Weiss, A. Alivisatos, *J. Phys. Chem. B.*, 105, 8861, (2001)
- [67] S. Pathak, S. K. Choi, N. Arnheim, M. E. Thompson, *J. Am. Chem. Soc.*, 123, 4103, (2001)
- [68] W. Guo, J. Li, Y. A. Wang, X. Peng, *Chem. Mater.*, 15, 3125, (2003)
- [69] G. J. Doherty, H. T. McMahon, *Annual Review of Biochemistry*, 78, 857, (2003)
- [70] S. S. Coe, S. J. S. Woo, M. G. Bawendi, V. Bulovic, *Nature*, 420, 800, (2002)
- [71] M. C. Schlamp, X. Peng, A. P. Alivisatos, *J. Appl. Phys.*, 82, 5837, (1997)

### **3. Development of Experimental Techniques**

#### **3.1 Introduction**

This section serves as an account of the experimental methods used to functionalise CQDs for study, acquire photoluminescence and absorption spectra in our CQD systems and to size CQDs, as performed by ourselves and other groups. The acquisition of absorption and photoluminescence measurements allows characterisation of many of the physical and electronic properties of the dots including the energy of the lowest conduction band state (which may be extrapolated to provide an estimate of the dot size) and the relative radiative recombination, in a variety of environments and levels of excitation. This will aid in achieving our objective of better understanding the effect of environment, especially those expected in cellular studies, upon the stability, toxicity and electronic properties of CdSe/ZnS colloidal quantum dots.

The bulk of the measurements in chapters 4 and 5 are performed on samples of 610nm CdSe/ZnS core/shell colloidal quantum dots with a HDA (hydroxylamine) coating supplied in toluene by Nanoco and functionalised in PMMA 200nm photoresist solution (Polymethylmethacrylate) supplied from Fisher Scientific. The HDA coating provides hydrophobic dots which should dissolve in a non-polar solvent. The study of these dots in this environment is significant as PMMA is widely used in the fabrication of micro-scale devices and has been proposed [1] as a suitable material for the development of optical devices and biological imaging systems which incorporate CQDs. This study will also yield some insight into the source and nature of the photo-dynamic processes which affect the dot quantum yield, and dependence on their environment.

Chapter 6 focuses on measurements performed on untargeted 655nm CdSe colloidal quantum dots coated with PEG (Polyethylene glycol) molecules, supplied by Invitrogen, which are widely used for cellular microscopy studies. These dots are hydrophilic, allowing dissolution in polar solvents, and most importantly in water based compounds. These dots were functionalised in pH buffers with the purpose of simulating biological, especially cellular, environments in order to further increase the knowledge base for research in bioscience where small changes in dot properties due to their environment lead to confusion in results.

The majority of absorption and PL measurements were performed on dots functionalised in glass capillary tubes, forming a cylindrical waveguide consisting the PMMA core ( $n \sim 1.55-1.6$ ) and glass capillary ( $n \sim 1.5$ ) and its boundary with the air around it ( $n=1$ ). This method poses a number of advantages over other approaches, such as studying dots in solution or on planar glass substrates:

- Processing of samples can be performed quickly and simply
- It removes the necessity of lithography techniques required to create waveguides on glass substrates
- Allows confidence that the same dots are being observed over long timescales, unlike studying dots in a large solution where mixing will introduce new dots and remove old dots from the observed area
- Transmission absorption and PL measurements can be performed simultaneously using fibre delivery
- Light can be used to measure PL, affect changes in the sample and measure absorption

For a schematic diagram of the capillary layout see Figure 12.

Photoluminescence measurements were performed in order to observe the radiative recombination in the CQD ensembles. This allowed study of the lowest transition energy of the material, and gave an indication of changes in dot size, as well as the evaluation of physical properties of the dots from photo-dynamic changes in the dot's quantum yield (photo-activation and photo-degradation).

Transmission absorption measurements were performed in order to obtain information on optical pumping level in the PL measurement and physical changes in the dot make-up. Absorption measurements also allowed determination of transition energies which allowed determination of changes in dot size. Transmission absorption measurements provided an arbitrary measure of absorption.

Where an absolute measure of absorption was required a technique involving imaging of the sample emission in-situ was utilised. The details of this approach are outlined in section 3.4. These measurements are of importance when determining the concentration of dots in a sample.

## **3.2 Sample Preparation and Characterisation**

### **3.2.1 610nm CdSe/ZnS dots in PMMA**

610nm CdSe/ZnS core-shell dots were supplied by NanoCo in a toluene solution with a HDA coating to allow dispersion in non-polar solvents. NanoCo do not specify the dot concentration in the supplied form. PMMA was sourced from Fisher in the form of PMMA 200nm photoresist solution. The two solutions were mixed in a vial in a 2:1 volume dot solution to PMMA ratio. The solution was allowed to rest for 2 hours while the toluene in which the dots were supplied and the chlorobenzene in which the PMMA was dissolved evaporated before it was agitated for a minute in order to give an even distribution of dots.

Once the solution was ready a glass capillary of length 10cm, outer diameter 1mm and inner diameter 0.6mm was allowed to take-up some of the solution from the vial via capillary action. Once about a centimetre of the capillary was full the sample was allowed to dry at room temperature for 24 hours, after which the PMMA was in a gel-like state.

After drying was complete a 0.5mm plastic optical fibre, used to deliver the light for transmission absorption studies, was inserted into the end of the capillary. Optical epoxy was used to seal the fibre in place and to seal the opposite end of the capillary in order to prevent any further exposure to air. The sample was then allowed a further 24 hours at room temperature to allow the epoxy to dry. All samples were refrigerated at 0-3°C when not in use and when they were required are removed from refrigeration and allowed to warm to room temperature before measurement is made.

Figure 12 demonstrates the schematic layout of the resulting sample.

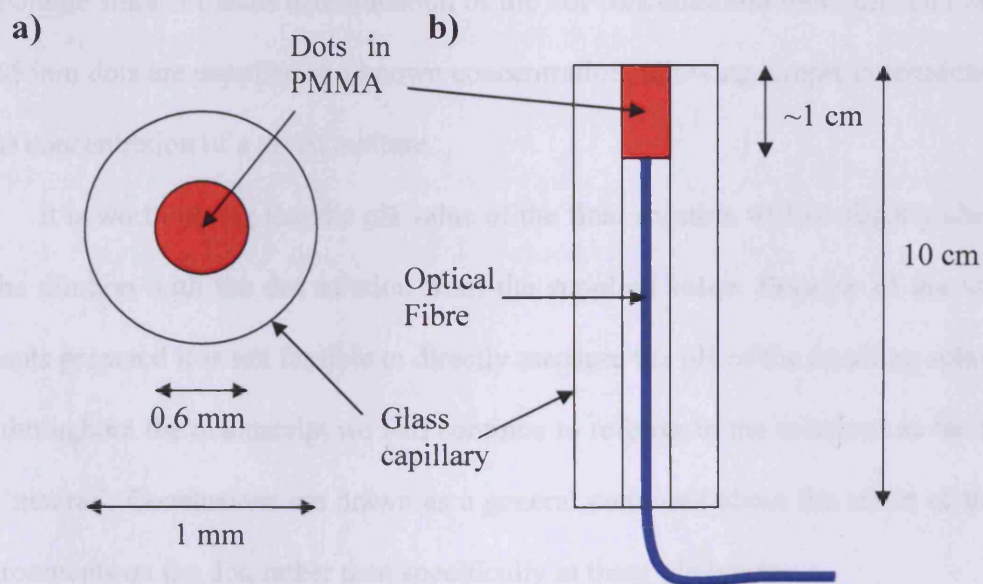


Figure 12 Schematic layout of capillary samples. Red areas indicate regions which contain CQDs

### 3.2.2 655nm CdSe Colloidal Quantum dots in pH buffers

The preparation method for these samples was very similar to that outlined in section 3.2.1 but varied in a few essential ways, which I will outline here.

Firstly the 655nm CdSe dots were sourced from Invitrogen and carry a PEG coating to allow dispersion in polar solvents. The solution had a molar concentration of 2 $\mu$ M. Buffer solutions were acquired from Fisher Scientific with pH of 4.0 (fisher product number J/2821C/05) and 6.87 (fisher product number J/2845/15). The solutions were mixed in a 2:1 volume of buffer to dot ratio and agitated for a minute in order to achieve a well distributed solution. The solution was allowed to settle for 10 minutes before uptake into the capillary in order to allow any bubbles formed during the agitation to escape the solution.

Unlike the PMMA samples the fibre was inserted and the capillary sealed immediately after the solution was incorporated, since drying of the material was undesirable since it makes determination of the dot concentration more difficult since the 655nm dots are supplied at a known concentration, allowing simple determination of the concentration of a given mixture.

It is worth noting that the pH value of the final solution will be slightly altered by the dilution with the dot solution from the supplied value. Because of the small amounts prepared it is not feasible to directly measure the pH of the resulting solution and throughout the manuscript we will continue to refer to the solutions as 'acidic' and 'neutral'. Conclusions are drawn as a general comment about the effect of these environments on the dot, rather than specifically at these pH levels.

### **3.3 Photoluminescence Measurements**

#### **3.3.1 Photoluminescence Measurements - Experimental Technique**

The detection of photons emitted via radiative recombination processes in semiconductor materials can be achieved in a number of ways. The vast majority of LED and Laser systems utilise electrical pumping in order to excite carriers into the conduction band and rely on dominant radiative recombination processes over non-radiative processes in order to achieve the required optical power out. Such a system requires good electrical contact with the device to be studied which is extremely difficult in the majority of colloidal quantum dot applications, and was certainly the case in our samples.

In the absence of an electrical pumping option most colloidal quantum dot studies are performed using optical excitation. This involves delivering excitation light of a wavelength which will be absorbed by the material. In colloidal dots this requires selecting a wavelength which is shorter than the emission wavelength of the dot ensemble which is to be studied. This can be seen more clearly in Figure 13, which demonstrates the emission and absorption spectra from various sizes of QTracker dots from Invitrogen (as studied in chapter 6 of this text).

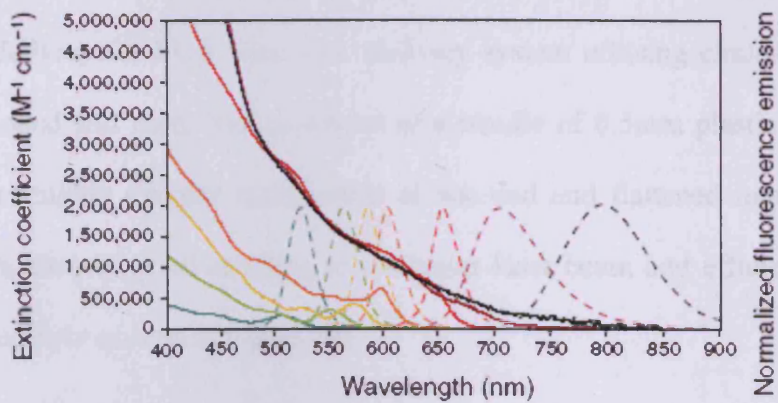
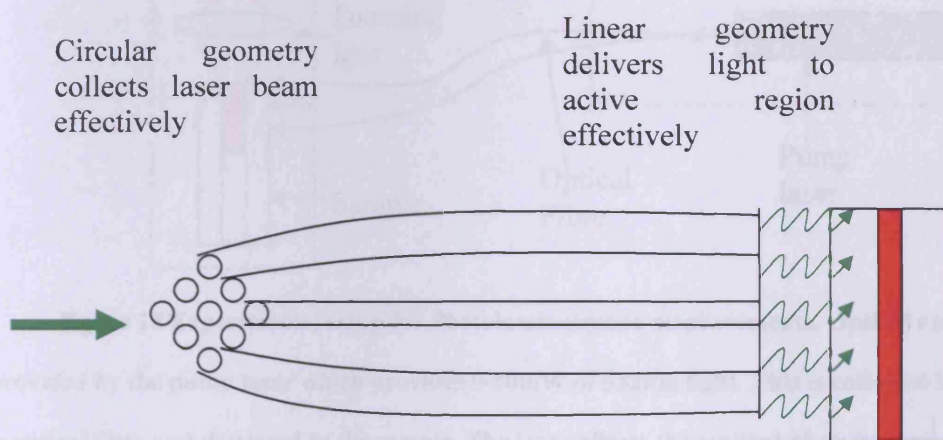


Figure 13 Absorption (solid) and emission (dotted) spectra for various sizes of Qtracker colloidal quantum dots taken from <http://www.invitrogen.com>. We pump our dots at 532nm.

For a more precise description of the processes involved in radiative and non-radiative recombination see chapter 2.

Because of the geometry of the capillary system, to maximise the efficiency of the light delivery for PL a fibre optic delivery system utilising circle-line geometry was developed and used. This consisted of a bundle of 0.5mm plastic optical fibres fixed in a roughly circular arrangement at one end and flattened into a line at the other. This allowed good coupling of a circular laser beam and efficient delivery to the linear sample as seen in Figure 14.



**Figure 14** Diagram depicting light collection and delivery geometry in the spot-line fibre setup

### 3.3.2 Photoluminescence Measurements - Experimental Setup

Photoluminescence measurements were performed using the apparatus illustrated in Figure 15. The excitation source was a diode pumped solid state laser (Power Technology, Inc., Model LCS-DTL-312), 532nm, and 50mW peak power with CW operation. The detected light was dispersed using an Oriel Instruments 74050 MS260i 1/4 m Imaging Spectrograph (model number 74050) and detected at an

Andor Technology iCCD (intensified charge-coupled device) (Model number DH501-18F-01, 1026\*1026 Pixels) .

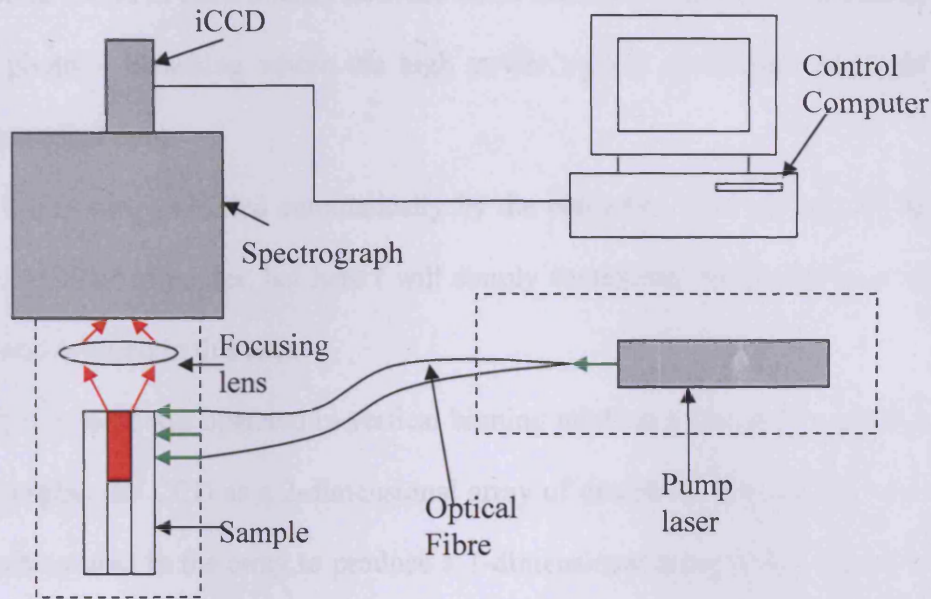


**Figure 15** Experimental setup for Photoluminescence measurements. Optical excitation is provided by the pump laser which provides 0-50mW of 532nm light. This is collected by a spot-line optical fibre and delivered to the sample. The lens collects the emitted photoluminescence and focuses onto the Spectrograph slit. The Spectrograph splits the light into its spectrum which is measured by the iCCD which is controlled by the computer. Dotted lines indicate areas which are optically isolated.

The focusing optics were used to maximise collection. Spectra were taken at wavelength windows appropriate to the wavelength of the particular dots used, usually a roughly 200nm window centred on 670nm or 630nm, keeping in mind the need to stay away from the wavelength of the exciting light. Where appropriate optical filters were used to prevent any overlapping light from falling on the sample.

While the resolution of the spectrometer is usually determined as a function of the path length and the grating line separation, in this case it is practically limited by the pixel width of the iCCD to around 0.3nm.

The powers used in our experiment (up to a few tens of milliwatts) compare to the powers used in typical confocal microscopy studies, depending on application (a balance must be found in most studies between noise reduction which requires more power, and photo – bleaching where the high power rapidly diminishes the light output of the studied dye).

The iCCD was controlled automatically by the computer. This device can be operated in a number of modes, but here I will simply summarise the modes used in the experiments covered in this text.

The CCD itself was operated in vertical binning mode at all times. To explain this mode, imagine the CCD as a 2-dimensional array of detectors. Binning involves summing each column in the array to produce a 1-dimensional array which is output as the result. In our case the output can be treated as a spectrum since the light incident on the spectrograph is split into its constituent wavelengths along the horizontal axis of the camera by the time it is imaged. The binning method is illustrated in Figure 16.

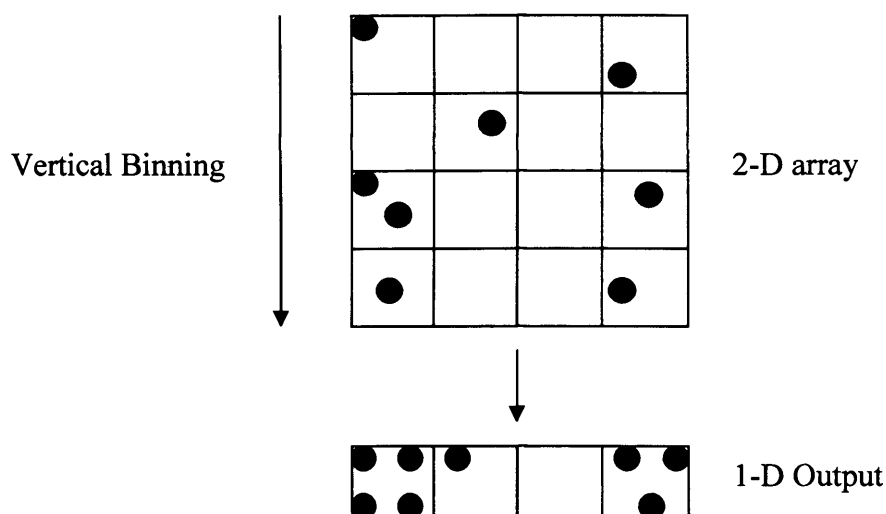


**Figure 16** Diagram depicting the vertical binning method whereby the camera created a 1-D data file from a 2-D array.

When producing spectra the iCCD uses an accumulation mode in which a series of spectra are taken and summed to provide a better signal to noise ratio in the resulting spectra. We typically used 1000 accumulations of 0.02 second exposures. This is preferable to a few long exposures since an excess build up of charge can be detrimental to the CCD, as well as causing saturation in the image.

The computer can automate a series of acquisitions in kinetic series mode. Here data acquisition is performed as outlined above but repeated for some number of times and at an interval set by the user. This outputs a sequence of spectra obtained at each time interval. The data can be acquired at extremely short intervals ( $>0.02s$ ) or over much longer periods, up to a few days. The number of acquisitions making up a series is limited only by the available memory to which the data can be stored.

In Figure 17 I have included an example of one photoluminescence measurement taken using the above arrangement.

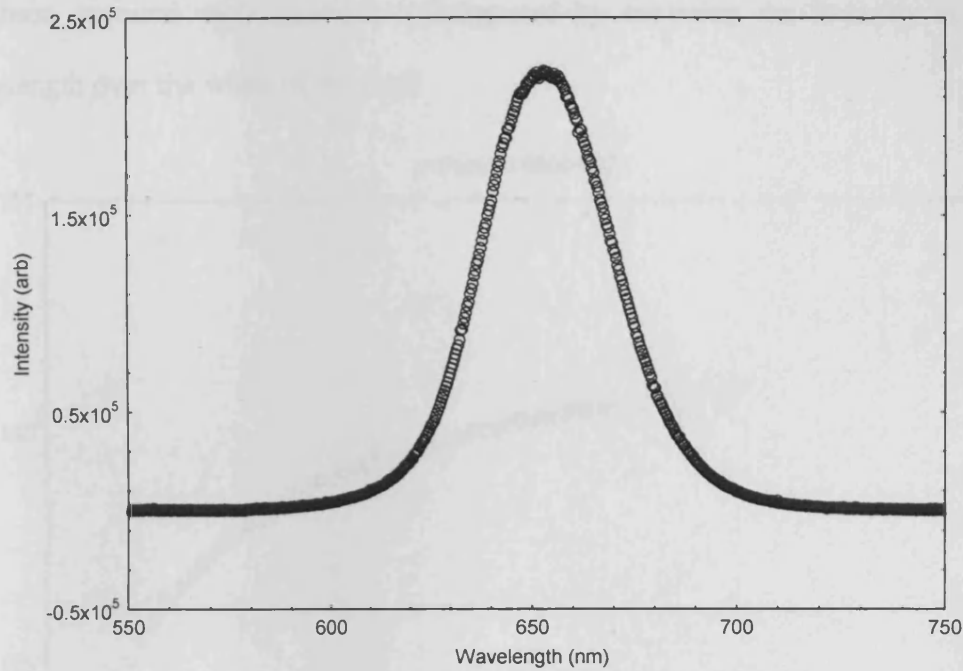


**Figure 17** PL spectrum taken from 655nm CdSe dots

Noise is minimised in the system by cooling the CCD in order to minimise the effect of thermally created charge in the detector array, and by subtracting the background signal, which is measured with no applied excitation, from the detected signal. This should provide a well zeroed signal with a low S-N ratio.

### **3.3.3 Extracting Photo-Activation Curves from Photo-Luminescence Measurements**

In a large number of cases our interest lies in the evolution of the CQD emission over time under various environmental and optical conditions. In order to observe temporal behaviour the kinetic series acquisition mode was used in the iCCD. This allowed the user to apply the pump source continually and leave the equipment to monitor the PL over a period of time, which could be anything from minutes to weeks. This was significant since in some samples it was necessary to monitor behaviour over several days in order to observe the whole dynamic range. Once data

has been acquired each spectrum is integrated by summing the intensity at each wavelength over the width of the peak.

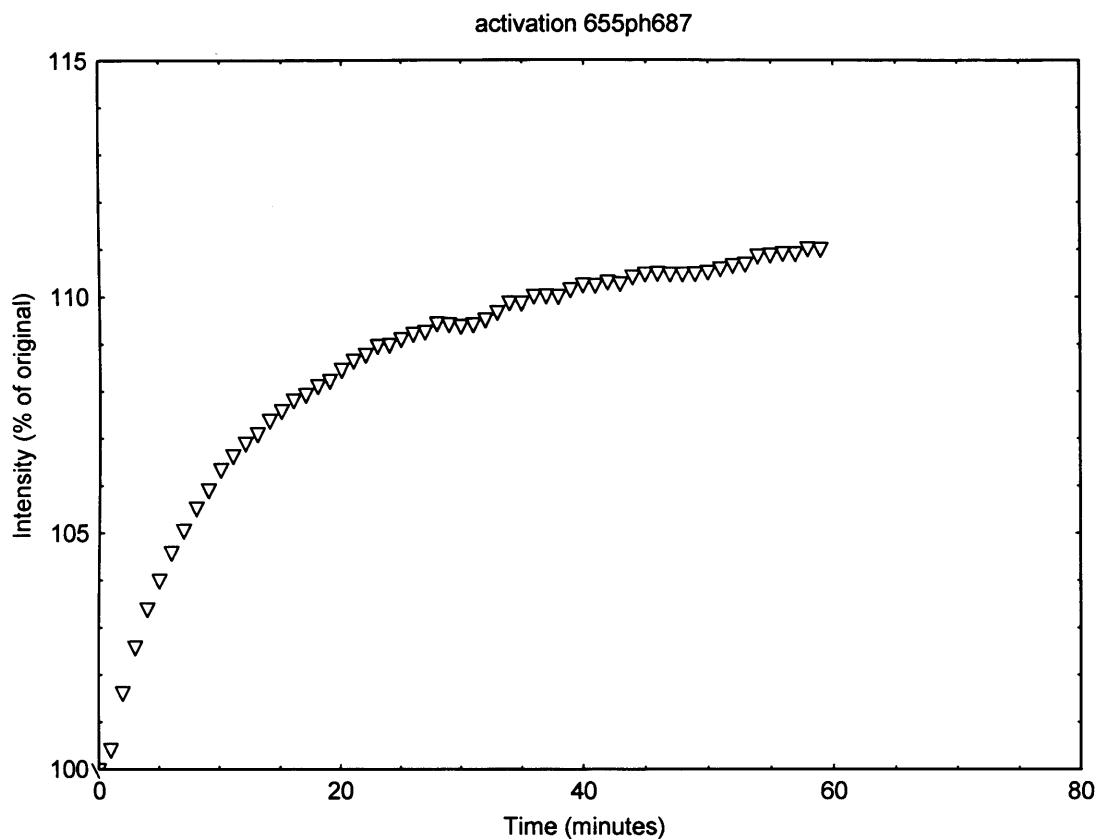


**Figure 18** Example of Photo-Dynamic measurement demonstrating extraction of intensity behaviour over time from a kinetic series. Intensity is normalised to 100 at its original value.

As can be seen in Figure 18 most photo-dynamic measurements took a roughly exponential form. In order to characterise the curves produced it was decided to use a curve fit, and compare this to a physical model of the behaviour. We used a simple formula shown in Equation 12, which represents an exponential transition from some initial intensity to another, to fit the curves above for photo-activation (increasing intensity, usually when optical pumping is applied constantly) and photo-degradation (decreasing intensity, usually when optical pumping is applied for measurement only).

$$I = I_0 + (I_\infty - I_0)(1 - e^{-\beta t})$$

**Equation 12**

In Equation 12  $I_0$  represents the initial photoluminescence intensity,  $I_\infty$  the long-term equilibrium photoluminescence intensity,  $\beta$  the rate constant of activation/degradation and  $t$  the time in minutes. The same data displayed in Figure 18 is shown with the fitted curve in Figure 19.

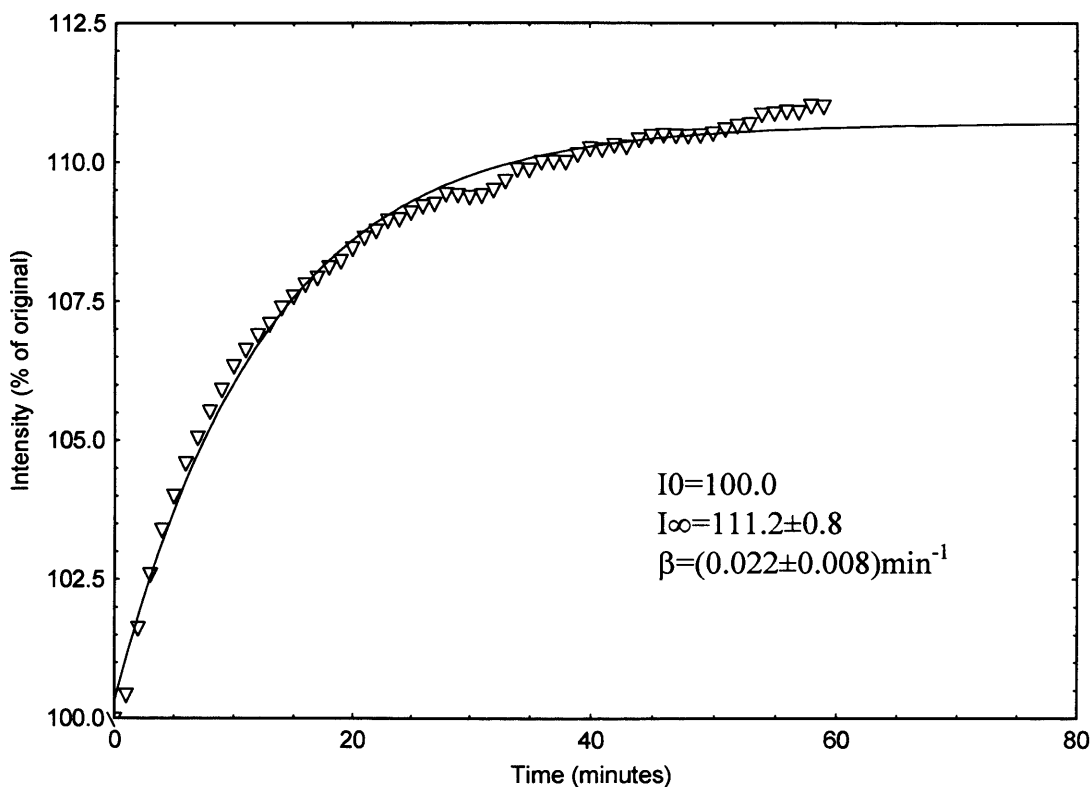


**Figure 19 Data shown in Figure 18 fitted using Equation 12.**

The curve was fitted in Easyplot using a least squares method. The program is fed guess values for each parameter and produces parameters and errors for the best a function fit to the given data.

For photo-activation measurements it was necessary to determine the optimum power at which to perform the experiment. By doing this it was possible to achieve

the maximum amplitude of activation for fitting, increasing the accuracy of the generated parameters. With this in mind it may seem appropriate to simply apply the maximum available power to the sample; however this often leads to photo-degradation of the sample in the long term, as can be seen in Figure 20. If the photo-degradation process becomes dominant before the system has reached its equilibrium point,  $I_{\infty}$  then it makes the curve fitting difficult or impossible.

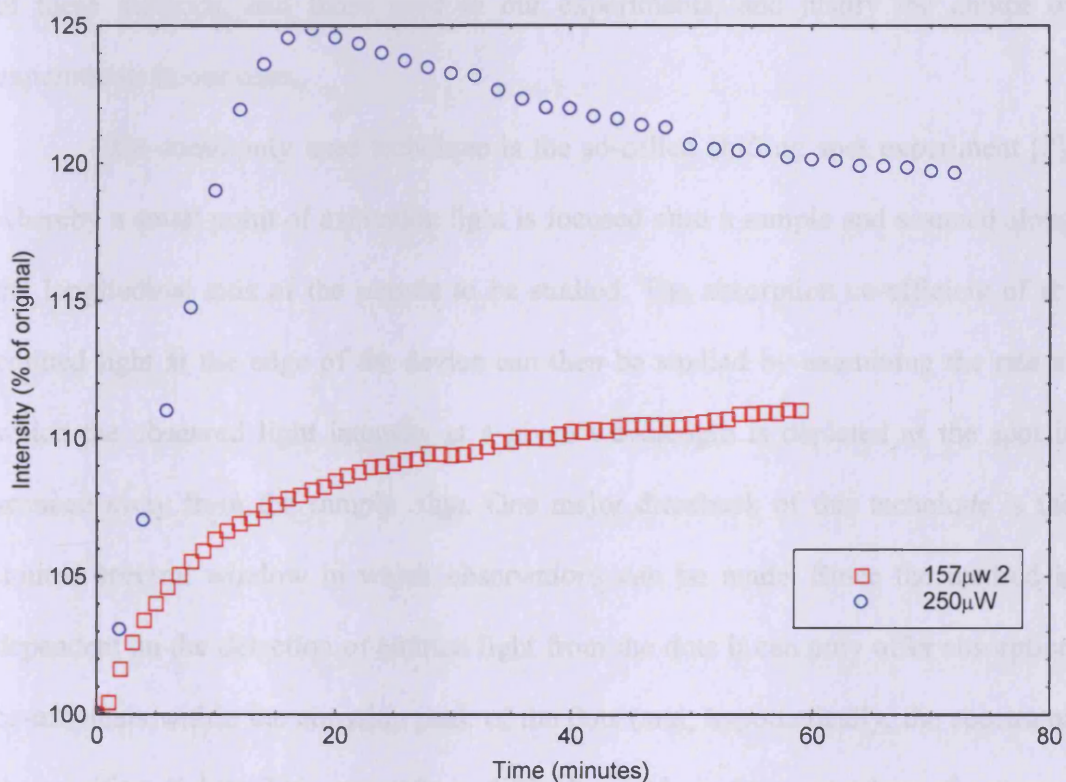


**Figure 20 Photo-activation measurements performed at 250μW and 157μW on 655nm dots in pH 6.87 Buffer**

Suitable powers were extracted for each measurement using a test sample, since no one ideal power existed for every measurement made. An identical sample was used, and the applied power raised until photo-degradation was observed, allowing us to pin a maximum allowed power to each experiment. The separate sample was used in order to prevent effects induced from this measurement from influencing further studies.

## **3.4 Absorption Measurements**

### **3.4.1 Absorption and Absorbance Measurements – Experimental Technique**

The measurement of the absorption as a function of wavelength of a material can be achieved through a number of methods. Here I will present a review of some of these methods, and those used in our experiments, and justify the choice of experiments in our case.

One commonly used technique is the so-called shifting spot experiment [2], whereby a small point of excitation light is focused onto a sample and scanned along the longitudinal axis of the sample to be studied. The absorption co-efficient of re-emitted light at the edge of the device can then be studied by examining the rate at which the observed light intensity at a given wavelength is depleted as the spot is scanned away from the sample edge. One major drawback of this technique is the limited spectral window in which observations can be made. Since the method is dependent on the detection of emitted light from the dots it can only offer absorption co-efficients within the emission peak of the dots (and, hypothetically, the spectra of the exciting light). This presents a difficult problem for a number of reasons. Colloidal quantum dots exhibit a large Stokes shift (see Figure 13 for reference), meaning there is little or no overlap between the absorption spectra and the emission spectra. Furthermore, for most applications, especially in optoelectronics and labelling applications, a narrow distribution of dots, and hence a narrow emission peak, is desirable. This exacerbates the problem of using this method to obtain absorption co-efficients in colloidal quantum dot systems.

Another possible approach to obtaining absorption measurements in our samples would be using the variable stripe length method first described by Shaklee *et al.* [3]. In this experiment, suited ideally to measurements of gain and absorption in flat slabs of material, excitation light is focused into a stripe on the surface of the material and the length of the stripe adjusted. By measuring spectra at each length one can determine a gain and absorption co-efficients for the material. Due to the difficulty of preparing our samples in flat sample geometry, and the absence of interest in optical gain, it was decided that this technique was unsuitable.

In this work the majority of the absorption spectra have been taken using a transmission absorption technique. The technique is well suited to the capillary geometry and importantly allows simultaneous measurement of absorption and Photoluminescence.

The transmission absorption experiment involves the measurement of light from some source, which is propagated through the absorbing media. This spectrum is compared to a reference spectrum which is taken from an identical sample which contains no absorbing media. In our case this involves preparation of a sample as outlined in section [3.2 Sample Preparation and Characterisation] in PMMA, but without the colloidal dots. This method makes a number of essential assumptions, as follows;

- The detected re-emitted fluorescence is negligible compared to the transmitted light.
- The fraction of light confined in the core of the capillary is the same with and without the presence of the absorbing media.
- The scatter from the dots is negligible.

When calculating the absorption from measured data we first consider the un-attenuated intensity at a given wavelength of light entering the absorbing region,  $I(0)$  and the intensity of the light at the same wavelength at some point  $x$  along the sample,  $I(x)$ . Light propagating along the axis of the material can be described by the equation

$$I(x) = I(0)\exp(-\alpha x)$$

**Equation 13**

where  $x$  is the distance travelled in the absorbing medium and  $\alpha$  is the total loss coefficient at some wavelength,  $\lambda$ . Re-arranging we obtain

$$\alpha = -\frac{1}{x} \ln\left(\frac{I(x)}{I(0)}\right)$$

**Equation 14**

from which  $\alpha$  can be determined if  $x$ ,  $I(0)$  and  $I(x)$  are well known. We make the assumption that the light measured from the sample containing no dots is equivalent to  $I(0)$ . While this is not strictly the case since the light measured from the end of the non-absorbing, dot free, sample has suffered from the intrinsic scattering losses within the capillary, the light from the dot sample should have suffered essentially the same scattering losses as that propagating along the non-absorbing sample. This assumption allows us to reduce the  $\alpha$  term in Equation 13, which is itself made up of each of the loss factors involved as shown in Equation 15

$$\alpha = \alpha_{dots} + \alpha_{capillary}$$

**Equation 15**

where  $\alpha_{dots}$  is the absorption from the dots and  $\alpha_{capillary}$  is the intrinsic loss from the capillary. Since the  $\alpha_{capillary}$  term is accounted for by using the measured light at the end of the non-absorbing sample as  $I(0)$  we can re-write Equation 14 as

$$\alpha_{dots} = -\frac{1}{x} \ln \left( \frac{I(x)}{I(0)} \right)$$

**Equation 16**

In order to extract the absorption co-efficient from Equation 16 it is necessary to know the distance propagated by the light along the x-axis (x). Although the length of the occupied area of the capillary can be measured it is difficult to ensure that path lengths are identical in absorbing and non-absorbing sample, so instead we opt to work in unit-less absorbance with a normalisation process. Since the absorbance can be written as

$$Abs = \alpha x$$

**Equation 17**

Equation 16 can now be written as

$$Abs = -\ln \left( \frac{I(x)}{I(0)} \right)$$

**Equation 18**

which can be used to calculate the absorbance using the data which we obtain. This is a qualitative measure of absorption and as such allows comparison of the shape of obtained absorption curves but not their magnitude.

In order for this method to be effective it is important that a good zero level is maintained when acquiring data and that the reference signal is well normalised (see section 3.4.2) to the studied signal (or vice versa). All normalisation must be done at a wavelength where no absorption is occurring; hence the absolute value of the measured light should be the same in each case.

In cases where it was important to know the absolute value of the absorption a technique was developed whereby absorption is measured via imaging. This involves transmission of light along the capillary and simultaneous top-down imaging of the emission from the sample. The resulting image can be analysed computationally by performing a line fit to the measured light intensity as a function of distance along the sample. Equation 13 can be fitted to the obtained line and hence the value of  $\alpha$  determined at the measured wavelength. In order to distinguish between absorbed light and scattered light a separate measurement is performed with longer wavelength light than should not be absorbed by the system. This gives a value for the scatter coefficient which allows separation of the real absorption coefficient of the dots.

### **3.4.2 Absorption and Absorbance Measurements – Experimental Setup**

Transmission absorption measurements were performed using the apparatus in Figure 21, whereby light is delivered from a light source to the sample via the optical fibre which lies in the plane of the capillary axis.

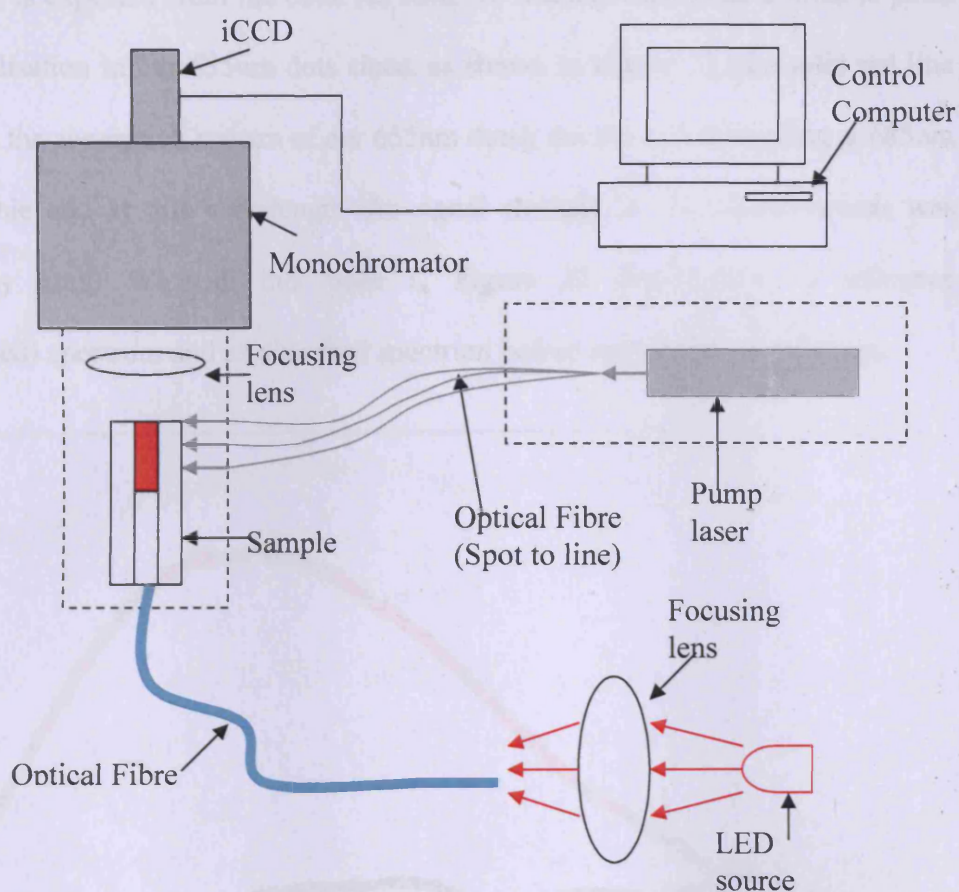


**Figure 21** Experimental setup for absorbance measurements. PL measurement equipment is shown as the greyed out items, in order to demonstrate how PL and Absorbance can be measured simultaneously.

Initially a measurement was made of the transmitted spectrum from the LED source through a sample containing no colloidal dots. We call this  $I_0$ . Subsequently a sample containing dots was placed into the system and the transmitted light from the LED source once again measured. With each spectrum a measurement was made of the background light and subtracted from the spectrum in order to eliminate any unwanted background signal. The next step was to normalise the unattenuated and attenuated spectra so that any discrepancy in light levels resulting from small changes in alignment of the absorbing media in the two samples would not alter the result. As detailed above it is necessary to perform normalisation at a wavelength where no

absorption is expected from the dots. As such we selected 685nm as a suitable point for normalisation in our 655nm dots since, as shown in Figure 13 (the solid red line represents the absorption spectra of our 655nm dots), the level of absorption at 685nm is negligible and at this wavelength the signal strength in our measurements was sufficiently high. We call this trace  $I_x$ . Figure 22 demonstrates a reference (unabsorbed) spectrum and an absorbed spectrum before and after normalisation.

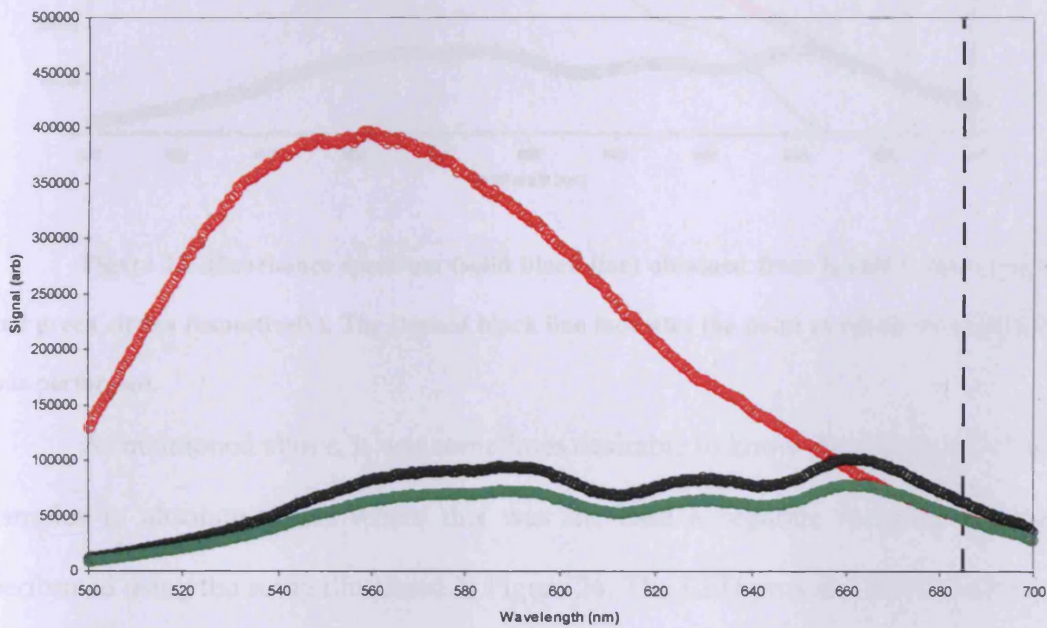


Figure 22 Transmitted spectra from dot-free sample (red squares) and colloidal quantum dot sample (black circles) and the colloidal dot sample normalised to the dot-free sample (solid green circles). The dashed black line indicates the wavelength at which normalisation is performed.

Absorbance spectra were obtained for the traces shown in Figure 22 by applying Equation 18 to  $I_0$  (Red squares in Figure 22) and  $I_x$  (Solid green circles in Figure 22). In Figure 23 the black line demonstrates the spectrum obtained from this data.

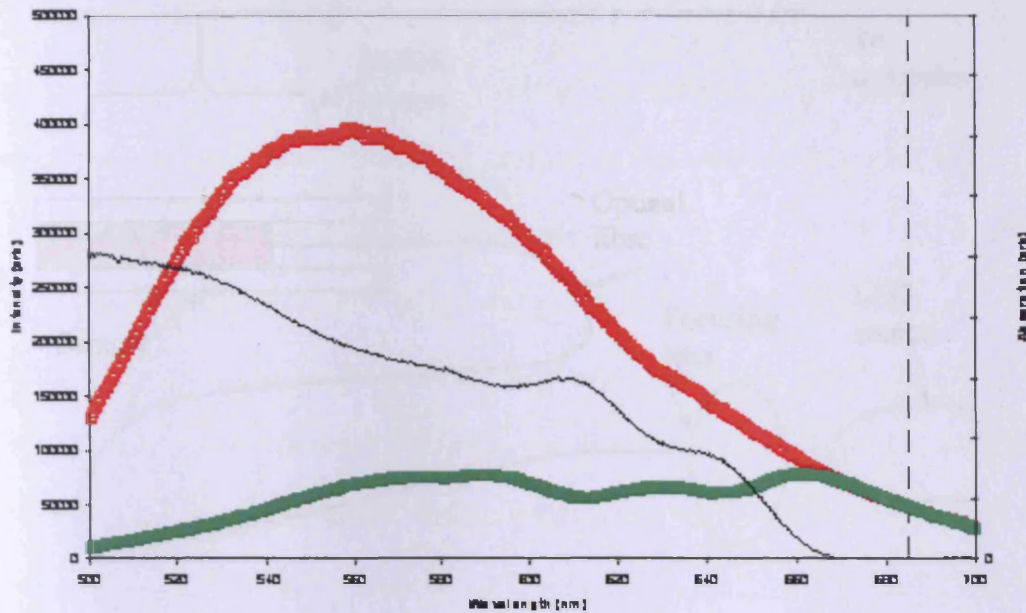


Figure 23 Absorbance spectrum (solid black line) obtained from  $I_0$  and  $I_x$  (red squares and green circles respectively). The Dashed black line indicates the point at which normalisation was performed.

As mentioned above, it was sometimes desirable to know the absorption of our samples in absolute units. Where this was the case a separate measurement was performed using the setup illustrated in Figure 24. The LED provides illumination via the fibre while a CMOS camera (HP 2100 Webcam) images the sample. Typically UV light is used for illumination, and re-emitted (red) light is measured. This approach relies on the assumptions that the light emitted is linearly related to the absorbed light, that the dot distribution is homogeneous and that the scattered light is independent of wavelength. An example of a raw image is shown in Figure 25. The acquired image was exported into Photoshop where it was split into the RGB constituents.

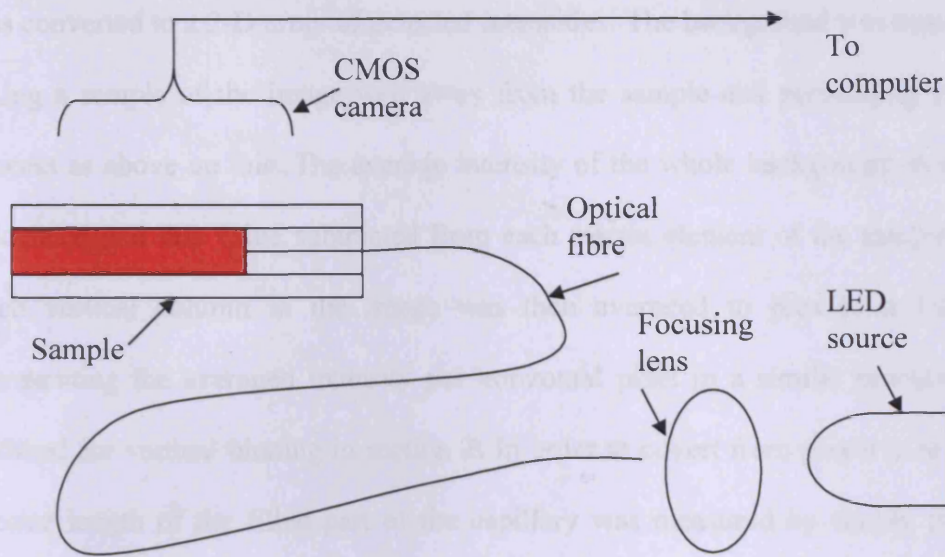


Figure 24 Experimental layout for absolute absorption measurements.

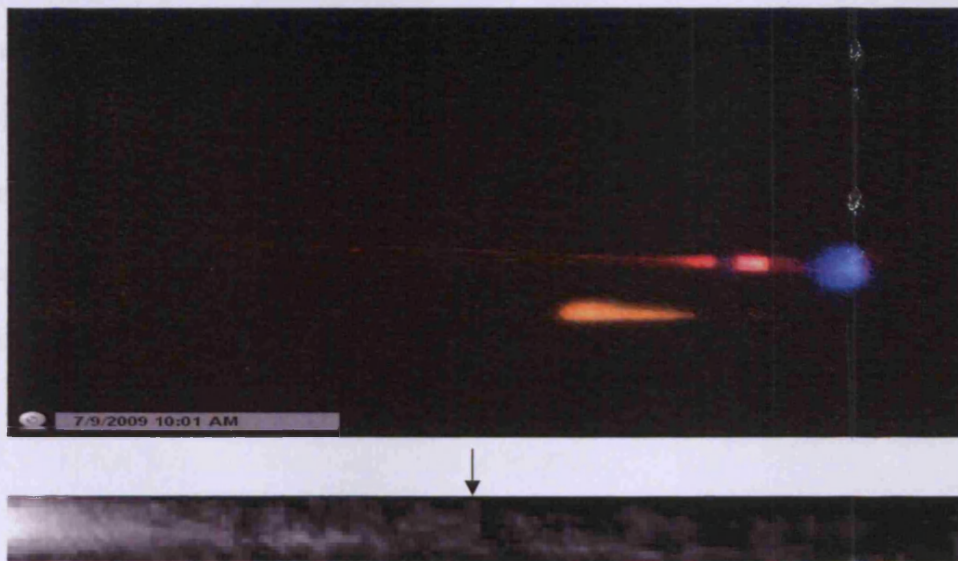


Figure 25 Raw image and result after processing demonstrating how the image is separated in colour to generate the greyscale depiction of the red element, rotated through 180 degrees and trimmed to provide only the relevant area

Once the image was split the green and blue elements were removed, leaving only the element detected by the red-sensitive element of the CMOS. The result was trimmed to provide only the area for study and exported to mathcad where the image

was converted to a 2-D array of detected intensities. The background was removed by taking a sample of the image well away from the sample and performing the same process as above on this. The average intensity of the whole background matrix was calculated and this value subtracted from each matrix element of the sample image. Each vertical column in the image was then averaged to provide a 1-D array representing the averaged intensity per horizontal pixel in a similar process to that outlined for vertical binning in section 2. In order to convert from pixels to length the precise length of the filled part of the capillary was measured by simply placing a measuring tape or ruler into the setup alongside the sample and taking a further image. This allowed calculation of the length per pixel. Finally the resulting trace was fitted using Equation 13, while bearing in mind that the  $\alpha$  value produced represented a sum of the absorption from the dots and the intrinsic scatter in the sample. In order to remove the scattered light element the measurement was repeated using a 680nm laser source which should be negligibly absorbed and the resulting  $\alpha_{\text{scatter}}$  value subtracted from the measured ( $\alpha_{\text{dots}} + \alpha_{\text{scatter}}$ ) value. An example of this fitting is demonstrated in Figure 26.

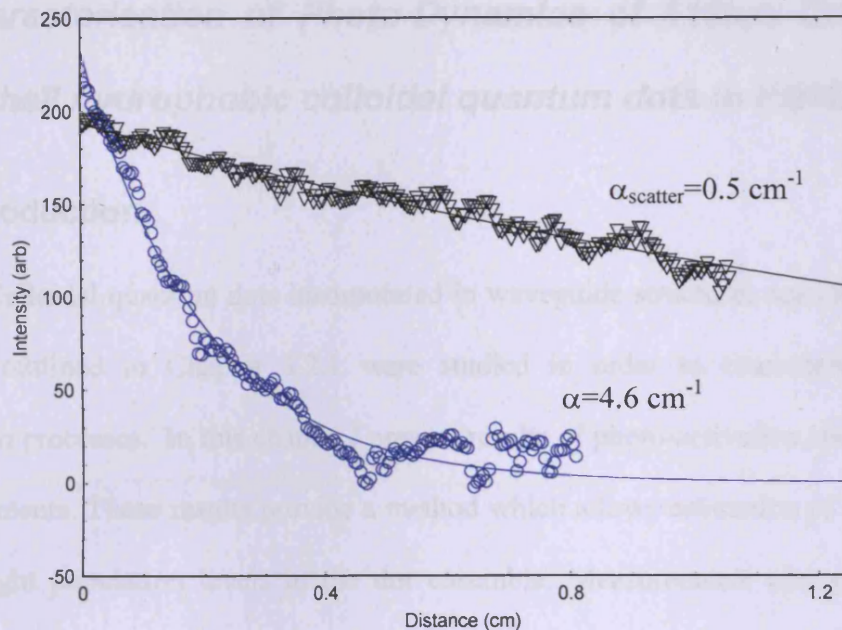


Figure 26 Example of traces resulting from scatter measurements (black triangles) and absorption measurements (blue circles) fitted with exponentials.

### 3.5 Summary

In this chapter I have outlined the methods used to create and characterise quantum dot samples studied in chapters 4,5 and 6 of this document. The majority of this work focuses on Transmission absorption measurements and photo-activation measurements obtained from photoluminescence. I have also outlined the method used to obtain absolute measurements of absorption.

### 3.6 References

- [1] L. Martiradonna, T. Stomeo, M. De Giorgi, R. Cingolani, M. De Vittorio, MicroElectronic Eng., 83, 1478, (2006)
- [2] S. Hoogland, V. Sukhovatkin, I. Howard, S. Cauchi, L. Levina, E. H. Sargent, Opt. Express, 14, 3273, (2006)
- [3] K. L. Shaklee, R. E. Nahori, R. F. Leheney, J. Luminescence 7, 284, (1973)

## **4. Characterisation of Photo-Dynamics of 610nm CdSe/ZnS core-shell hydrophobic colloidal quantum dots in PMMA**

### **4.1 Introduction**

Colloidal quantum dots incorporated in waveguide structures according to the method outlined in Chapter 3.2.1 were studied in order to characterise photo-activation processes. In this chapter I present results of photo-activation and recovery measurements. These results provide a method which allows estimation of initial and final bright population levels in the dot ensemble. Measurements also provide an indication of how long-term degradation of CQDs affects measurements and hinders precise characterisation. Interpretation of wavelength shifts in the PL spectra of the dots provide a means to study this physical degradation, and a possible link between photo-oxidation and photo-degradation is identified.

### **4.2 Effect of Functionalisation in PMMA**

Before the main bulk of our results were taken it was necessary to know of any effects brought about by the transfer of dots from their supplied state into the PMMA matrix. As such two samples were prepared, one containing the dots as supplied in toluene from Nanoco, and one containing dots prepared in PMMA 200nm photoresist solution from Fisher Scientific. A single Photoluminescence measurement was performed on each sample under identical conditions. As seen in Figure 27 the functionalisation in PMMA brings about a reduction in PL intensity which is far larger than that expected due to the reduction in dot concentration (mixed in a 2:1 ratio as detailed in 3.2.1) or small alignment differences.

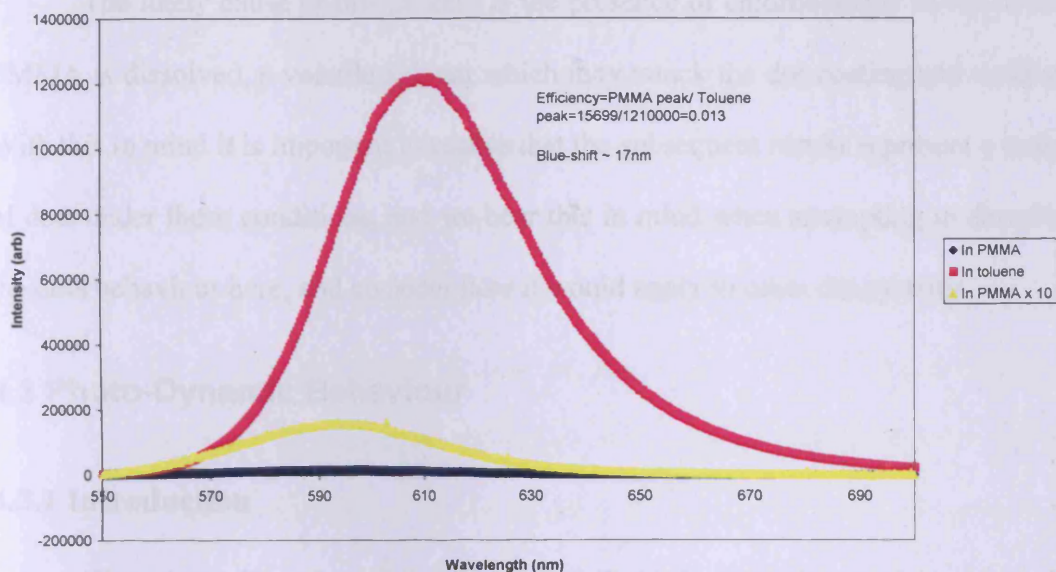


**Figure 27** PL spectra of 610nm CdSe colloidal quantum dots as supplied in toluene (pink squares) and in PMMA x 10 (yellow triangles) . Spectra in PMMA is multiplied by 10 for clarity.

The original spectrum is shown by the blue diamonds.

Identifying the source of the decrease in PL intensity in the colloidal quantum dots poses some difficulty without a thorough understanding of the chemical processes involved, but the blue shift in the emission wavelength provided some clues to its source. A blue shift of ~17nm in the emission corresponds to a reduction in dot size of around 1nm according to chapter 2 equation 4, or roughly 1-2 monolayers of material from the dot surface in an idealised situation where the overall structure of the dot is unaffected. In these dots the ZnS shell is understood to be of a similar thickness to the proposed removed material, thus we can deduce that it is possible that the majority of this layer has been removed which will result in a significant decrease in PL efficiency as a result of increased non-radiative recombination routes introduced by surface states. Furthermore in order for any surface material to be removed it is likely that some or all of the surface coating HDA has been removed during the process since any chemical interaction with the dot material would require physical access to the dot, which would be hindered by the large capping molecules.

The likely cause of this process is the presence of chlorobenzene in which the PMMA is dissolved, a volatile solvent which may attack the dot coating and surface. With this in mind it is important to realise that the subsequent results represent a study of dots under these conditions, and we bear this in mind when attempting to describe the dots behaviour here, and consider how it would apply to other dot systems.

## **4.3 Photo-Dynamic Behaviour**

### **4.3.1 Introduction**

The photo-dependent behaviour of CdSe/ZnS colloidal quantum dots in PMMA was measured under several conditions. Initially the sample was periodically photo-activated and allowed to recover using cyclic modulated excitation.

Once a scheme was established which allowed description of the observed processes a study was performed of the magnitude of photo-activation against excitation power. A method was then derived which allowed estimation of the population of dark (non-radiative) and bright (radiative) dots in the ensemble before and after photo-activation.

### **4.3.2 Characterising Photo-Dynamic Behaviour**

Figure 28 illustrates photo-dynamic behaviour in a CdSe/ZnS CQD ensemble in PMMA. The teal step function shows the modulation of the pump intensity. In this case the pump intensity was never brought to zero, but rather modulated between a high power ( $250\mu\text{Wcm}^{-1}$ ) and low power ( $2.5\mu\text{Wcm}^{-1}$ ) level. The low power level is  $\sim 1\%$  of the high power in order that some PL can still be observed allowing monitoring of recovery from any photo-induced changes. It is assumed that behaviour at very low pump intensity is negligibly different to behaviour with no applied power.

To confirm this, the sample is left under low power illumination initially until equilibrium is reached. As can be seen in Figure 28, the result is a small (~10%) change in the PL output, which quickly reaches equilibrium. Note that in Figure 28 low power data intensity is scaled to match the high power measurements by normalising the data at the points where the two meet. Application of high power pumping initiates a photo-activation process and removal of this brings about a recovery of PL intensity, as can be seen by the saw tooth shape of the trace in Figure 28. The light blue line in Figure 28 shows the effect of prolonged exposure to high power excitation. The system reaches equilibrium before a degradation process becomes dominant and begins to deplete the PL output significantly. This is followed by a low pump power recovery which shows the system returning to slightly less than its initial PL intensity.

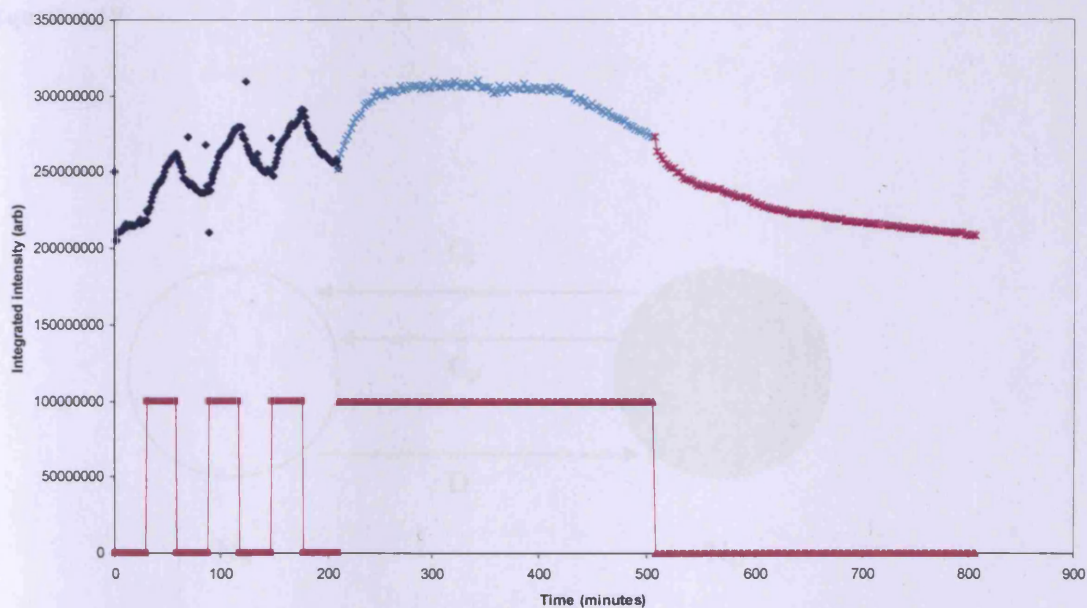


**Figure 28 Photo-Dynamic behaviour in CQD ensemble in PMMA. The purple step function denotes the modulation of applied pump intensity.**

### 4.3.3 Describing Photo-Dynamic Behaviour

In order to describe and analyse the behaviour observed above it was decided that an approach involving a two state system in which dots are either bright (i.e. radiative recombination dominates) or dark (non-radiative recombination dominates) would be adopted. Here we recognise work on so-called ‘blinking’ in single dot studies and assume that behaviour in large ensembles is essentially an extension of this model. Hence we begin by stating that the ensemble consists of some fraction of ‘bright’ dots ( $N_B$ ) in a state where radiative recombination is dominant, and some fraction of dark dots ( $N_D$ ) where non-radiative recombination paths dominate. Equation 19 demonstrates that the total of these two fractions must be equal to 1.

Equation 18

$$N_B + N_D = 1$$

Equation 19

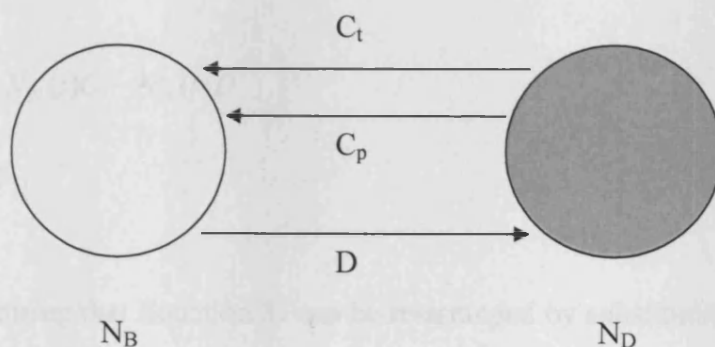


**Figure 29** Diagram depicting proposed two level system and associated transitions between bright and dark states.

Figure 29 depicts the proposed system, as well as the routes by which the dots may move from one state to the other.  $C_t$  is the rate of photo-independent brightening

of the dots. This co-efficient is necessary since we do not assume that all of the dots begin in a dark state and there must therefore be some factor balancing against the effect of darkening,  $D$ , the rate at which dots darken.  $C_p$  is the rate at which dots are driven into a brighter state by an applied optical flux. This factor is proportional to the applied flux. For simplicity we define a factor  $C$ , defined in Equation 20 which comprises the sum of both of the brightening processes. Note at this point that long-term degradation processes such as those observed in Figure 28 are ignored for the purpose of this model.

$$C = C_i + C_p$$

**Equation 20**

From this it is possible to develop a rate equation solution to the problem, firstly by stating that the rate at which the population of bright dots is changing can be described by

$$\frac{dN_B(t)}{dt} = N_D(t)C - N_B(t)D$$

**Equation 21**

and recognising that Equation 21 can be re-arranged by substituting Equation 19 such that

$$\frac{dN_B(t)}{dt} = (1 - N_B(t))C - N_B(t)D$$

**Equation 22**

Integrating Equation 22 with respect to time provides an expression which should describe the fraction of bright dots at some time  $t$  after applying or removing some optical flux, and the result is shown in Equation 23, where  $N_0$  is the initial fraction of bright dots.

$$N_B(t) = \frac{[N_0(C + D) - C]\exp[-(C + D)t] + C}{C + D}$$

**Equation 23**

The approach demonstrated above gives us a simple characterisation of the main processes in the dot system. It is important at this point to draw parallels with the curve fitting method outlined in section 3.3.3. By comparing equivalent factors it is possible to equate measured values in the fit to physical quantities in Equation 23. Firstly consider that the measured PL intensity ( $I$  in 3.3.3 Equation 12) is related to the number of bright dots by

$$I = kN_B(t)$$

**Equation 24**

where  $k$  is related to the total number of dots in the ensemble. We assume that ‘dark’ dots are entirely non-radiative and thus make no contribution to PL. Bearing this in mind one can re-arrange Equation 20 and Equation 23 to produce the following relations:

$$I_{\infty} = k \left( \frac{C}{C + D} \right)$$

**Equation 25**

$$I_0 = kN_0$$

**Equation 26**

$$\beta = C + D$$

**Equation 27**

We also observe that the fractional increase brought about by any activation which starts at the ‘dark’ equilibrium (i.e. before any optical excitation is applied or the system has entirely recovered) and reaches the ‘bright’ equilibrium can be described by

$$A = \frac{I_{\infty} - I_0}{I_0} = \frac{\left[ \frac{C}{C + D} \right] - N_0}{N_0} = \frac{\frac{\beta - D}{\beta} - N_0}{N_0}$$

**Equation 28**

Since D is assumed to be independent of the activation which it follows this enables us to study the activation of a sample under various intensities and thus deduce an estimate of the initial population of bright dots, as well as how applied optical intensity effects the rate of photo-activation.

## 4.4 Measurements

Measurements were taken on a single sample, which was illuminated under various intensities in a quasi-random order. The intensity of the pump light was modulated using neutral density filters. Recovery measurements were taken after each activation by applying low intensity pump light for short intervals (typically around 20s) in order to generate PL spectra, whilst allowing much larger timescales between measurements which we assume will have a negligible effect on the overall behaviour, due to the relatively massive timescales involved.

Figure 30 demonstrates the traces which resulted from the experiment. There is evidently some non-ideal behaviour occurring, especially in the measurement at  $180\mu\text{W}$ . This will be discussed in further detail later, but first we will review the results.

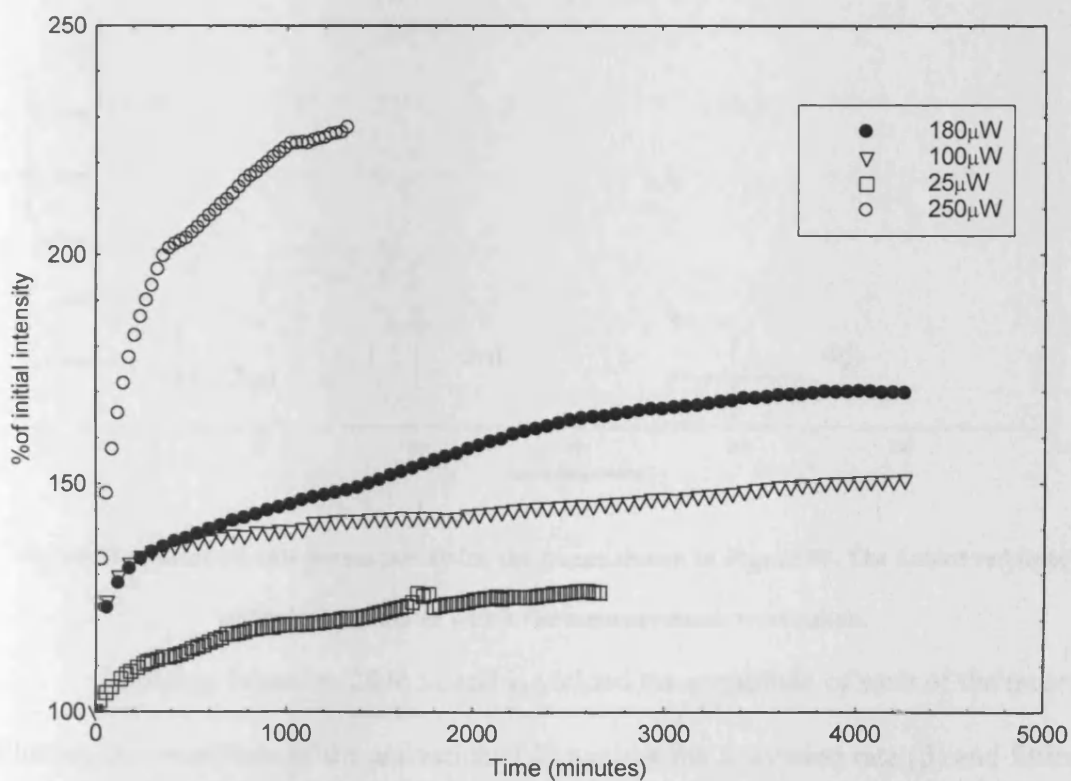
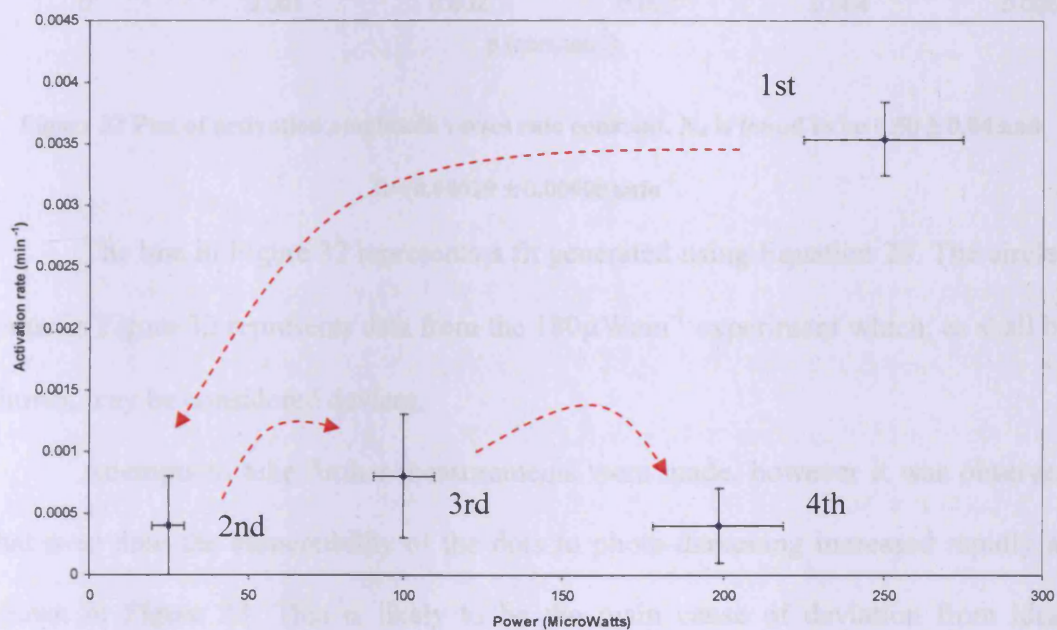


Figure 30 Photo-activations at various powers. The  $250\mu\text{W}$  trace was taken first, followed by  $25\mu\text{W}$ ,  $100\mu\text{W}$  and finally  $180\mu\text{W}$ .

Curves were fitted to each of the results shown in Figure 30. In each case values of  $I_{\infty}$ ,  $I_0$  and  $\beta$  were extracted along with corresponding uncertainties. For each activation the recovery rate was also measured. This gave us a value for  $C_t + D$ , since  $\beta = C_t + D$  if  $C_p = 0$ . The value of  $C_t + D$  used was an average of the recovery constant following each activation studied. Figure 31 demonstrates the fitted photo-activation rate versus the applied power. The behaviour seen is investigated later in this chapter as well as the subsequent chapter, but the reader should be aware of the order in which measurements were taken. As mentioned above, results were taken in a quasi-random order, and Figure 31 illustrates this order.



**Figure 31** Activation rate versus power for the traces shown in Figure 30. The dotted red lines indicate the order in which the measurements were taken.

Applying Equation 28 to  $I_{\infty}$  and  $I_0$  yielded the amplitude of each of the traces. Plotting the amplitude of the activations ( $A$ ) against the activation rate ( $\beta$ ) and fitting using Equation 28 produced the trace seen in Figure 32 which provides values for  $N_0$  and  $D$ .

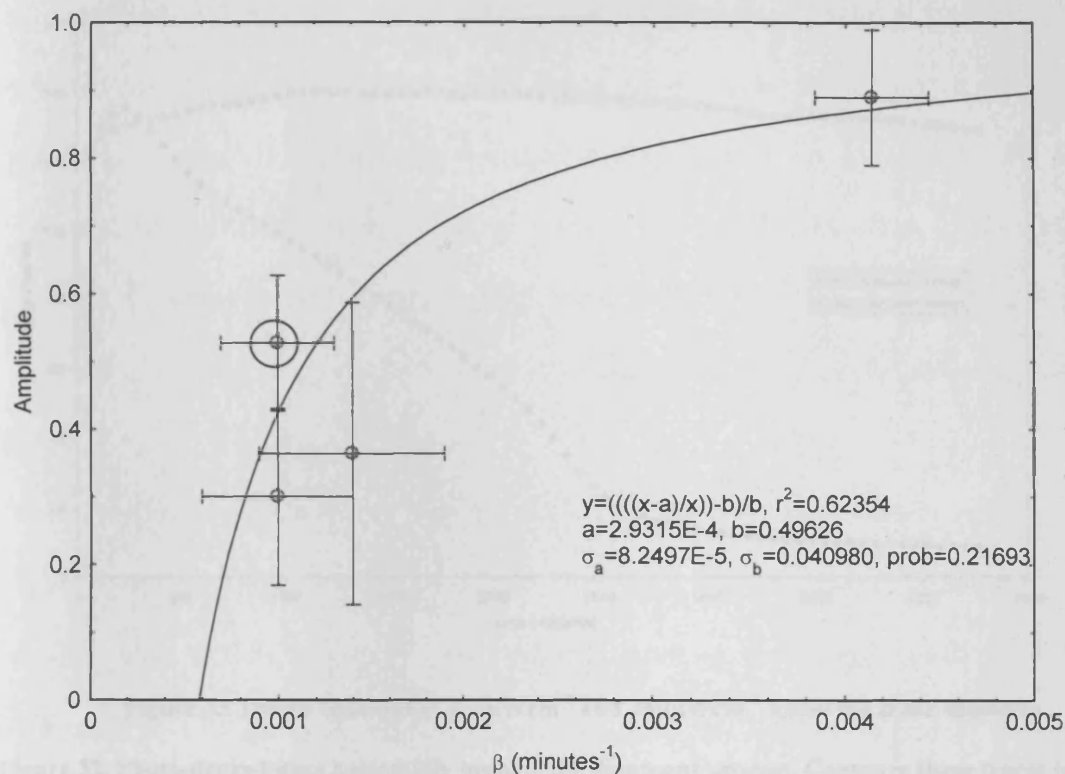
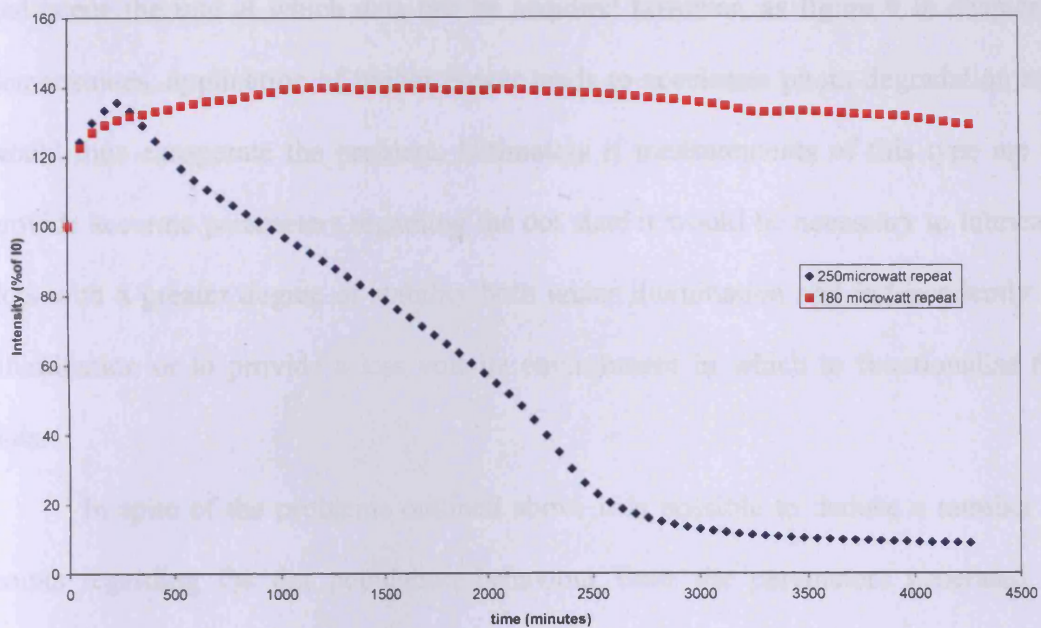


Figure 32 Plot of activation amplitude verses rate constant.  $N_0$  is found to be  $0.50 \pm 0.04$  and

$$D=(0.00029 \pm 0.00008)\text{min}^{-1}.$$

The line in Figure 32 represents a fit generated using Equation 28. The circled value in Figure 32 represents data from the  $180\mu\text{Wcm}^{-1}$  experiment which, as shall be shown, may be considered deviant.

Attempts to take further measurements were made, however it was observed that over time the susceptibility of the dots to photo-darkening increased rapidly as shown in Figure 33. This is likely to be the main cause of deviation from ideal behaviour in the  $180\mu\text{Wcm}^{-1}$  experiment, which was the last measurement to be taken chronologically. There also appears to be an increasingly large irrecoverable element to the activation which will affect the calculated amplitude.



**Figure 33** Traces obtained at  $180\mu\text{Wcm}^{-1}$  and  $250\mu\text{Wcm}^{-1}$  following those shown in **Figure 32**. Photo-degradation has rapidly become the dominant process. Compare these traces to those in **Figure 30** for reference.

## 4.5 Discussion

The above measurements present a difficult problem which may be ubiquitous to application of colloidal quantum dots in PMMA. The physical properties of the dots appear to be changing with time, resulting in deviation of the ensemble behaviour from initial measurements. These effects result in an inherent inaccuracy in measurements such as those shown in **Figure 32**, and as such the factors generated should only be treated as estimates of initial values. Attempting to address this problem poses further problems. For accurate parameters to be generated it is necessary to activate the dots to their equilibrium point, and recover them to within a small tolerance of their initial state, assuming that activation is wholly recoverable. Given that the ensemble appears to deviate from ideal behaviour over some time period it may seem appropriate to apply higher power in order to accelerate activation

and hence the rate at which data can be acquired however, as figure 9 in chapter 3 demonstrates, application of higher power tends to accelerate photo-degradation and would thus exasperate the problem. Ultimately if measurements of this type are to provide accurate parameters regarding the dot state it would be necessary to fabricate dots with a greater degree of stability both under illumination and independently of illumination or to provide a less volatile environment in which to functionalise the dots.

In spite of the problems outlined above it is possible to deduce a number of points regarding the dot population behaviour from the parameters generated as outlined above. The  $N_0$  generated is  $0.50 \pm 0.04$ , suggesting that almost half of the dots are initially in a bright state. This is evidently not the case, since as Figure 27 shows; the PL intensity has already been decreased by a much more significant factor by mixing the dots in PMMA. These two points can be reconciled by considering that  $N_0$  is in fact the proportion of dots available for brightening which are initially in a bright state. It is thus possible that a large proportion of the dots are unavailable to the brightening process, implying that they are permanently darkened, or destroyed, by the PMMA mixing process. Figure 34 illustrates the proposed state of the dot population after the mixing is performed. Photo-activation can be envisaged as an increase in the size of the white circle, limiting at the point where it entirely occupies the shaded circle (i.e. all the dots which may still be photo-activated have done so).

The  $C_t$  value, which can be calculated by realising that the measured rate constant of recovery ( $0.0006 \text{min}^{-1}$ ) is equal to  $C_t + D$ , represents the photo-independent brightening of dots. This process is very scarcely covered in literature and the precise mechanism is unclear, however the presence of such a process is required in order that the dots not be entirely 'dark' when under no illumination. Study of the process is

necessarily indirect since in order to observe photoluminescence some optical excitation must be applied, inducing the photosensitive element of the process,  $C_p$ . The calculated value of  $C_{i\text{is}}$  is  $(0.00031 \pm 0.00008) \text{min}^{-1}$ .

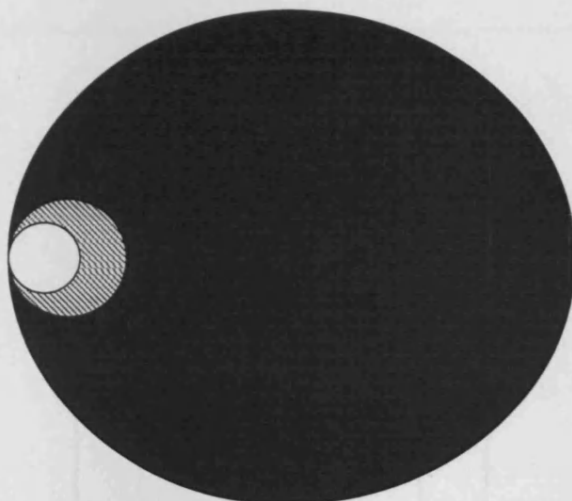


**Figure 34** Depiction of dot population after mixing with PMMA. The Black area depicts permanently darkened dots, the shaded area represents dots which are currently dark but may be photo-activated, while the white area represents currently bright dots. A large number of the dots are permanently darkened by the PMMA mixing process and make no contribution to the photo-dynamic process.

Throughout the measurements made above the peak wavelength of the PL was monitored. Figure 35 shows the evolution of the wavelength peak over time spent under excitation. The shift in wavelength is attributed to changes in the confinement potential within the nanocrystals brought about by a physical change in the size of the dot. The trend corroborates observations made above, that the dots have extremely limited stability in this environment, and measurements must be taken with these dynamics in mind. The plot indicates that the dots maintain their size for a short period, before rapidly deteriorating, and subsequently stabilising. Interestingly the end of the wavelength change at around 30000 minutes coincides with the start of the

180 $\mu\text{Wcm}^{-1}$  measurement shown in Figure 33, where significant photo-degradation is first observed. This may indicate a link between the two processes, specifically that whatever process causes the reduction in dot size also prevents photo-degradation of the sort seen in Figure 33.

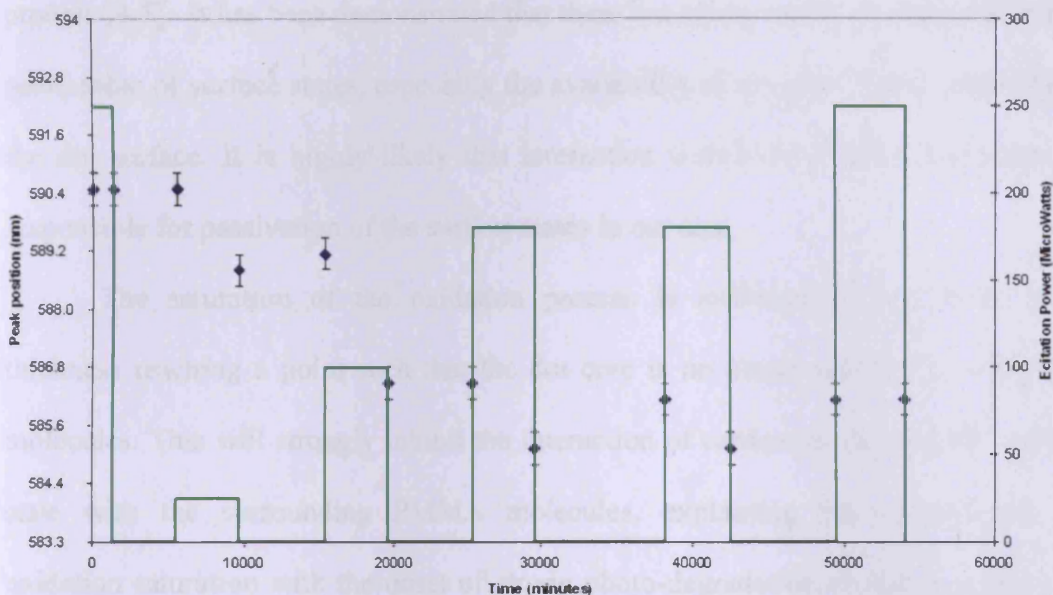


Figure 35 PL peak wavelength vs. time. The green line indicates the applied excitation.

Based on previous work [1] we may hypothesise that the reduction in dot size is caused by oxidation of the dot surface. Kim et al.[2] have demonstrated limiting in the oxidation process of small nano-wires (<150nm thickness), which reflects the peak position behaviour which we observe. The onset of photo-degradation upon saturation of the oxidation process might suggest that whatever process is driving the photo-oxidation process also drives photo-degradation process, but drives photo-oxidation preferentially.

Precisely understanding these processes requires careful consideration of the dot environment as well as processes within the dot itself. It has been demonstrated that PMMA is photo-stable, experiencing little or no photo-oxidation at wavelengths above ~255nm [3]. This is significant since it allows us to eliminate any changes

brought about in the PMMA matrix as a likely culprit for the dot behaviour and focus on processes within the dot itself.

Whilst the process by which surface traps are passivated, bringing about photo-activation, is disputed, it is widely accepted that they play a pivotal role in the process [4,5]. It has been demonstrated that there is a strong environmental role in the passivation of surface states, especially the availability of oxygen [4] and water [5] at the dot surface. It is highly likely that interaction with local PMMA molecules is responsible for passivation of the surface states in our case.

The saturation of the oxidation process is attributed to the oxide shell thickness reaching a point such that the dot core is no longer exposed to oxidising molecules. This will strongly inhibit the interaction of carriers occupying the surface state with the surrounding PMMA molecules, explaining the co-incidence of oxidation saturation with the onset of strong photo-degradation as surface states are no longer passivated.

#### **4.4 Conclusions**

Photo-activation, photo-degradation and photo-oxidation processes were studied in 610nm CdSe/ZnS core-shell colloidal quantum dots. A model is developed whereby the whole ensemble is treated as a two-state system consisting of a population of dots, existing in a bright or a dark state. It is shown that a large proportion of the dot population is irreversibly darkened by the preparation process in PMMA. Estimated values are generated for the photo-independent rate of photo-brightening, as well as the initial distribution of the population available for photo-brightening between bright and dark dots. A link is proposed between photo-oxidation and photo-degradation.

## 4.6 References

- [1] L. Liu, Q. Peng, Y. Li, *Inorg. Chem.*, 47, 3182, (2008)
- [2] S. Y. Kim, S. W. Kim, H. J. Chang, H. K. Seong, H. J. Choi, *Mat. Sci. in Semicon. Processing*, 11, 182, (2008)
- [3] Y. Fukada, Z. Osawa, *Polymer degradation and Stability*, 34, 75, (1991)
- [4] S. R. Cordero, P. J. Carson, R. A. Estabrook, G. F. Strouse, S. K. Buratto, *J. Phys. Chem. B*, 104, 12137, (2000)
- [5] J. Muller, J. M. Lupton, A. L. Rogache, J. Feldmann, D. V. Talapin, H. Weller, *App. Phys. Lett.*, 85, 381, (2004)

## **5. Calculation of Optical Cross Section and Photo-Activation Probability in 610nm CdSe/ZnS Colloidal Quantum Dots in PMMA**

### **5.1 Introduction**

Having studied colloidal quantum dots' photo-dynamic behaviour in chapter 4, here we calculate the optical cross section of dots using the extinction co-efficient (and vice versa) and use measured absorption values to calculate the dot concentration. With this information as well as measured photo-activation rates from the previous chapter it was possible to calculate the probability of photo-activating a colloidal quantum dot upon absorption of a photon under certain circumstances. This was considered important as in order to better understand the transient behaviour in the dots observed in chapter 4 it was desirable to eliminate the power dependence of the fitted photo-activation rates and obtain a value with greater physical relevance. We go on to propose a physical model to describe the observed behaviour and hypothesise mechanisms behind the model.

### **5.2 Calculation of the Optical Cross Section**

#### **5.2.1 Rationale**

It is important to clarify the comparison being made between two different experiments. Once the optical cross section has been calculated from the extinction co-efficient supplied by the manufacturer it is used to calculate the concentration of dots in the sample, which is possible due to measurement of the absorption co-efficient as per the imaging method outlined in chapter 3.4. These values are then

used in calculating a photo-activation probability, where the value of the photo-activation rate is obtained from a separate experiment where light is incident normal to the sample. Figure 36 demonstrates the difference between the two approaches.

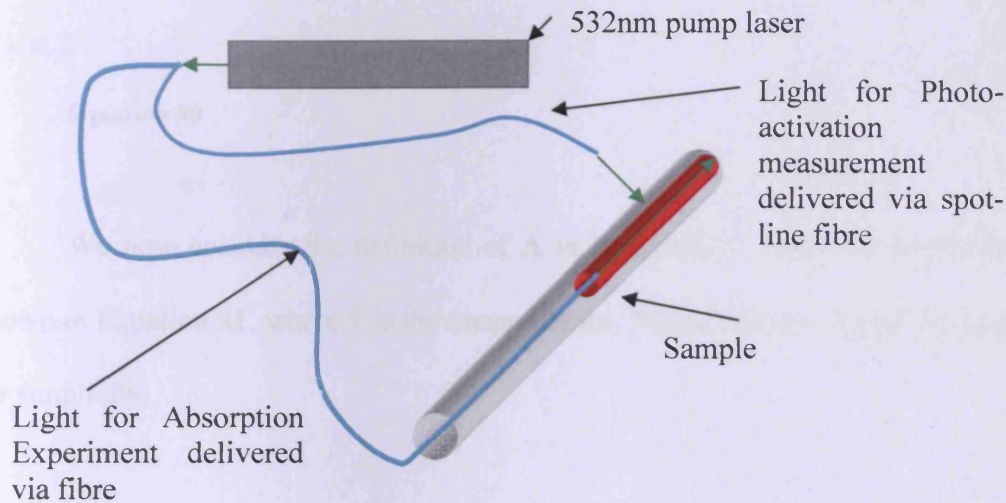


**Figure 36** Diagram showing different geometries of Photo-activation and absorption measurements. Note that the two experiments are not run simultaneously.

### 5.2.2 Derivation of Optical Cross Section

We begin by considering Equation 29, which defines the absorption coefficient of a material containing  $N$  absorbing dots per unit volume, each with optical cross section  $\sigma$  square centimetres. We assume that the dots do not shadow each other.

$$\alpha = N_{vol} \sigma$$

**Equation 29**

We next consider Equation 30 from [1] which provides the fractional absorbance,  $A$ , effected by a concentration of  $C$  dots per litre, the dots having a molar extinction co-efficient of  $\epsilon$  [(mol litre<sup>-1</sup>)<sup>-1</sup>cm<sup>-1</sup>], along a path of length  $L$  cm.

$$A = \epsilon CL$$

**Equation 30**

We now consider the definition of  $A$  in Equation 30, which is expressed as shown in Equation 31, where  $T$  is the transmittance. Notice that we denote  $\log_{10}e$  by  $\gamma$  for simplicity.

$$A = -\log_{10} T = -\log_{10} e \cdot \log_e T = -\gamma \log_e T$$

**Equation 31**

Re-arranging Equation 31 and substituting Equation 30 yields Equation 32. The last term on the right of Equation 32 is the definition of transmittance.  $\Phi(L)$  indicates the optical flux at some point along the length  $L$ .

$$T = \exp\left(\frac{-A}{\gamma}\right) = \exp\left(\frac{-\epsilon CL}{\gamma}\right) = \frac{\Phi(L)}{\Phi_0}$$

**Equation 32**

We now compare Equation 32 with Equation 33, which defines the absorption co-efficient,  $\alpha$ . Doing so gives Equation 34, which expresses the absorption co-efficient in terms of the extinction co-efficient,  $\epsilon$ .

$$\frac{\Phi(L)}{\Phi_0} = \exp(-\alpha L)$$

**Equation 33**

$$\alpha = \frac{\varepsilon C}{\gamma}$$

**Equation 34**

We now substitute Equation 29 into Equation 34;

$$N_{vol} \sigma = \frac{\varepsilon C}{\gamma}$$

**Equation 35**

and realise that

$$N_{vol} = N_{Avo} C$$

**Equation 36**

where  $N_{Avo}$  is Avogadro's number. Equation 36 can be substituted in Equation 35 to yield an expression for the optical cross section of the dot in terms of the extinction co-efficient, as expressed in Equation 37

$$\sigma = \frac{\varepsilon}{N_{Avo} \gamma}$$

**Equation 37**

Figure 37 demonstrates the physical meaning of some of these factors for clarity. It is important to note that the extinction co-efficient is commonly supplied in units of  $[(\text{mol litre}^{-1})^{-1}\text{cm}^{-1}]$  and it is therefore important to make a conversion to  $[(\text{mol cm}^{-3})^{-1}\text{cm}^{-1}]$  if the cross section is to be obtained in  $[\text{cm}^2]$ , which is achieved by re-writing Equation 37 as per Equation 38.

$$\sigma = \frac{\epsilon \times 10^3}{N_{\text{Avo}} \gamma}$$

Equation 38

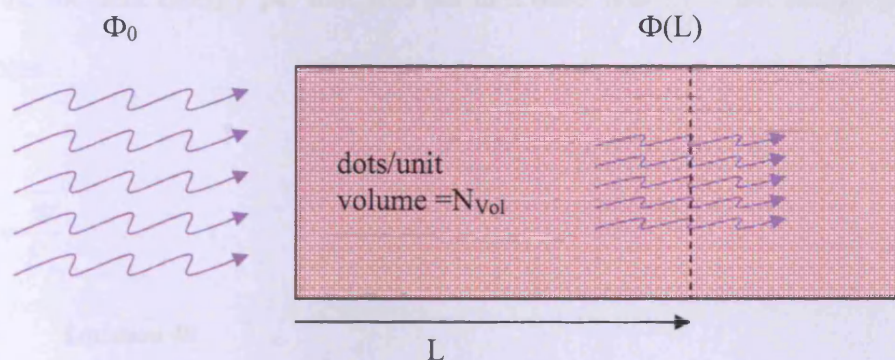


Figure 37 Demonstration of the physical significance of constant involved in derivation of Equation 38.

The above allows calculation of the optical cross section using supplied data (the extinction co-efficient) for a system of dots.

### 5.2.3 Calculation of the dot concentration

Once  $\sigma$  is known the dot concentration is calculated using Equation 39 where  $\alpha$  is the measured absorption co-efficient (according to section 3.4.2), and  $N_{\text{vol}}$  is the

number of dots per cubic centimetre. Converting  $N_{vol}$  to the number of dots per litre, and dividing by Avogadro's number yields the concentration in moles per litre.

$$\alpha = N_{vol} \sigma$$

**Equation 39**

#### **5.2.4 Calculation of the photo-activation probability**

In order to establish the probability of photo-activating a dot upon absorption of a photon we begin by establishing the incident photon flux which is defined by Equation 40, where  $\phi$  is the number of incident photons per unit area per unit time,  $\Phi$  is the incident Energy per unit area per unit time, and  $E_p$  is the energy per photon in joules.

$$\phi = \frac{\Phi}{E_p}$$

**Equation 40**

At this point we recall that we are using the second geometry outlined in section 3.2.1 in order to obtain the photo-activation rate, whereby light falls normally on the capillary. Since the distance travelled in the absorbing media is now small we use the approximation that the dots do not shadow each other.

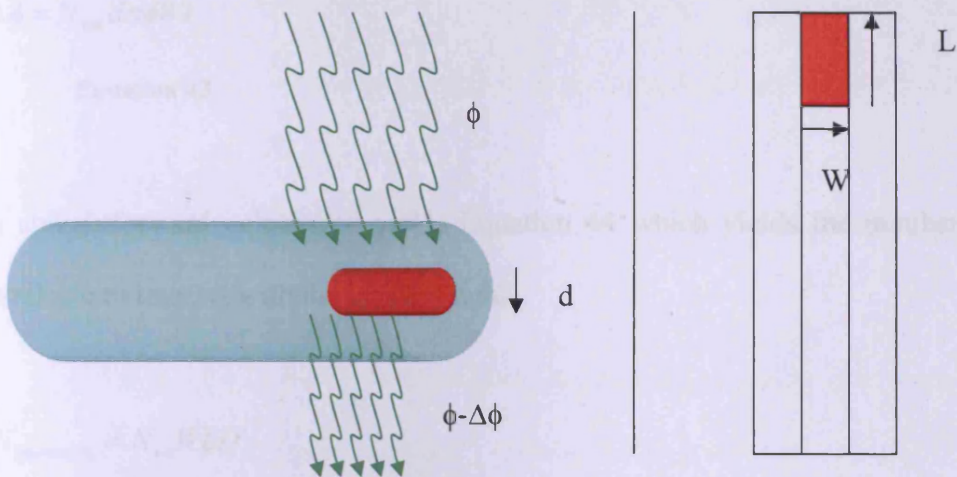


**Figure 38** Diagram depicting light incident on sample and the depth of the material, as well as top-down view depicting the width and length of the sample used.

We now consider that the number of dots per unit area presented to the incoming light is calculated as per Equation 41.

$$N_{Area} = N_{vol} d$$

**Equation 41**

Substituting Equation 41 in Equation 29 yields Equation 42,

$$\frac{\Delta\phi}{\phi_0} = N_{vol} d\sigma$$

**Equation 42**

hence the number of absorbed incident photons in the sample per unit time is given by Equation 43 where  $W \times L$  represents the area of the sample presented to the incoming light.

$$\Delta\phi = N_{vol} d\sigma\phi WL$$

**Equation 43**

A straightforward calculation yields Equation 44 which yields the number of dots available to interact with the incident light.

$$N_{Interacting} = N_{vol} WLD$$

**Equation 44**

At this point we have assumed for simplicity that the sample is rectangular, and as we see below, the area terms cancel so this assumption has no effect on the result.

Dividing Equation 43 by Equation 44 yields the average number of absorbed photons per dot per unit time, as shown in Equation 45.

$$\eta = \frac{N_{vol} d\sigma\phi WL}{N_{vol} WLD} = \sigma\phi$$

**Equation 45**

Finally the probability of photo-activating a dot is given by Equation 46, where P is the probability of photo-activating a dot upon absorption of a photon, and  $C_p$  is the rate of photo-driven activation. We note that this result is expected, however it serves to demonstrate that the terms we are using are valid in this context.

$$P = \frac{C_p}{\eta} = \frac{C_p}{\sigma\phi}$$

**Equation 46**

Below we present results of application of these equations to our results.

## 5.3 Results

### 5.3.1 Optical Cross Section

Data supplied with 610nm colloidal quantum dots states their extinction coefficient to be  $4.7 \times 10^5 \text{ mol}^{-1} \text{ litre cm}^{-1}$ , yielding a value of  $\sigma$  of  $1.6 \times 10^{-15} \text{ cm}^2$ . We assume that functionalisation into PMMA does not effect the extinction co-efficient. This value is significantly lower than the physical area of the dot which is roughly  $2.5 \times 10^{-13} \text{ cm}^2$ , it is however in agreement with the work by Leatherdale et al. [2] which calculated cross sections of CdSe colloidal dots on the scale of  $10^{-15} \text{ cm}^2$ .

### 5.3.2 Dot Concentration

The calculated dot concentration, using absorption measured at 400nm via the method outlined in 3.2.1, is  $0.9 \times 10^{15} \text{ dots/cm}^3$  which is equivalent to a  $1.6 \mu\text{M}$  solution, which is a reasonable for a solution which is diluted only a little from its supplied form (typically a few micro molar). The absorption measured at 400nm was  $(0.60 \pm 0.05) \text{ cm}^{-1}$  after correction for scatter, and this was adjusted to  $(0.20 \pm 0.05) \text{ cm}^{-1}$  after consulting standard absorption data for the expected ratio of absorption at 400nm and near the band edge, where the extinction co-efficient is measured.

### 5.3.3 Photo-Activation Probability

Here we show calculated photoactivation probability,  $P$ , per dot per photon for each of the measurements made in chapter 4 using Equation 46. As the probability is calculated per photon we would expect the probability to be roughly the same for each case assuming there is negligible chance of two-photo absorption. In Table 1 we see

that this is not the case. The examples shown in Table 1 are in chronological order (i.e. the order in which they were taken), with the powers which the measurement were taken included for reference only since probabilities stated are calculated per photon. We see a clear drop off in the probability of a photon activating a dot after the second exposure and further after the third.

**Table 1**

Order of acquisition/Excitation power for period	Photo-activation Probability per photon per dot ( $\text{min}^{-1}$ )	Error in Photo-activation Probability ( $\text{min}^{-1}$ )
1 <sup>st</sup> (250 $\mu$ W)	5.51E-05	6.8E-06
2 <sup>nd</sup> (25 $\mu$ W)	6.22E-05	2.78E-05
3 <sup>rd</sup> (100 $\mu$ W)	3.11E-05	1.15E-05
4 <sup>th</sup> (190 $\mu$ W)	7.83E-06	2.48E-06

In order to be certain that two photon effects are not playing a part a transmission absorption measurement was performed with and without applied PL excitation. It is expected that if the dots are receiving enough light to drive such processes then we would expect to see saturation of the absorption spectra as the conduction band energy levels became unavailable to further electrons as the pump fills these states. In this experiment it was necessary to measure the PL before performing the experiment in order that the PL signal could be subtracted from the measured transmission signal in order to eliminate its effects from the resulting absorption spectra. The investigation showed no determinable change in the absorption spectra due to the pump light at every power used to obtain the results

demonstrated in Table 1. An example of measured absorption spectra with and without maximum power excitation is shown in Figure 39.

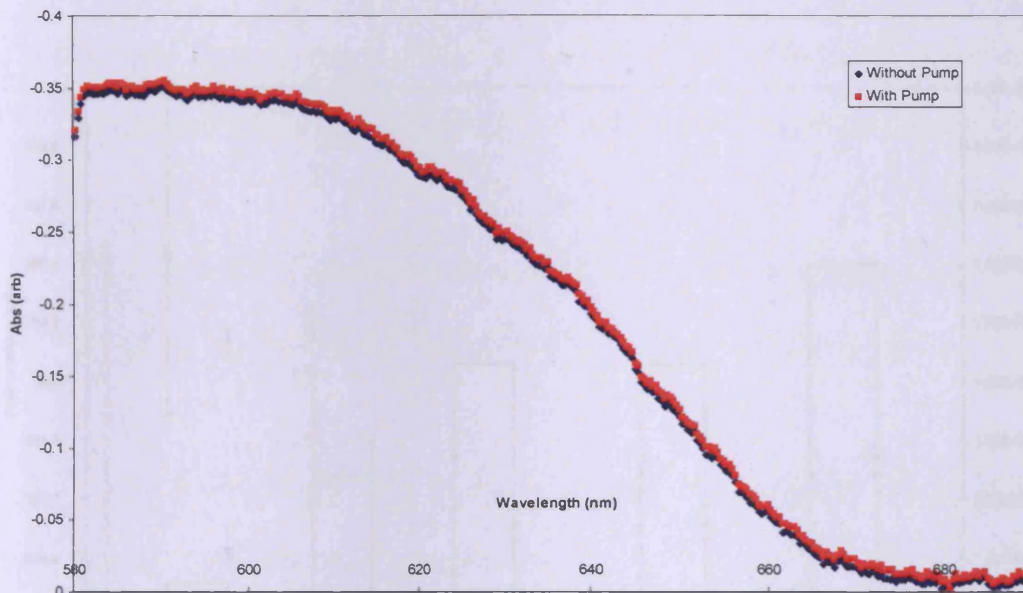


**Figure 39** Measured absorption spectra with and without 250 $\mu$ W excitation.

Importantly this measurement agrees with calculations made during the calculation of the activation probability where the number of absorbed incident photons per dot per second was found to be extremely low, the highest rate being 1 photon per second per dot for the case of 250 $\mu$ W $\text{cm}^{-1}$  excitation. Given that relaxation times are obviously vastly smaller than this we would be very surprised to see any non-linear processes occurring in our sample.

The results in Table 1 are shown in chronological order, so as to demonstrate that the photo-activation probability is dropping off over time. In order to demonstrate this we plot the photo-activation probability against time and overlay this onto Chapter 4 Figure 8 where the change in the peak wavelength position was shown as a function of time, which is displayed here in Figure 40. We observe a clear correlation between the onset of significant photo-oxidation, to which we attribute the shift in the peak wavelength of the photoluminescence, and the decrease in the probability of

photo-activating a dot upon absorption of a photon. Probabilities are not calculated for later times since reliable values of the photo-activation rate cannot be obtained due to the onset of significant photo-degradation preventing accurate fitting.

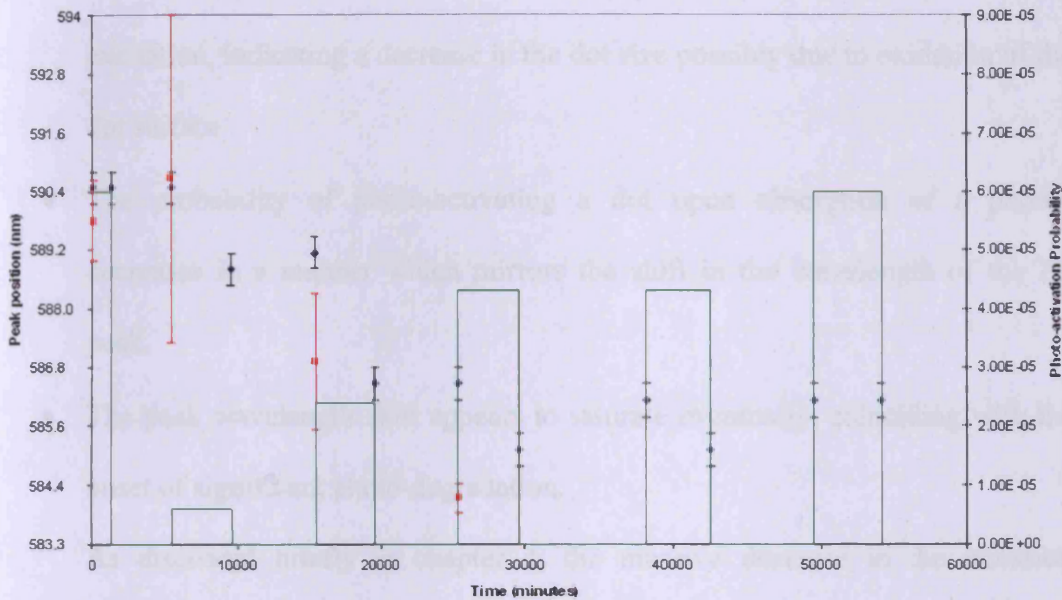


**Figure 40** Photo-Activation probability per absorbed photon per dot over time under illumination (red points) overlaid against the peak wavelength value (blue points), showing the correlation between the decrease in the photo-activation probability and the acceleration of photo-oxidation of the dot surface. The green line indicates the modulation of the applied power.

In the absence of an axis for this data refer to chapter 4 figure 9 for values.

## 5.4 Analysis and Proposed Physical Model

Here we present the physical model to which the above behaviour is attributed, as described in chapters 4 and 5.

We begin by listing the behaviour which we have observed which requires explanation;

- The PL Intensity of the dots decreases massively upon functionalisation in PMMA

- Under modulated excitation at various powers photo-activation behaviour deviates from expected behaviour after some period of time
- After further excitation photo-degradation becomes the dominant process
- A blue shift in the emission wavelength of the dots is observed under excitation, indicating a decrease in the dot size possibly due to oxidation of the dot surface
- The probability of photo-activating a dot upon absorption of a photon decreases in a manner which mirrors the shift in the wavelength of the PL peak.
- The peak wavelength shift appears to saturate eventually, coinciding with the onset of significant photo-degradation.

As discussed briefly in chapter 4, the massive decrease in the emission intensity of the dots upon functionalisation is attributed to partial or complete removal of material from the dot surface. It is likely that most if not all of the passivating ligands have been removed, as well as some of the ZnS shell.

Firstly we consider that the most likely explanation for the shift in the PL peak wavelength under excitation is photo-driven oxidation of the dot surface (as alluded to earlier) or removal of material from the dot. Given the other behaviour which is observed, especially the saturation of the process, it is felt that this behaviour is very likely to be an oxidation process rather than removal of material. We propose a picture in which an increasingly thick shell of oxide material builds up around the dot, until such time as the approximately spherical particle is wholly surrounded by the oxide layer, preventing any further oxidation of the surface. Having formed this picture we may consider what effect we expect it to have on the other dot properties

and what conclusions regarding the photo dynamic mechanisms within the dot may be drawn.

We now consider the gradual decrease in the photo-activation probability per absorbed photon, correlating well with the observed wavelength shift. In order to properly characterise this we must first have some sense of the driving force behind the photo-activation process. As discussed earlier the precise mechanism behind colloidal quantum dot photo-dynamics is still uncertain, however it is widely accepted that surface defect states and their passivation are integral to the process. The photo-sensitive mechanism which passivates the states is, however, less well understood. Bearing in mind the system proposed for the oxidation mechanism above, it is the author's opinion that these results are consistent with a mechanism arising due to photo-assisted binding of local molecules to the dot surface, passivating the surface defect. This mechanism would explain the decrease in photo-activation probability as the oxidation becomes more extensive, preventing access to the surface sites by the molecules responsible for the passivation.

The eventual saturation of the oxidation and coincident onset of photo-degradation also fit well with this picture, since once the oxide shell has surrounded the dot and no passivating molecules may access the dot surface, allowing a run away build up of surface states or charge on the dot surface, possibly driven by photo-ionisation of the dot surface. This is discussed in further detail below.

Below we present the proposed model for the observed behaviour as a whole. We assume that initially the dot coating has been removed and that the ZnS shell no longer plays a significant role in the mechanics. The mechanism is shown in Figure 41.

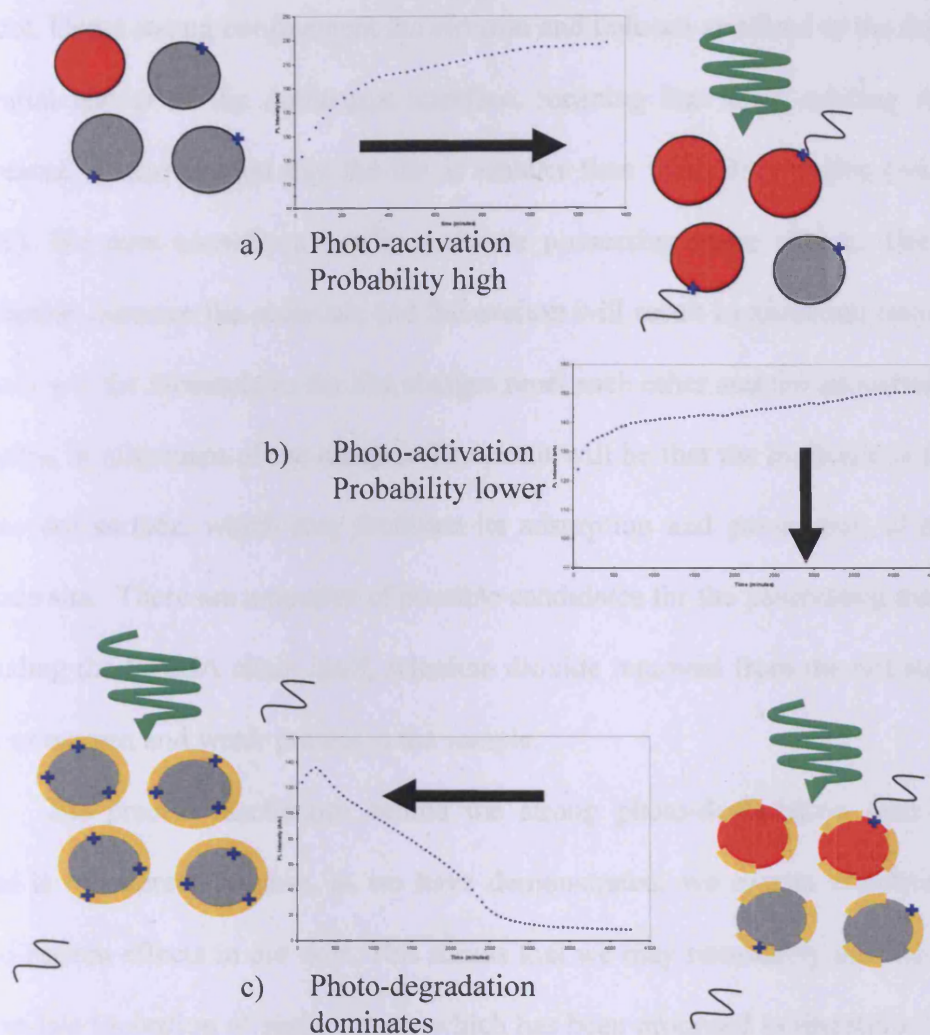


**Figure 41** Depiction of the proposed mechanism for the observed behaviour, as well as data supporting the hypothesis; a) Initially some number of the dots are bright, and the others have their fluorescence quenched by unoccupied surface states b) Upon application of excitation a photo-driven process allows passivation of the dot surface state by environmental molecules c) After prolonged exposure the dot surface begins to photo-oxidise, preventing access to some surface states by passivating molecules and slowing the photo-activation process d) Eventually the dot surface is entirely covered by the oxide layer, preventing passivation of any formed surface states and photo-degradation as the surface charges unabated.

Whilst the exact chemical nature of the surface passivation is unclear, we here propose a mechanism which may go some way to explain the observed behaviour in a

more precise way. We consider first the nature of the photo-generated exciton within the dot. Under strong confinement the electron and hole are confined to the dot by the potential barrier at the dot/matrix interface, meaning that their orbiting radius is decreased by the amount that the dot is smaller than their Bohr radius ( $\sim 4.8\text{nm}$  in CdSe). We now consider a nearby molecule possessing some charge. The mutual interaction between the molecule and the exciton will result in attraction between the exciton and the molecule as the like charges repel each other and the opposites attract, resulting in alignment of the charges. The result will be that the molecule is attracted to the dot surface, which may facilitate its adsorption and passivation of a vacant surface site. There are a number of possible candidates for the passivating molecules, including the PMMA chain itself, selenium dioxide removed from the dot surface as well as oxygen and water present in the sample.

The precise mechanism behind the strong photo-degradation seen at later times is of interest because, as we have demonstrated, we expect effectively zero multi-photon effects in our dots. This means that we may reasonably assume that the Auger-like ionisation of surface states which has been proposed in literature [3] is not responsible in this case. In our case we consider that the oxide layer which has been generated around the dot will consist of cadmium oxide, a semiconductor with a band gap of  $2.16\text{eV}$  [4]. This is only very slightly larger than the band gap of CdSe ( $1.74\text{eV}$ ) and, significantly, lower in energy than our excitation source photons ( $532\text{nm} \sim 2.33\text{eV}$ ). This may mean that electrons excited in the core may pass into the oxide layer, resulting in the rapid depletion of the dot PL.

## 5.5 Conclusions

We have calculated the optical cross section of our  $610\text{nm}$  CdSe/ZnS colloidal quantum dots and used this to calculate the probability of photo-activation of a single

dot by absorption of a single photon. We subsequently observe a correlation between the decrease in this probability and the photo-oxidation process in the measurements seen in chapter 4. Using this information we have constructed a robust physical model where oxidation of the dot surface prevents access by passivating molecules, which described the observed behaviour and have gone on to propose possible quantum mechanical mechanisms which may be driving this behaviour. We go on in the next chapter to conduct similar tests in a pH buffer solution environment and observe how this model applies in the cell-like acidic environment as well as attempting to expand on the hypothesis and conclusion drawn here.

## 5.6 References

- [1] A. Beer, *Annal. Phys. Chem.*, 86, 78 (1852)
- [2] C. A. Leatherdale, W. K. Woo, F. V. Mikulec, M. G. Bawendi, *J. Phys. Chem. B*, 106, 7619, (2002)
- [3] R. M. Kraus, P.G. Lagoudakis, J. Muller, A. L. Rogach, J. M. Lupton, J. Feldmann, *J. Phys. Chem. B*, 109, 18214, (2005)
- [4] P.H. Jefferson, S. A. Hatfield, T. D. Veal, P.D.C. King, C. F. McConville, J. Zuiga-Perez, V. Munoz-Sanjose, *App. Phys. Lett.*, 92, 106103, (2008)

## **6. Optical Study of 655nm Untargeted CdSe/ZnS Colloidal Quantum Dots in pH Buffer Solutions**

### **6.1 Introduction**

This chapter presents results and analysis of photoluminescence and optical absorption measurements performed on untargeted 655nm CdSe/ZnS colloidal quantum dots in pH buffer solutions. The aim of the study is to characterise the effect of local environment pH on dot behaviour for better understanding of optical properties of colloidal dots in biological systems, where dots are often used to image and study samples on a cellular and organism scale. We shall first present the results and continue to analyse and discuss the results at length.

The study will focus on two samples at different pH with the following stages of measurements taken on each.

- I. Initial measurement of PL and absorption in each environment
- II. Measurement of absorption over 24Hrs at room temperature in darkness and PL before and after
- III. Measurement of Absorption under 24Hr low level white light illumination and PL before and after
- IV. Measurement of PL under 24Hr high intensity optical excitation with absorption measured before and after, followed by 24Hr recovery with absorption and PL measurements made at the beginning and end of this period. This was repeated three times for each sample
- V. Measurement of PL under 96Hr high intensity optical excitation, with absorption measured before and after.

## 6.2 Effect of Functionalisation into pH Buffers (Stage I)

Samples prepared as described in chapter 3.2.2 in pH 4.0 and 6.87 (henceforth called acidic and neutral) were prepared and studied using photoluminescence and absorption techniques. Before detailed study was undertaken the properties of the photoluminescence and absorption spectra in each buffer were studied in order to identify changes which had occurred due to the ionic activity in the dot environment. Detailed information on the buffer make up can be found in information sheets using the product codes provided in chapter 3. Figure 42 shows the photoluminescence and absorption spectra in each buffer after 24 hours in ambient conditions, during which time the epoxy which seals the sample was allowed to set, and shows evidence of stronger absorption and photoluminescence levels in the neutral buffer. The fractional magnitude of the integrated PL in the acidic buffer with respect to the neutral sample is calculated to be 0.20, while the ratio of the integrated absorption spectra in the excited region (taken as 520:540nm from inspection of the laser line) gives a value of 0.61. It must be implied from this that the change in PL cannot be attributed to decreased pumping due to absorption alone, and that the dot ensemble is less efficient due to some non-radiative pathways introduced by incorporation into the acidic buffer.

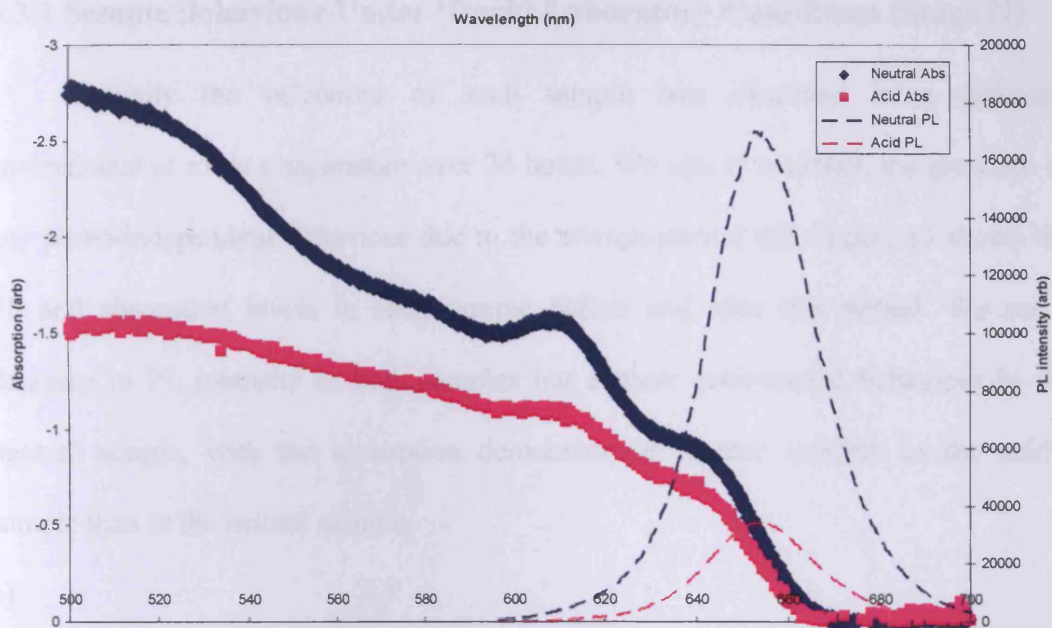


**Figure 42** Absorption and photoluminescence levels in neutral and acidic buffers

Interestingly a multi-Gaussian analysis of the absorption curve in Figure 42 shows a small but significant ( $\sim 5\text{meV}$ ) blue shift of the first transition energy in the neutral sample compared to the acidic sample. The wavelengths of the PL peaks have not shifted significantly with respect to each other.

In order to further investigate this behaviour we studied the transient behaviour of PL and absorption in each sample under a number of conditions as set out at the beginning of the chapter.

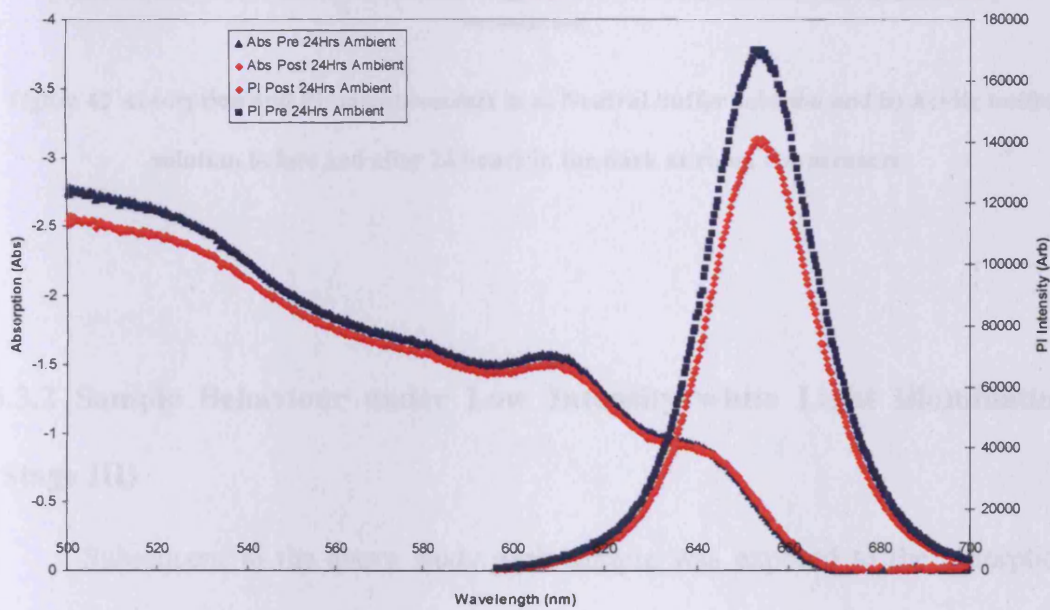
### 6.3 Transient Absorption Measurements

In this section we present transient measurements of absorption and PL behaviour in different pH buffers under various illumination levels. For each sample we monitor both characteristics under ‘dark’ laboratory conditions, under low-level white light illumination, under low intensity excitation and under high intensity illumination.

### 6.3.1 Sample Behaviour Under 'Dark' Laboratory Conditions (Stage II)

Initially the behaviour of each sample was observed in a darkened environment at room temperature over 24 hours. We aim to establish the presence of any photo-independent behaviour due to the environmental pH. Figure 43 shows the PL and absorption levels in each sample before and after this period. We see a decrease in PL intensity in both samples but a more pronounced behaviour in the neutral sample, with the absorption demonstrating greater stability in the acidic sample than in the neutral sample.

a)



b)

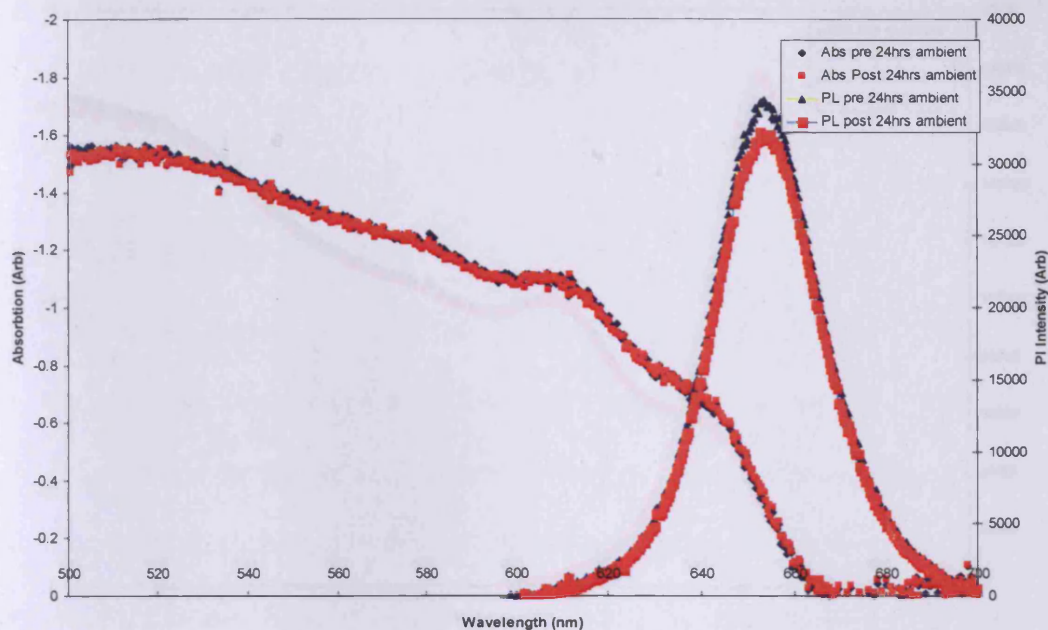
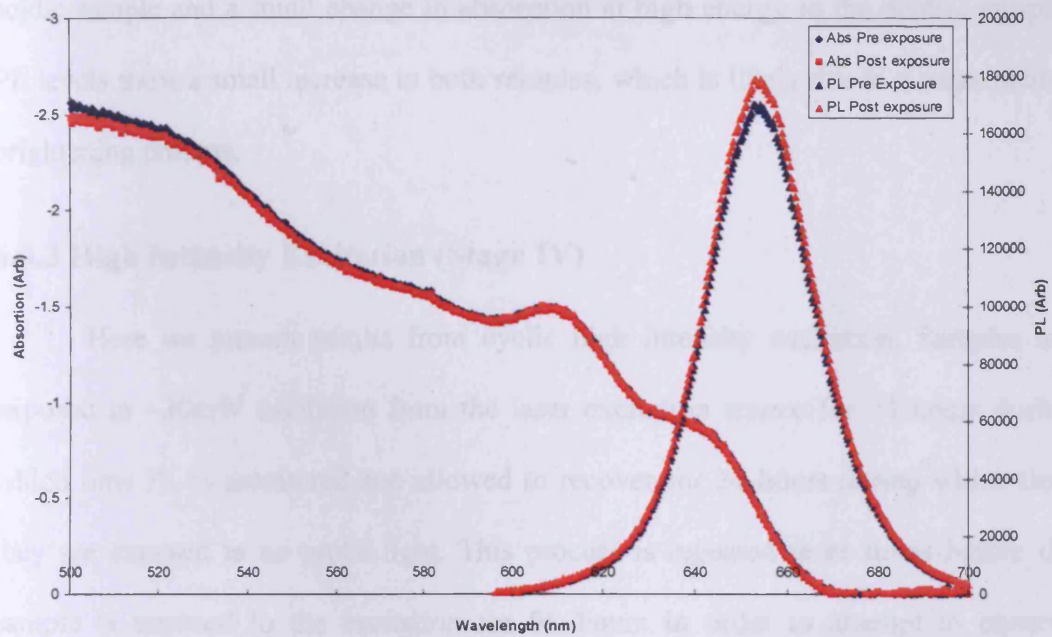


**Figure 43 Absorption and PL measurements in a) Neutral buffer solution and b) Acidic buffer solution before and after 24 hours in the dark at room temperature.**

### **6.3.2 Sample Behaviour under Low Intensity white Light Illumination (Stage III)**

Subsequent to the above study each sample was exposed to the absorption probe light for 24 hours in order to investigate any behaviour which may be induced by the probe. PL measurements were taken before and after and absorption was monitored throughout the process.

a)



b)

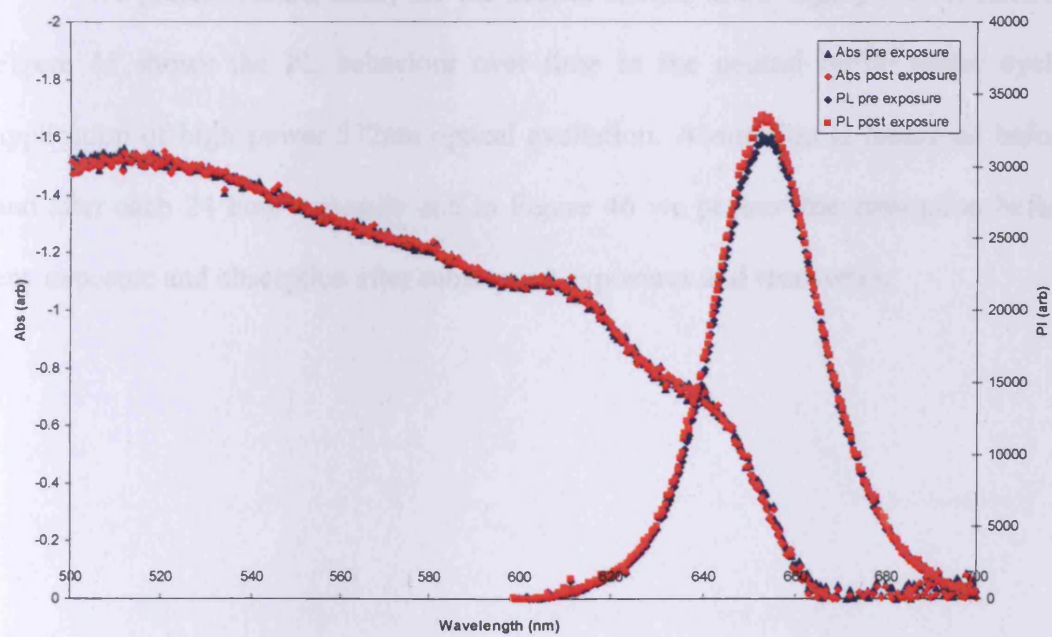


Figure 44 Absorption and PL measurements in a) Neutral buffer solution and b) Acidic buffer solution before and after 24 hours under low intensity white light illumination.

As Figure 44 demonstrates there is little or no change in the absorption in the acidic sample and a small change in absorption at high energy in the neutral sample. PL levels show a small increase in both samples, which is likely due to a weak photo-brightening process.

### **6.3.3 High Intensity Excitation (Stage IV)**

Here we present results from cyclic high intensity excitation. Samples are exposed to ~30mW excitation from the laser excitation source for 24 hours during which time PL is monitored and allowed to recover for 24 hours during which time they are exposed to no probe light. This process is repeated three times before the sample is exposed to the excitation for 96 hours in order to attempt to observe degradation behaviour.

We present results firstly for the neutral sample under high power excitation. Figure 45 shows the PL behaviour over time in the neutral buffer under cyclic application of high power 532nm optical excitation. Absorption is measured before and after each 24 hour exposure and in Figure 46 we present the absorption before any exposure and absorption after subsequent exposures and recoveries.

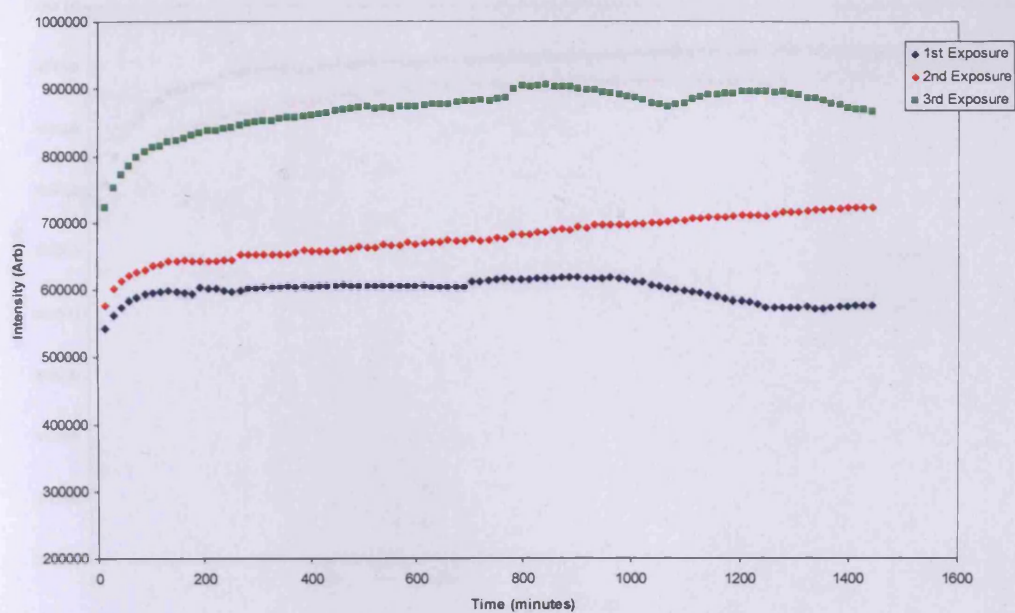


**Figure 45 Integrated PL over time in pH 6.87 buffer over three exposures**

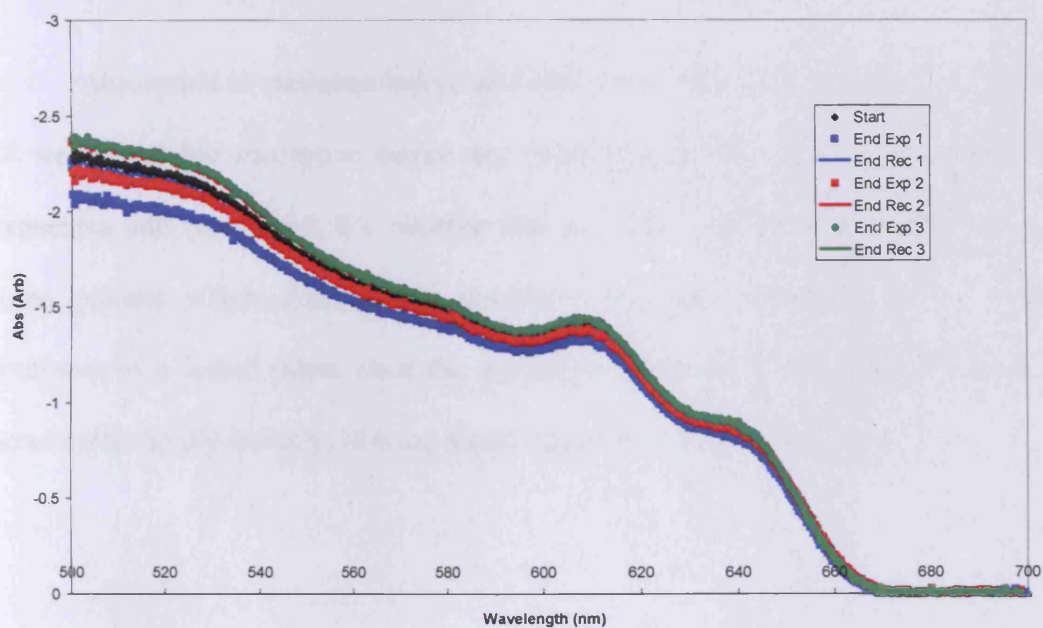


**Figure 46 Absorption spectra before and after each exposure in pH 6.87 buffer**

We now consider results from the acidic sample. Figure 47 shows the spectrally integrated photoluminescence over time in the acidic buffer when the high intensity 532nm light is applied.

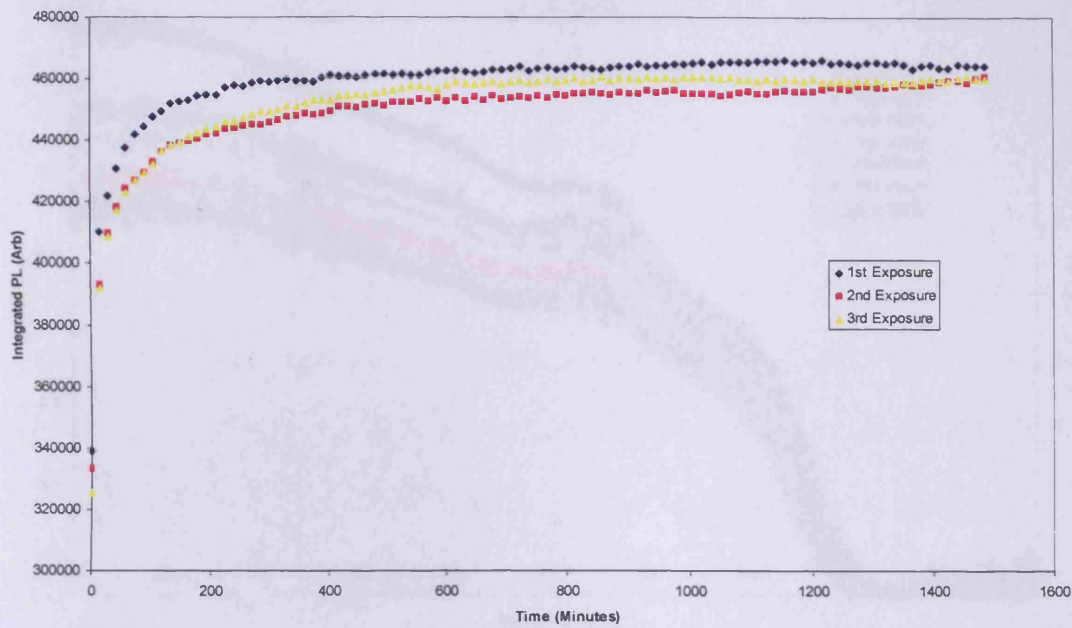


**Figure 47 Integrated PL over time in acidic buffer under high intensity excitation**

Absorption is measured before and after each 24 hour exposure and in Figure 48 we present the absorption before any exposure and absorption after subsequent exposures and recoveries. We observe that the more intense illumination initiates some process which depletes the absorbing capability of the ensemble which continues to a lesser extent once the excitation is removed. The process seems to occur quite rapidly initially, slowing significantly after the second cycle.

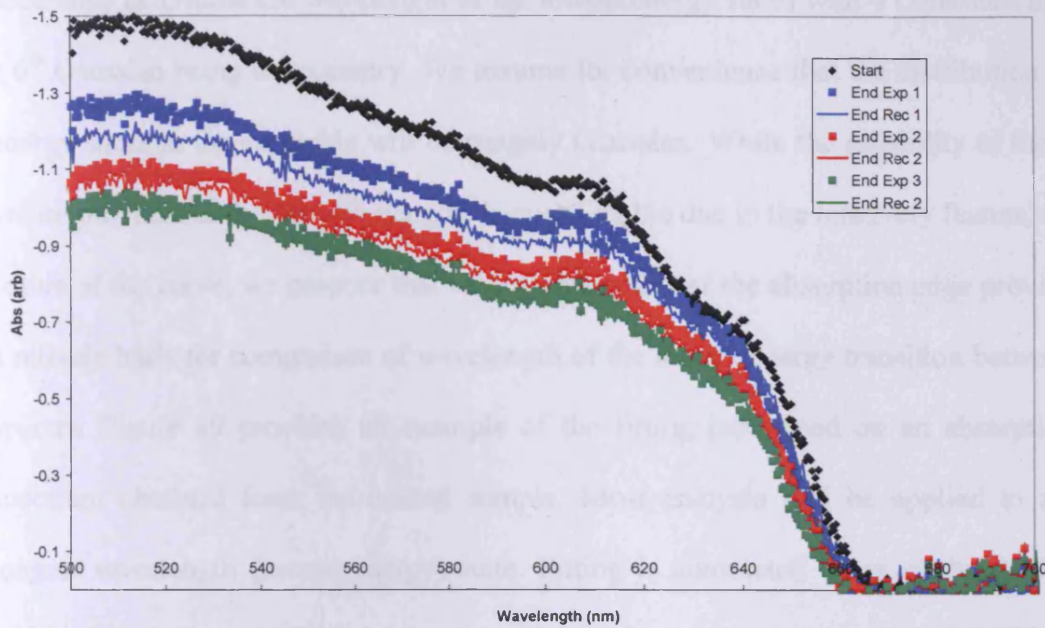


**Figure 48** Absorption spectra before and after each exposure. The black points indicates the absorption before any exposures. Subsequently points indicate absorption after an exposure while solid lines indicate absorption after 24hrs recovery.

## 6.4 Analysis of Results

Here we present systematic analysis of the results displayed above. Initially we use a five Gaussian fitting and a single Gaussian fitting to characterise the absorption and PL respectively. We shall present analysis for the acidic and neutral samples separately in order to draw comparison between the environmental effects on the dot later.

### 6.4.1 Absorption Analysis

Fitting the absorption spectra obtained above with a five Gaussian system was performed in order to identify the energy of the ground state transition for characterisation of dot size as well as the magnitude of the ground state absorption. Five Gaussians were used arbitrarily based on an unsatisfactory fit (due to inability to

accurately determine the wavelength of the lowest energy state) with 4 Gaussians and a 6<sup>th</sup> Gaussian being unnecessary. We assume for convenience that the distribution of energy states in the ensemble will be roughly Gaussian. While the reliability of these values provided at shorter wavelengths is questionable due to the relatively featureless nature of the curve, we propose that values obtained near the absorption edge provide a reliable basis for comparison of wavelength of the lowest energy transition between spectra. Figure 49 provides an example of the fitting performed on an absorption spectrum obtained from the neutral sample. Most analysis will be applied to the longest wavelength (lowest energy) state. Fitting is automated using mathcad. The width of each Gaussian is fixed in each pH in order to ensure comparability of the obtained parameters.

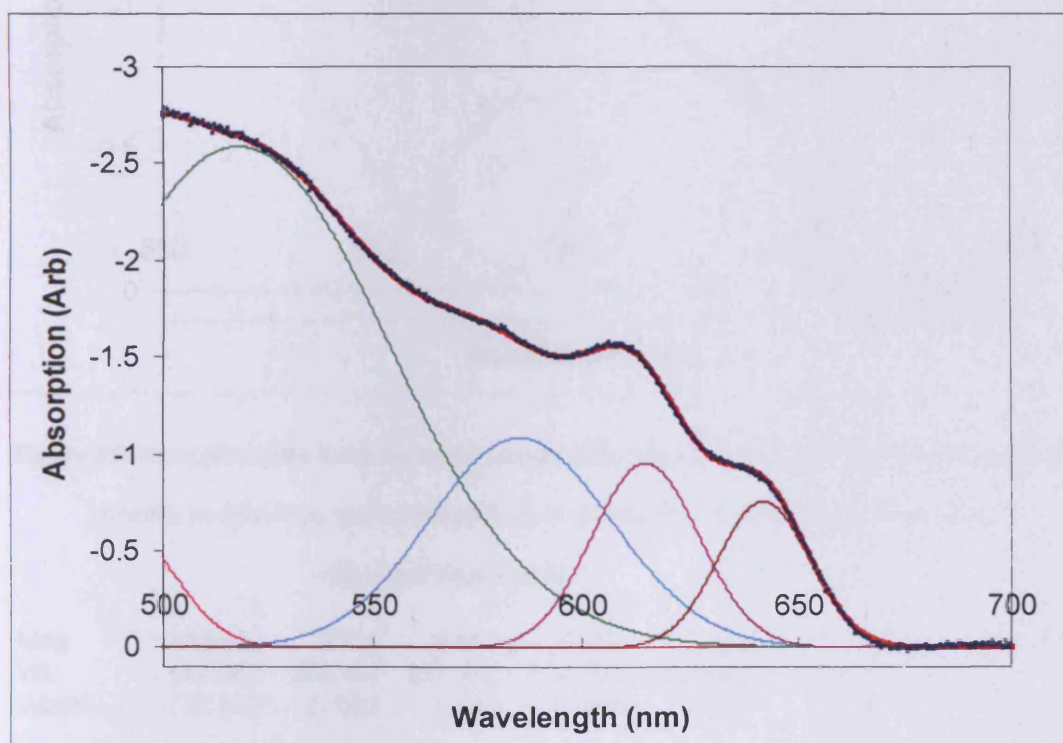


**Figure 49** Absorption data from the neutral sample (Blue points) fitted with five Gaussians (solid brown, purple, blue, green, and pink lines) giving the solid red line as their sum.

4.2.1.1. Plot of absorbance vs wavelength

The absorbance spectra of the poly (vinylidene fluoride) (PVDF) film is shown in Figure 49.

	Gaussian Parameters				
	1	2	3	4	5
Mag	6.08E-01	2.587	1.082	0.953	0.755
WL	491.156	517.479	585.248	614.725	642.156
Width	11.626	36.015	21.589	12.445	10.662

Table 2 Parameters for fit shown in Figure 49.

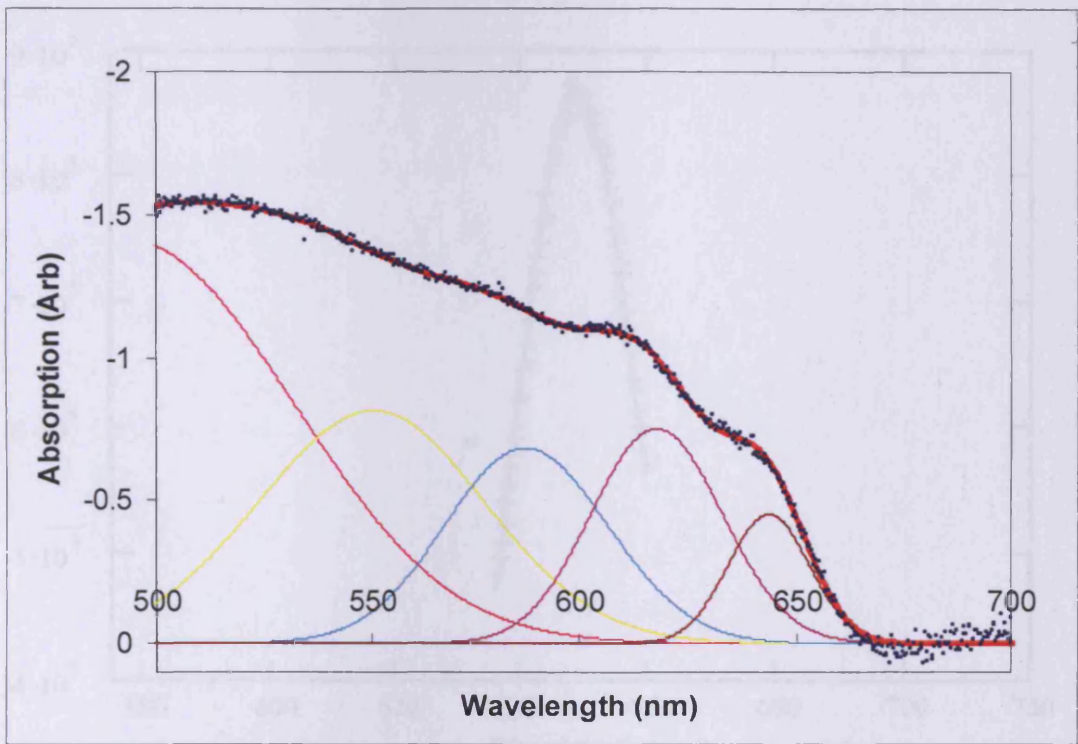


Figure 50 Absorption data from the acidic sample (Blue points) fitted with five Gaussians (solid brown, purple, blue, green, and pink lines) giving the solid red line as their sum.

	Gaussian Parameters				
	1	2	3	4	5
Mag	1.41E+00	0.814	0.683	0.752	0.452
WL	493.345	550.487	587.213	617.795	643.635
Width	37.539	27.031	19.345	15.098	9.397

Table 3 Parameters for fitting shown in Figure 50.

### 6.4.2 Photoluminescence analysis

In order to identify the peak wavelength of the ensemble PL we fit a Gaussian to the spectral centre of the PL peak. While the peak itself is not described well by a Gaussian, this method simply allows determination of the desired quantity (i.e the peak wavelength) Figure 51 shows an example of fitting performed in this way.

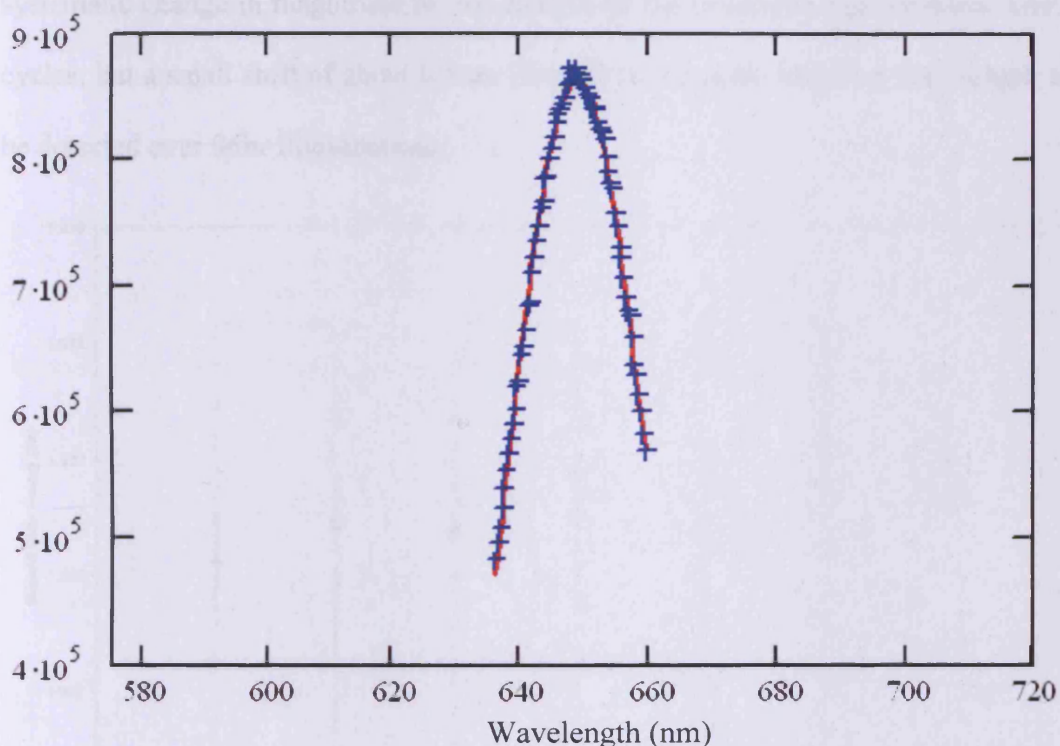


Figure 51 Gaussian fitting to the tip of the PL peak in the acidic sample, allowing determination of the peak wavelength

Determination of integrated PL intensity is achieved by summing values in the data, rather than from any fitting process.

### 6.4.3 Neutral Sample Analysis Results

We firstly characterise PL and absorption spectra before any perturbations are applied to the sample. Fitting as outlined in 6.4.1 yields energies of the four lowest

energy peaks to be 2.396, 2.118, 2.017 and 1.93eV. The PL peak is found to be at 653.9nm, or 1.896eV.

The integrated absorption and PL magnitudes are seen to drop under 'dark' conditions as seen in Figure 43 a). Under low level illumination there is a small drop in the absorption magnitude at long wavelength, as shown in Figure 44 a).

Under 24 hour intense laser illumination the neutral sample demonstrates no systematic change in magnitude or wavelength of the lowest energy transition over 3 cycles, but a small shift of about 0.5nm (1meV) in the peak emission wavelength can be detected over 96hr illumination.

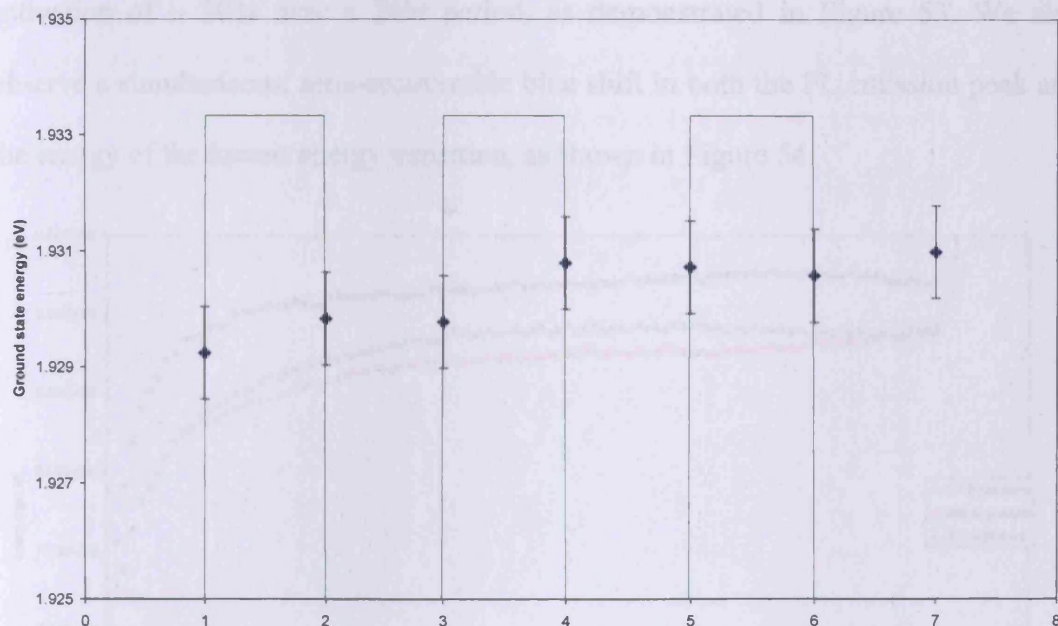


**Figure 52 cyclic application of high power illumination effecting no significant change in the measured energy of the ground state transition.**

#### 6.4.4 Acidic Sample Analysis Results

We begin by characterising the absorption and PL before any intentional perturbations have been imposed on the sample in order to determine a start point against which subsequent measurements may be compared. It also allows

determination of any effects brought about by the buffer itself. Fitting as outlined in 6.4.1 to the absorption spectrum yields the energies of the four lowest energy peaks to be 1.926, 2.007, 2.111 and 2.252 eV. The peak of the PL was found to be at 653.3nm, or 1.897 eV.

As can be seen in Figure 43 and Figure 44 there is very little change in the absorption characteristics in the dark or under low level white light illumination. The PL peak remains at the same wavelength within the spectrometer resolution in the dark and under low level white light illumination.

Under intense laser illumination we consistently observe a recoverable photo-activation of  $\sim 20\%$  over a 24hr period, as demonstrated in Figure 53. We also observe a simultaneous, semi-recoverable blue shift in both the PL emission peak and the energy of the lowest energy transition, as shown in Figure 54.

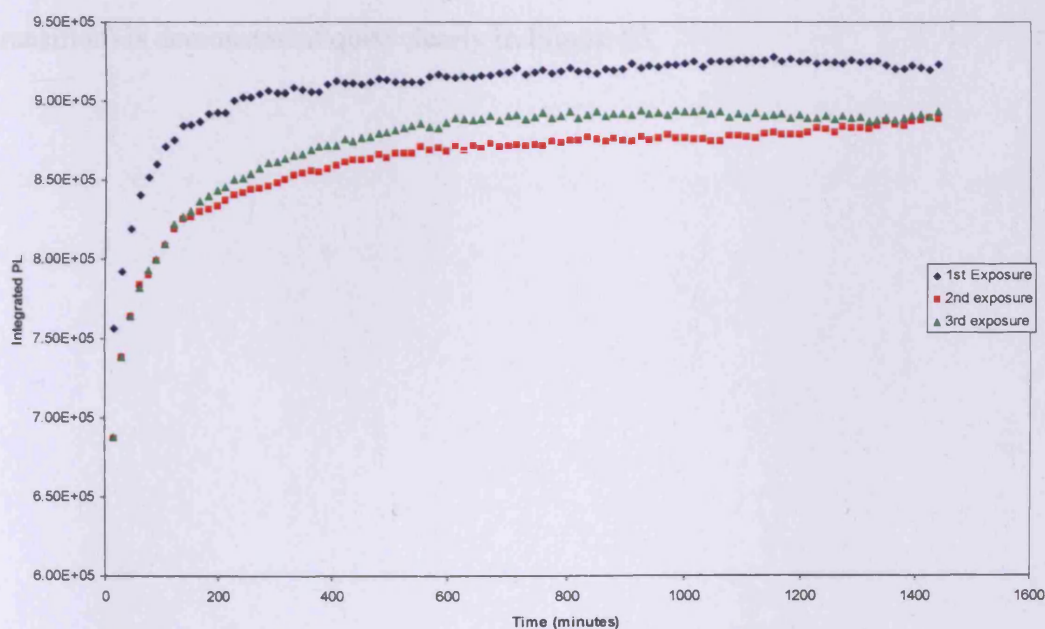


**Figure 53 Photo-Luminescence levels in acidic buffer under cyclic 24hr exposure to high intensity 532nm light.**

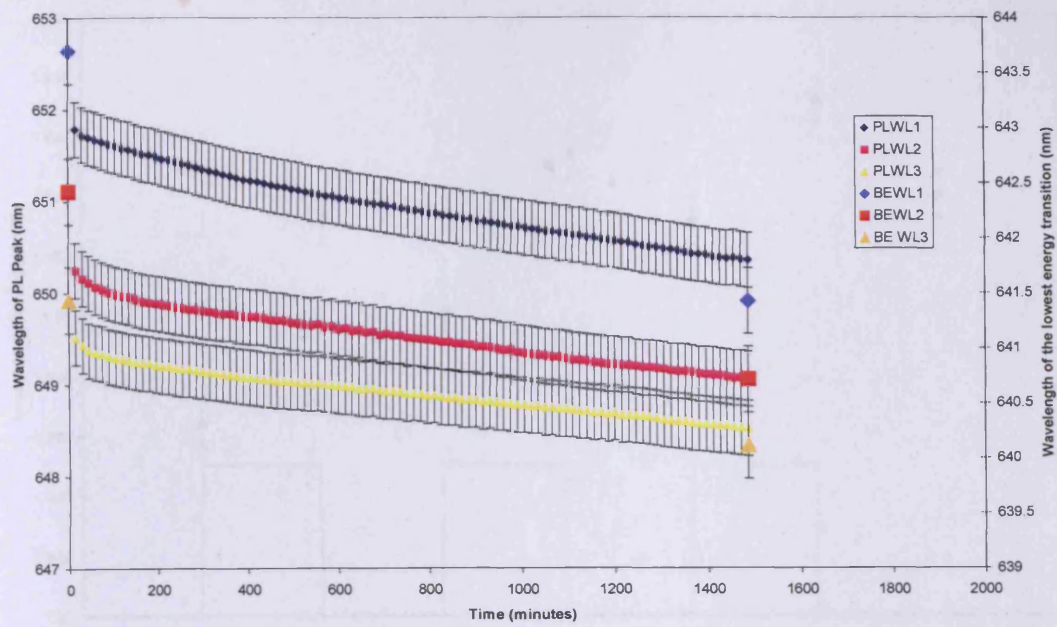


**Figure 54 PL peak and Wavelength of the lowest energy transition in acidic solution under consecutive 24 hour exposures to high intensity 532nm excitation.**

The semi-recoverable nature of the effective band edge (lowest energy transition) is demonstrated quite clearly in Figure 55.

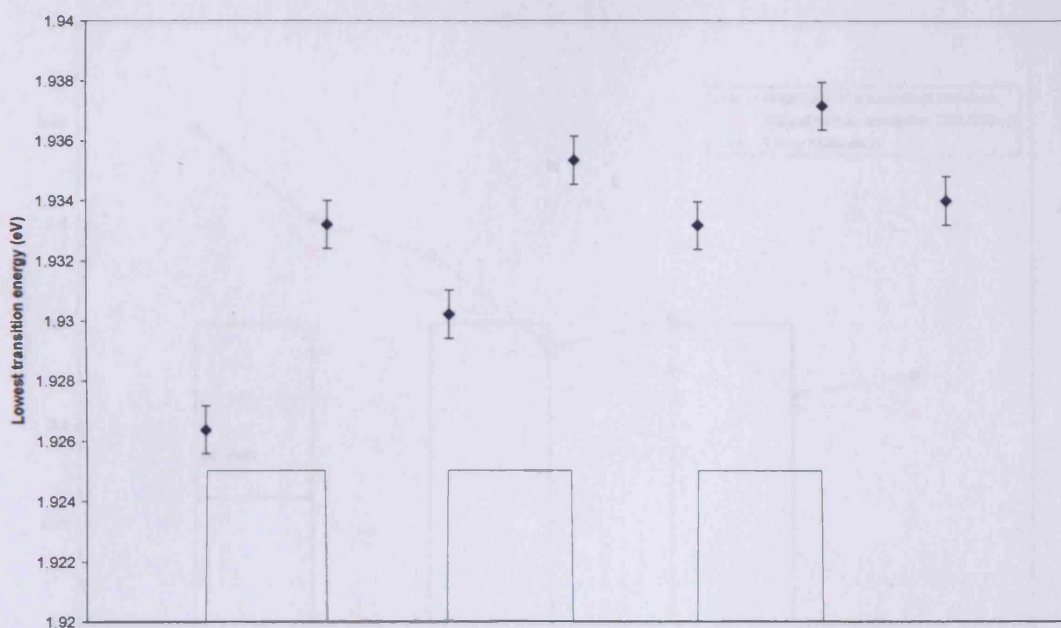


**Figure 55** Lowest transition energy (points) over three twenty four hour exposures and recoveries in the acidic buffer. The green line indicates intensity modulation over the course of the study.

The magnitude of the dot absorption taken from the Gaussian fit to the first state, and the integrated area under a higher energy region (530-535nm) is demonstrated in Figure 56. This allows comparison of the behaviour in the ground state which is strongly confined, and the higher energy states which are expected to behave in a more ‘bulk like’ manner.

As the intensity of the lowest energy transition, or otherwise said, decreases upon exposure to the exciting light but the detection decreases after the first exposure, and recovers a little after the second and third.

Under this illumination the blue shift of the lowest energy transition can be seen more clearly, and with subsequent measurements under no illumination the partial recovery can be traced, as shown in Figure 57.

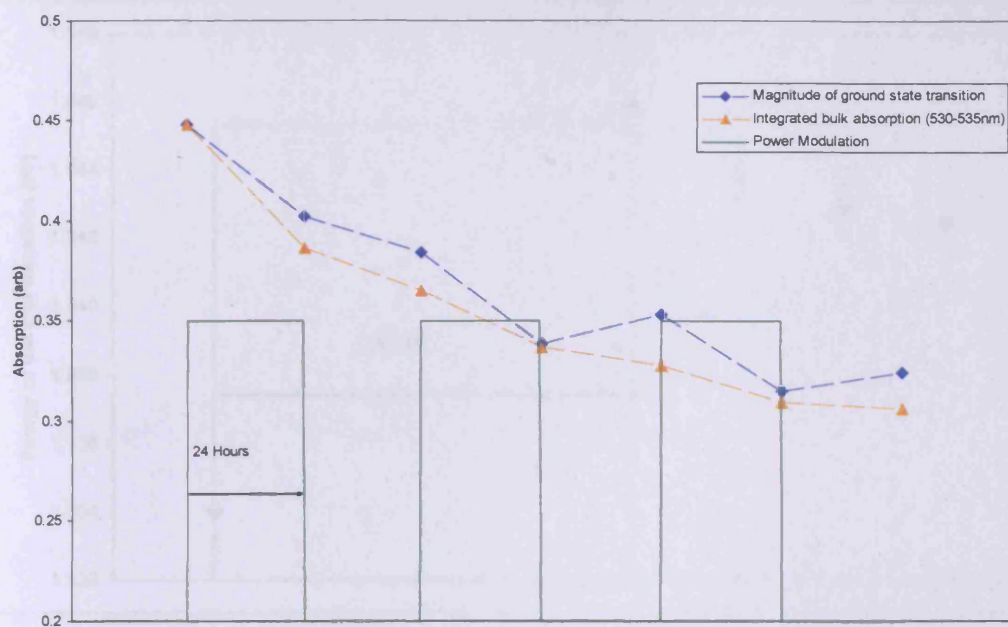


**Figure 56** Magnitude of the absorption at the excitation wavelength (orange triangles) and magnitude of the fitted Gaussian at the lowest excited transition (blue squares) over cyclic application of high intensity 532nm excitation in the acidic buffer. The integrated absorption from the shorter wavelength absorption is normalised to the lowest excited state magnitude values for clarity.

As we see there is a continual decrease in the strength of the absorption in the ‘bulk’ like states (i.e. in the excited region) while the decrease in the magnitude of the absorption in the lowest energy transition, or effective band gap, decreases upon exposure to the exciting light but the decrease decelerates after the first exposure, and seems to recover a little after the second and third.

Under 96hr illumination the blue shift of the lowest energy transition can be seen more clearly, and with subsequent measurements under no illumination the partial recovery can be tracked, as shown in Figure 57.

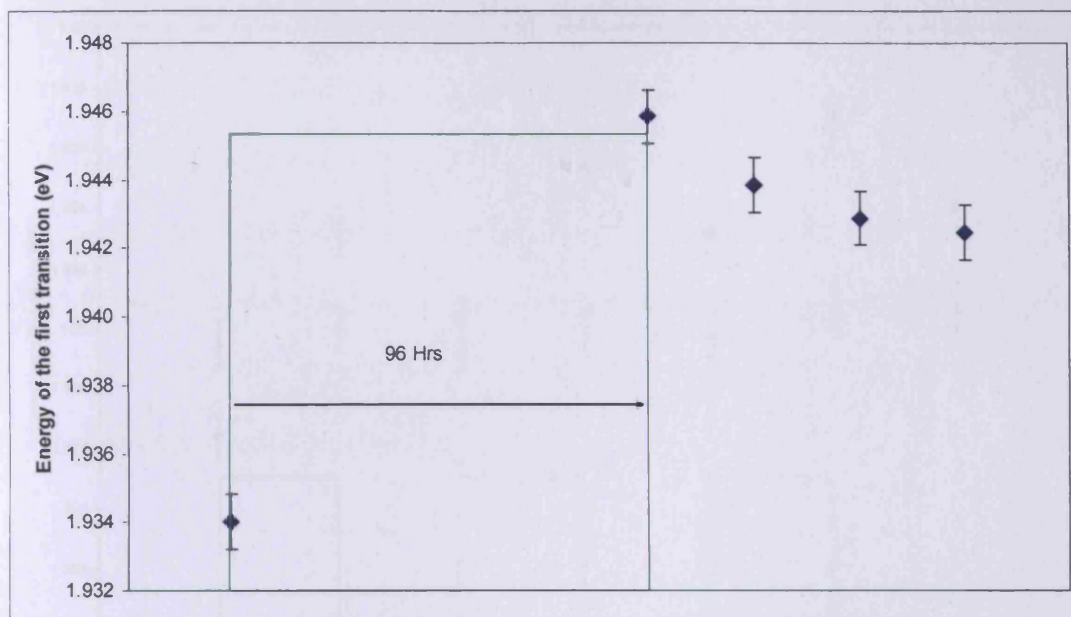


**Figure 57: Energy change in the first transition and subsequent recovery after 96hours of intense 532nm illumination.**

In order to emphasise the magnitude of the changes in the energy of the lowest transition Figure 58 shows the energy of the lowest transition in the acidic and neutral buffers over the application of the three high power exposures. We see almost no change in the neutral sample but a large, semi-reversible changes in the energy of the acidic sample.

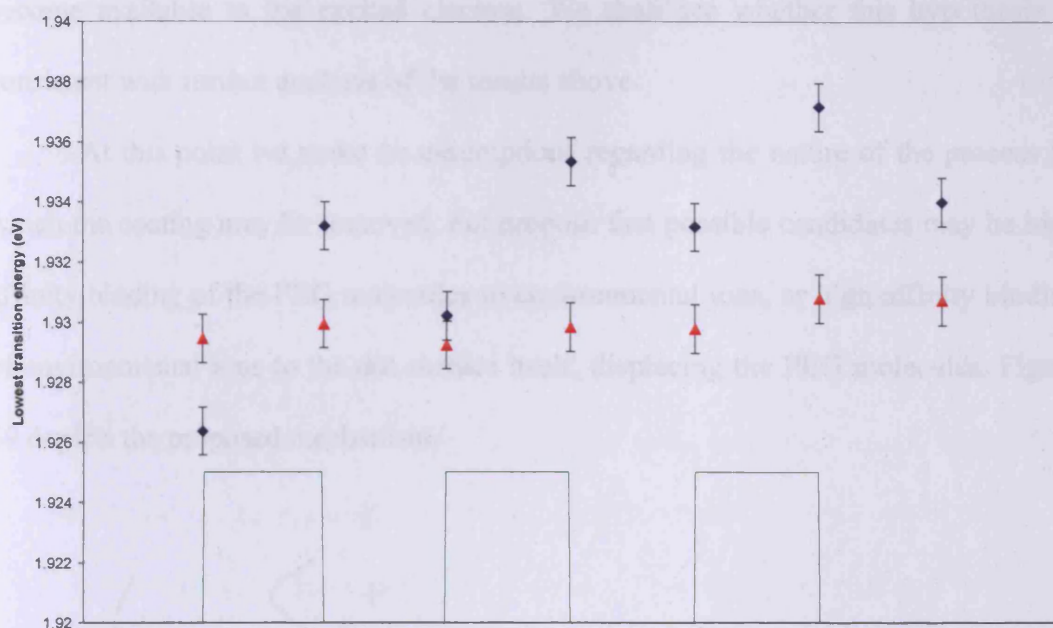


**Figure 58** Plot of energy of the lowest transition in neutral and acidic buffer over modulated application of high power excitation. Data in the acidic buffer is shown in blue while data in the neutral buffer is shown in red.

## 6.5 Discussion

We begin by considering the effect of buffer functionalisation alone on the dots. We have already demonstrated that the observed difference in PL cannot be explained by the drop in absorption alone. As such we must conclude that the PL output of the ensemble has decreased. We do not observe any significant change in the energy of the PL peak wavelength or the wavelength of the lowest energy transition which leads us to assume that no physical changes have been effected in the core of the dot. With this in mind we hypothesise here that functionalisation into the acidic buffer has partially or entirely removed the polymeric coating (PEG) around the dot, reducing the passivation of surface states and resulting in a drop in the quantum yield of the ensemble as more non-radiative recombination pathways

become available to the excited electron. We shall see whether this hypothesis is consistent with further analysis of the results above.

At this point we make no assumptions regarding the nature of the process by which the coating may be removed, but propose that possible candidates may be high affinity binding of the PEG molecules to environmental ions, or high affinity binding of environmental ions to the dot surface itself, displacing the PEG molecules. Figure 59 depicts the proposed mechanism.

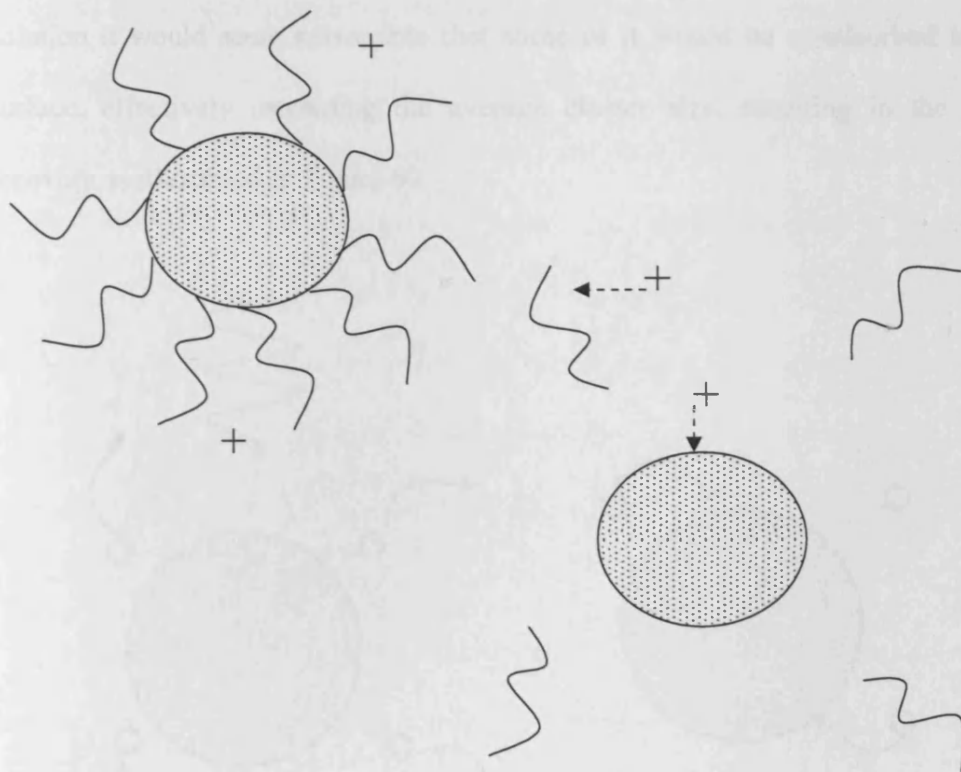


**Figure 59: Depiction of removal of surface passivation molecules due to bonding of environmental ions to either the dot surface or to the molecules themselves. The exposed surface states lead to a drop in PL efficiency due to an increased number of non-radiative recombination pathways.**

The above hypothesis is supported by the observation of a significant blue shift in the PL peak and ground state energy of the dots in acidic buffer under high intensity illumination. This implies that the acid is obtaining access to the dot surface to attack it or that the surface itself is oxidising. Due to the large size of the polymer bonds on the dot surface we would expect them to strongly inhibit access to the dot surface by any such articles. The observation of a recoverable element in the blue shift of the absorption edge and the PL lends itself to the idea that the acid is attacking the dot surface, causing material to dissociate. Since this material would remain in solution it would seem reasonable that some of it would be re-adsorbed to the dot surface, effectively increasing the average cluster size, resulting in the observed recovery as illustrated in Figure 60.

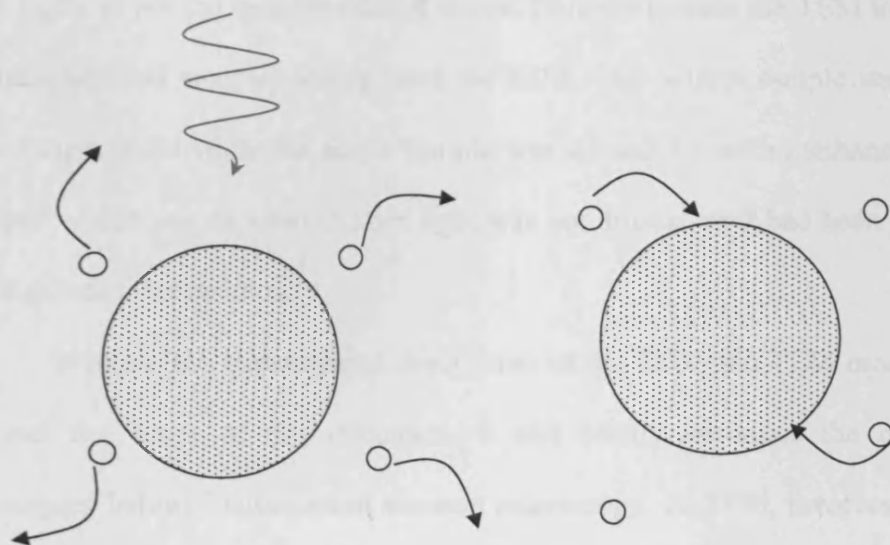


**Figure 60: Depiction of removal of material from dot surface under illumination, followed by partial re-adsorption of material upon removal of illumination.**

The dynamics observed in Figure 56, unique to the acidic sample, show a consistent decrease in absorption across the spectrum under illumination but a partial

recovery or deceleration of the degradation of the lowest energy transition contrasting with a continued decrease in higher energy absorption upon removal of illumination.

In order to satisfactorily explain this behaviour we must consider the expected behaviour of the optical cross section (and hence the absorption) under the various changes which the dots are undergoing.

## **6.6 TEM and EDX measurements**

Three samples were sent to Nicole Hondow and Andy Brown at the University of Leeds Institute of Materials Research for transmission electron microscopy (TEM) and energy dispersive X-ray spectroscopy (EDX) in order to investigate the validity of the hypotheses above. Samples studied were dots in a neutral buffer, dots in an acidic buffer and dots in an acidic buffer given a long (~96hr) exposure to high intensity laser light as per the samples studied above. Here we present the TEM images as well as the chemical analysis arising from the EDX. The neutral sample was diluted 5:1 with isopropanol while the acidic sample was diluted 5:1 with methanol. The acidic sample which was exposed to laser light was not diluted, as it had been prepared in a more dilute mixture initially.

While a full experimental description of the EDX and TEM measurements is beyond the scope of this document, I will briefly introduce the reader to the techniques below. Transmission electron microscopy, or TEM, involves the imaging of a sample (usually a very thin sample) by studying the interaction of electrons with the sample as a small conducting tip is scanned across it. Energy dispersive X-ray spectroscopy (EDX) is often conducted in parallel with such studies due to the experimental convenience of using essentially the same setup. Material in the studied sample is bombarded with charged particles and the emitted x-ray spectrum is

observed, and by precise knowledge of the frequency of the lines in the spectrum one is able to deduce, or narrow down, the material composition of the studied material.

### 6.6.1 Dots in Neutral Buffer

Figure 61 demonstrates images of dots in the neutral buffer. We see evidence of aggregation of the dots, although it is possible that this is brought about by the dilution in solvent. The dots appear to be somewhat elongated along one axis, with a dimension of roughly 4-5nm in one direction and 9nm in the other. Figure 62 shows a higher magnification image of the dots and, significantly, dots sitting over the edge of the carbon film support, which indicates that the dots possess an amorphous coating; consistent with the passivating PEG layer which we have already hypothesised is stable in the neutral buffer.

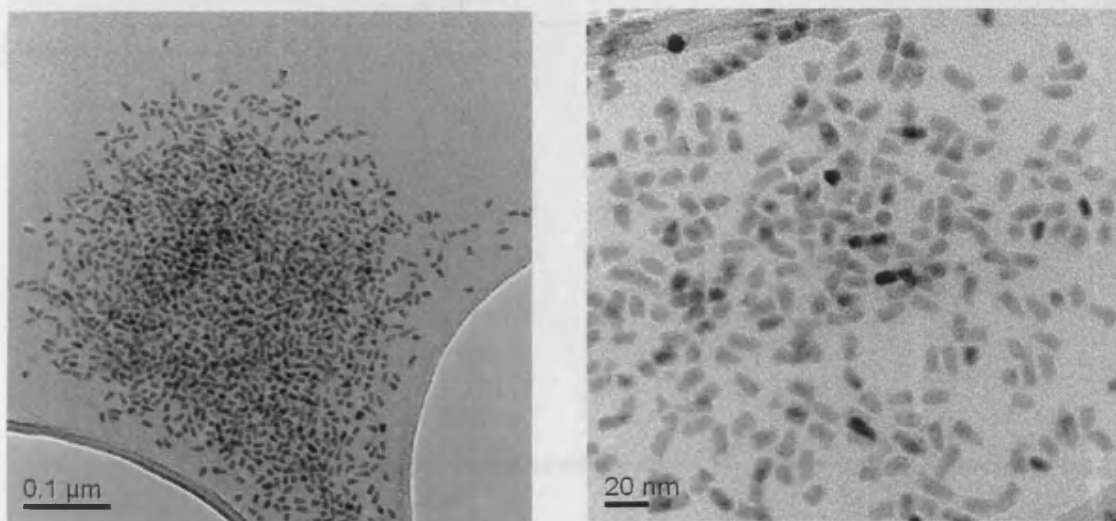
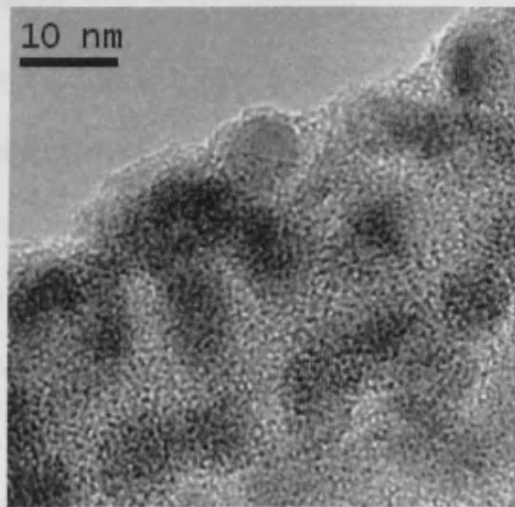
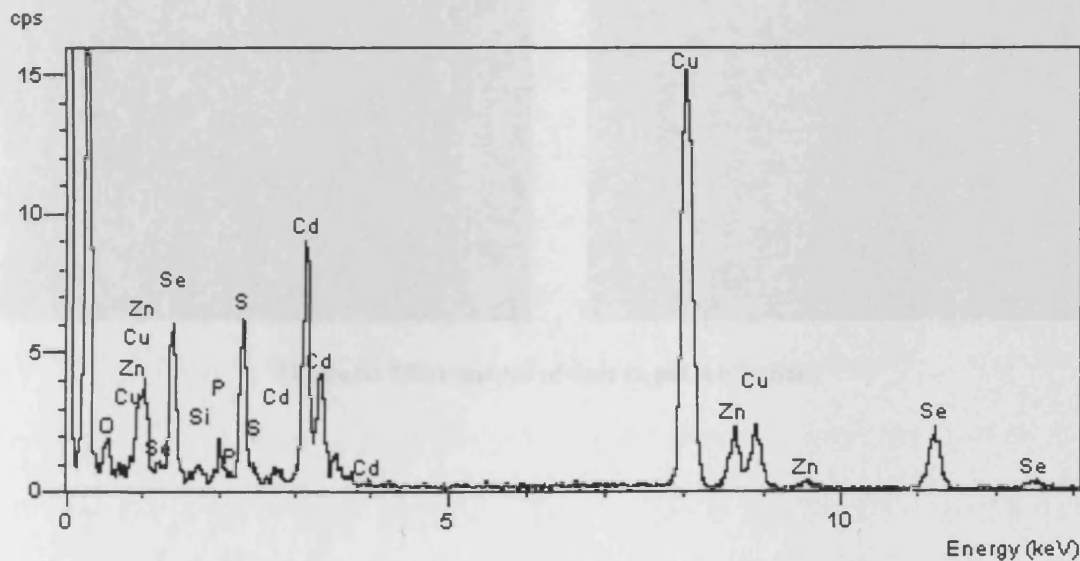


Figure 61 TEM images of dots in neutral pH buffer



**Figure 62** High magnification image of colloidal quantum dots in neutral buffer solution. The appearance of dots which sit over the edge of the carbon indicate the presence of an amorphous coating, consistent with the passivating PEG layer.



**Figure 63** EDX spectrum of a dot in the neutral buffer

In Figure 63 we see EDX spectra from a dot in neutral buffer. We shall return to consideration of the EDX spectra when we have observed equivalent spectra from the other samples, however we note that we observe clear Cd, S and Se lines (the Cu lines arises from the plate on which the samples are prepared) as well as weak O and P lines.

## 6.6.2 Dots in Acidic Buffer

Below we present TEM images of dots in pH 4.0 buffer solution. Figure 64 demonstrates that the dots in the acidic buffer have not aggregated as per the neutral dots. Inspection of the images shows no evidence of dots on the edge of the carbon film, indicating that the amorphous film seen in Figure 62 is no longer present. Figure 65 shows EDX measurement of a dot in the acidic buffer. The differences between this dot and that shown in Figure 63 are minimal, but we note that this measurement is very insensitive to the polymer coating.

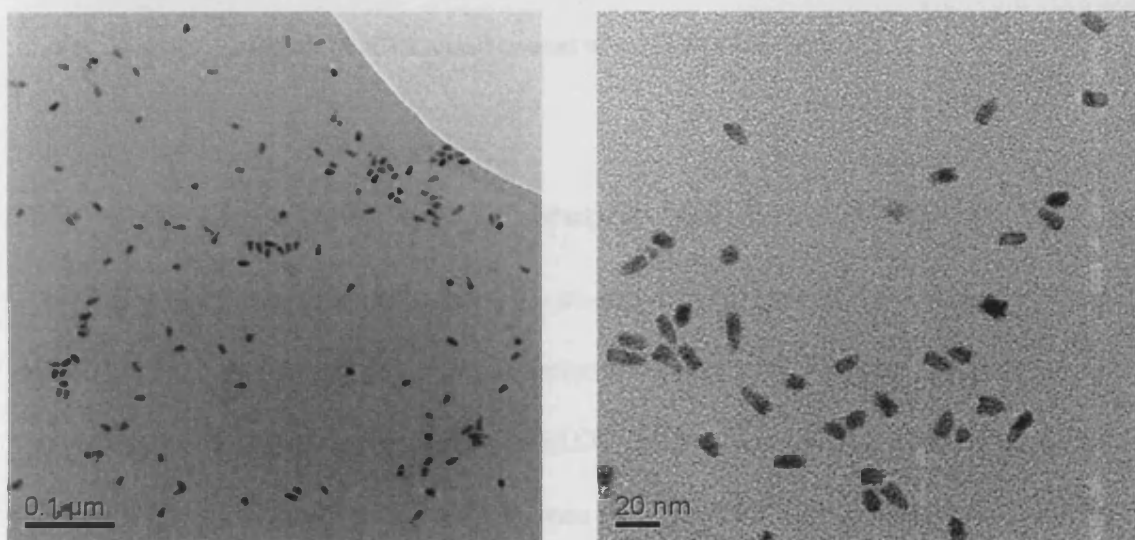


Figure 64 TEM images of dots in pH 4.0 buffer.

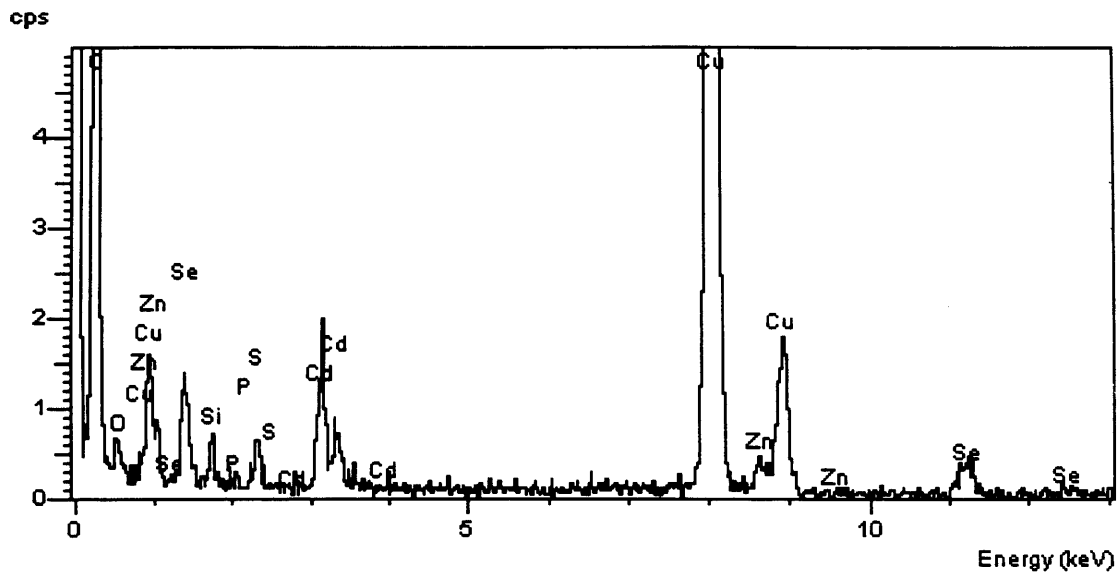


Figure 65 EDX measurement of a dot in acidic buffer.

### 6.6.3 Dots in Acidic Buffer with Exposure to High Power Excitation

Here we present similar results to section 6.6.2, but where the sample has been exposed to high power excitation for an extended period. While the TEM images do not yield any additional information the EDX measurement shows some significant changes in the dots chemical makeup as seen in Figure 66. Careful inspection shows the presence of a strong K (3.31 keV) or Cd L $\beta$  (3.32 keV) line as well as a small indication of Fe in the sample. Most importantly we observe a much stronger O line in this sample (Cd/O ratio is  $\sim 1.16$  as opposed to  $\sim 3.3$  in the sample without exposure to excitation), indicating that the dot has been oxidised to some extent. Below we discuss the application of this to the hypothesis above.

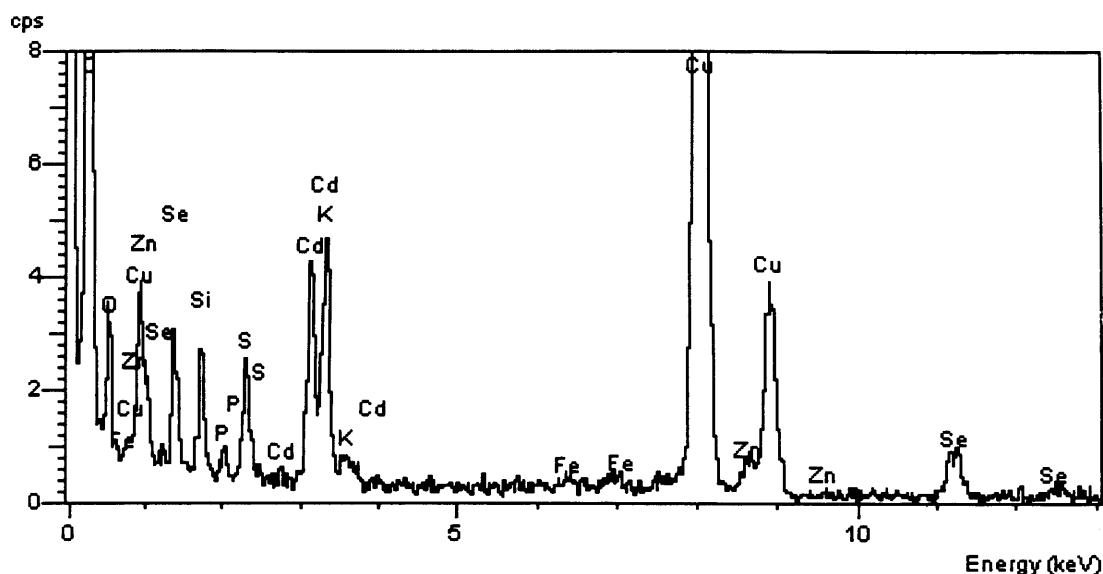


Figure 66 EDX spectra of dots in acidic buffer after prolonged high power excitation

## 6.7 Conclusions and Application

We conclude that in the acidic sample the dots have undergone a significant alteration to their surface chemistry, arising due to the ability of environmental ions to access the dot surface because of the removal of the polymer shell. A number of measurements including a drop in PL output, TEM images indicating the absence of the shell as seen in the neutral sample, and the oxidation of the dot surface from EDX, support the hypothesis that the coating shell has been removed and the dot core exposed. Upon removal of this shell exposure to excitation causes photo-oxidation of the dot, resulting in a semi-reversible blue-shift of the PL peak and the band edge absorption. We may now state with some certainty as a result of the EDX measurements, that the observed blue shifts are associated with the oxidation of the surface. We cannot dismiss the possibility that the removal of material from the dot is still occurring, however if this process is occurring then it is on a small scale since there is no observable change in the dot size on inspection of TEM images of samples which have undergone extensive photo-excitation at high power.

This sensitivity of the dots to the environmental pH provides a number of interesting applications, especially in the field of cellular imaging. A number of observable factors including a lower PL output, a drop in the observed absorption magnitude and blue shifting of both the above provide the potential for use of quantum dots as pH sensors in imaging setups, especially in a cellular environment where the pH gradient between the early and late endosomes can be observed as the dots progress through the structure.

Conversely this work also has an impact on work currently undertaken and work which will be undertaken in the future. The goal of using colloidal quantum dots in a number of medicinal and diagnostic capacities *in vivo*, as well as work more commonly performed currently *in vitro* rely on dot stability for reliability and interpretation of results, as well as the reliability of the organic capping layer to prevent access to the toxic, inorganic, dot core. In this work we have demonstrated that in a moderately acidic environment the capping layer is removed and the dot core exposed. The implications of this for *in vivo* use of CdSe/ZnS dots are many, since the exposure of the dot could allow release of toxic cadmium ions. Ultimately this field will rely on the development of dots made of less toxic material, and/or the development of more stable capping materials for the existing materials.

*In vitro* studies are much less affected by the issue of toxicity (although studies on live cells may need to take this into account) however the release of material from the dot, and the change to the dots makeup and subsequent alteration of its optical properties will be of concern. Material coming from the dot's inorganic core is of concern due to the possibility of it affecting the function of the imaged cell, as well as returning false positives on tandem measurements. To demonstrate the latter consider detection of K channels in a cell. Many of the dyes commonly used as

K-indicators are also highly sensitive to the presence of Cadmium ions. The release of cadmium from the dot core, or simple exposure of the inorganic surface, could result in false detection, and subsequent error in results.

In closing, the development of less toxic material systems for colloidal quantum dots in biological applications and the ability to coat these dots with more stable surface materials is essential if dots are to fulfil their potential for use in living organisms, especially for medicinal purposes in humans. In the short term, however, dots possess great potential as cellular indicators of environmental processes due to their highly environmental sensitive optical properties.

In the context of biomedical imaging our results indicate that under ambient conditions dots which have been incorporated into a cellular environment will initially demonstrate a pH sensitive change in their properties over a timescale of approximately 24Hrs. After this period the dots will provide a stable photoluminescence output under excitation up to  $25\mu\text{Wcm}^{-1}$ , with no significant change in the absorption profile. We have shown that above  $250\mu\text{Wcm}^{-1}$  significant photo-dynamic behaviour is induced over a 24Hr timescale, with photoluminescence output increasing by ~50% in the acidic environment. There is also a large change in the shape of the absorption spectra, especially near the band edge, in the acidic environment. This implies that when using higher power densities in biomedical imaging application, great care is needed where an acidic cellular environment is involved as pH sensitive processes will drive changes in the photoluminescence output of the dots. Indeed, even when working at power densities one must be aware that the acidic environment alone will bring about changes in the dots, and that dots photoluminescence output must be allowed to stabilise before measurements are made if quantification of changes in PL intensity is important.

## **7. Conclusions and Further Work**

Here I will summarise the results presented in this document and go on to suggest work which could be done in order to further test the hypotheses which have been constructed, expand on the knowledge gained and apply the results of this work.

### **7.1 Conclusions**

The work contained in the document is divisible into two main parts: the study of colloidal quantum dots in PMMA to develop an understanding of their photo-dynamic behaviour, and the study of colloidal quantum dots in pH buffers to simulate cellular environments. Here I will discuss the conclusions drawn from each of these areas and their impact on the field.

#### **7.1.1 Colloidal Quantum Dots in PMMA**

In chapters four and five we used a two state model to describe photo-dynamic behaviour in quantum dot ensembles contained in a PMMA matrix. In doing so we were able to estimate values of the initial bright and dark population of dots available for photo-brightening to be approximately 50% in our case, as well as separating the natural process by which dots enter into a bright state from the photo-driven element.

This work also identified a trend whereby, once the power-sensitive element of the photo-activation was removed by calculating the probability of photo-activating a colloidal dot upon absorption of a photon, the photo-activation probability of dots became increasingly inhibited over time exposed to excitation. This was linked to possible oxidation of the dot surface, identified by a gradual blue shift in the emission wavelength, and a model describing the link was proposed.

In the above work we have been able to expand on previous work detailing sensitivity of photo-dynamics to environmental oxygen and the role of surface passivation in the emission intensity of dot ensembles. We have drawn a link between these two processes by hypothesising that oxidation of the dot surface eventually inhibits passivation of surface states by preventing access to the dot surface by environmental molecules which may affect passivation.

### **7.1.2 Colloidal Quantum Dots in pH Buffers**

In chapter six we studied the behaviour of colloidal quantum dots coated with a hydrophilic polymer shell and functionalised in pH buffers. This enabled identification of key elements of their behaviour which will have an impact on their use in biological systems.

We identified that in a neutral environment the dots maintained a good level of photo-stability, enabled by the polymer shell around the dot providing a degree of protection from environmental factors. Conversely dots in acidic buffer showed dramatic changes to their behaviour under optical excitation, leading to the hypothesis that the organic shell had been partially or completely stripped by the acid. We arrived at this hypothesis by studying the emission and absorption properties of the dots under a variety of optical conditions, and applying curve fitting in order to characterise these observations. It was observed that under high intensity light the PL peak and wavelength of the absorption ground state altered dramatically in the acidic environment, behaviour which was not observed in the neutral environment, implying that the dot core was exposed to environmental effects to a greater extent.

The above hypothesis was tested by EDX, TEM and FTIR measurements conducted by Leeds University. The TEM results obtained indicated the presence of an amorphous coating around the dots in the neutral buffer, which does not appear in

the acidic sample, consistent with the presence of the polymer coating in the neutral sample and its absence in the acidic sample. EDX studies indicated approximately three times the presence of oxygen at the surface of the dots in the acidic buffer after exposure to excitation, which suggests that the changes observed may have been driven by an oxidation process. As a result we concluded that our hypothesis regarding removal of the ligand shell was accurate and that this enables oxidation of the dot surface which drives changes in its optical behaviour.

The above work identifies a number of potential pitfalls for dots in biological tagging and imaging applications including toxicity brought about by exposure of the inorganic core, possible interference generated by dot by-products in tandem measurements, and undesirable changes in the magnitude and wavelength of the dot emission in certain elements of cells and organisms.

## **7.2 Further Work**

In order to further test some of the hypothesis we propose a number of further studies could be performed, including attempting to detect free cadmium ions in the solution under excitation, which will provide confirmation of the release of material from the dot core, the implications of which are discussed below. This may be possible with sensitised dyes, which demonstrate photo-dynamic behaviour dependent on the presence of heavy metal ions. Such a study, should it prove that there was evidence of release of such ions from the dot surface, would pose some very serious problems for studies where the detection of K ions is used to identify biological pathways, since the tandem use of dots in such a study would return a false positive. It would also be of concern due to the highly toxic nature of Cadmium ions in biological systems, especially if the goal of incorporating dots into medical treatment is to be realised.

The work detailed in this document could be supplemented by studies of dots with a wider variety of polymeric coatings, since we have addressed the specific case of dots coated with the PEG molecule. In addition it would be useful to expand the study to dots made of other materials widely used in imaging applications such as CdTe. The end goal of such studies must be to develop a material system whereby the polymer shell is sufficiently well bound to the dot surface as to remain stable in volatile environments.

The results discussed above also provide the potential for use of colloidal dots in identifying pH in imaging applications, whereby, if the magnitude and/or wavelength of dot in a cell can be spatially resolved, the relative pH of each area could be determined by comparison with standard data obtained in buffer solutions, provided other environmental factors could be ignored. While it is currently possible to perform such studies using dyes the many advantages of colloidal dots over dyes, such as their relatively high photo-stability allowing much greater periods of activity to be observed, means that they would be a useful alternative for studies where there was call for more flexibility.